TAMPEREEN TEKNILLINEN YLIOPISTO
TAMPERE UNIVERSITY OF TECHNOLOGY
Julkaisu 743 • Publication 743

Antti Stenvall

An Electrical Engineering Approach to the Stability of MgB_2 Superconductor

Tampere 2008

Tampereen teknillinen yliopisto. Julkaisu 743
Tampere University of Technology. Publication 743

Antti Stenvall

An Electrical Engineering Approach to the Stability of MgB_2 Superconductor

Thesis for the degree of Doctor of Technology to be presented with due permission for public examination and criticism in Rakennustalo Building, Auditorium RG202, at Tampere University of Technology, on the 8th of August 2008, at 12 noon.

Tampereen teknillinen yliopisto - Tampere University of Technology
Tampere 2008

ISBN 978-952-15-1996-3 (printed)
ISBN 978-952-15-2034-1 (PDF)
ISSN 1459-2045

Abstract

The high critical temperature, 39 K, and usable critical current characteristics of MgB_2 make it a highly interesting superconductor for practical applications. Unlike conventional low temperature superconductors, it can be used around 20 K where cooling is relatively easy with a cryocooler. In addition, long-length MgB_2 conductors can be manufactured of inexpensive materials with standard techniques. Though the MgB_2 was found superconductive only in 2001, industrially manufactured conductors are already now available and several promising demonstration projects are underway. To develop a new application using the MgB_2, detailed design methods are required. Many modelling tools, but not all, can be adopted from devices constructed of conventional superconductors.

This thesis begins by introducing readers to the mathematical formulation of phenomenon models required for the research presented in the attached publications. After this background, I first study conductor characterisation in a conduction-cooled measurement station, because short-sample characterisation forms the basis of magnet design. From there I move to propose a model for computing the critical current of coils consisting of a ferromagnetic matrix. Based on the coil design, a stability margin must be determined for the coil. Here, I present a numerical model for computing the minimum propagation zone, a model that can be further used to determine the minimum quench energy and the normal zone propagation velocities. At the end of the thesis, I consider a scientific industrial-scale induction heater project ALUHEAT. First, I introduce the basics of quench analysis and, then simulate a quench in the main coil of the induction heater with the developed quench program. In the quench analysis, I also design protection for the coil.

Preface

The summer of 2004 was the first time I worked at the Institute of Electromagnetics (IoE) at Tampere University of Technology (TUT). Before that I had taken the course Superconductivity in Electric Power Grid, but that summer was the first time when I worked in the field of superconductivity.

Our group leader, Risto Mikkonen, had been involved in superconductor research for more than two decades. Because of his contacts and reputation, IoE was invited to participate in an European project, called ALUHEAT, for the design, constructing and testing of a DC induction heater using the superconducting material MgB_2. The project began on 1 June 2005 with IoE responsible for cryostat design and coil stability analysis. Somehow I managed to convince Risto and his right hand, Aki Korpela, for my capabilities of shouldering the stability analysis, and I was consequently hired to do my M.Sc. thesis on the stability of the MgB_2 superconductor. The work began already on 2 January 2005, and I have since then been working with IoE, now part of the Institute of Electronics and known as Electromagnetics at TUT.

My M.Sc. thesis work introduced me to the stability of superconductors and the superconducting material MgB_2 from the electrical engineering perspective. However, the thesis did not fulfil the requirements of the ALUHEAT system coil stability analysis. The more I learnt, the more I realised that the less I know, the more there is to be done; a phenomenon that still happens daily. By spring 2005, I had accumulated enough data for an M.Sc. thesis. The thesis was not a comprehensive study of the details examined in it, yet it suggested several topics for further study in a Ph.D. thesis and prepared me to make a quench simulation program for the ALUHEAT magnet and propose system for protecting the coil and detecting quench.

Since my first conversation with Risto in spring 2004, when I had applied for the summer job, I had stressed my willingness for postgraduate study. Because of constantly tight budgets for the basics at the university, Risto made no promises until the money was guaranteed. We had the ALUHEAT

project though, but money only for one worker. My colleague, Iiro Hiltunen, currently a Ph.D. student, was then working on the cryostat, which made it impossible for me to continue working at IoE, participate in the ALUHEAT project, and to do a Ph.D. without extra funding.

* * *

When in autumn 2001 I started the Degree Programme of Electrical Engineering at TUT, I practically hated electricity and especially magnetism. It was not because of the subjects themselves but because of the useless book I had studied in high school. I chose Electrical Engineering because my friends, Vesa Karhu and Tuomas Kovanen, did so too. During my first course on circuit analysis, given by Aki, I enjoyed his transcendental teaching skills but was not yet fascinated by electromagnetism. During spring 2002, I and Vesa decided to finish off all our required studies that had something to do with electromagnetism in TUT and were taught by IoE. Thus, in addition to an advanced course on circuit analysis, we took two second year courses on electromagnetic fields and waves lectured by professor Lauri Kettunen, who was also head of IoE during my time in that encouraging unit. These three courses took my breath away. I had never seen such good lecturers as Lauri, Risto and Aki. TUT boasts many good, but the teaching methods of these three gentlemen were ideal for freshmen and equally so at advanced levels, including their discussion based management. To me, each in his own way had correctly understood correctly the purpose of technical university; to give high-level education to prepare students for innovative work and provide facilities for credible research. While I was doing my Ph.D., they provided me with great opportunities to carry out this fascinating research in my way.

The compact and feasible theory of the electromagnetic phenomena, with relevant roughening, and the level of education at IoE made me start a vocational subject at IoE already in my second year. I sought to take all the courses at IoE for which I had the necessary pre-requirements. Practically a student could do two majors at IoE. The first, my official major, was about renewable energy and modern electrical engineering, supervised by Risto. The second, electromagnetism and mathematical physics, was supervised by Lauri. I decided to take as many courses as possible from both, and I did well expect for one course. Mechanics of electromagnetic systems was a bit too much for a second year student. But, that was my first contact with Saku Suuriniemi, one of the most demanding lecturers at TUT, a word of praise, mind you. I consider Electromagnetic modelling, given by Saku, the best course I have taken ever. Luckily, I took that in my fourth year with few other courses to add to the load.

However, in my third year, Tuomas had also started to study electromagnetism, and we took a few courses together. I believe that Guided waves, given by Lauri in spring 2004, influenced on my possibility to do Ph.D. at IoE. Each time I took an IoE course, I tried to do superb work to learn and get a good grade. However, during that course I broke my wrist in a floorball game. Lauri gave as some challenging home exercises to code 1D and 2D FDTD programs, and admittedly niche guidance, which probably was intentional. Because of my broken wrist, I had more time for homework and less for sports, and I think I managed the programs rather well and convinced Lauri of my ability to solve given bugger tasks. I believe Lauri remembered me from the course, because a couple of years later he asked me about the FDTD codes and if I could do a lecture demo for him. I could no more even remember what FDTD stood for.

But back to how I ended up as a Ph.D. student. Lauri is head of National Graduate School on Applied Electromagnetism. One day in summer 2005, Risto came to me and said that I could get into Lauri's school. I thought Risto had suggested to Lauri to enrol me; after all, my grades were good enough for admission. I graduated in August 2005 to M.Sc. (tech.) and immediately started work towards Ph.D. I had then already tentatively sketched a couple of manuscripts based on the ideas developed in the M.Sc. thesis or immediately afterwards. One publication, excluded here, was directly based on the M.Sc. thesis. In August 2006, I celebrated my 25^{th} birthday in a local pub in Seattle, where with Risto and Iiro I was attending the Applied Superconductivity Conference. Somehow the conversation turned to my graduate school position, and Risto told me that Lauri had suggested I should apply to his school. Surely, it was not all about one piece of homework, but if one seeks to do one's tasks to the best of one's ability in a reasonable time, things generally turn out well.

This thesis summarises my work at IoE, TUT, over three years. Thanks to the position in the graduate school, I was given a free hand to do what I wanted, a privilege I really enjoyed. I started by studying the computation of critical current and magnetic flux density distributions in coils with a conductor consisting of ferromagnetic matrix. I then proceeded to coil quench analysis. At some point, I realised that it can be quite difficult to get initial data for modelling a coil. In practice, the n-values of some MgB_2 conductors seemed quite high. We then built a test coil and observed considerable heat generation at sub-critical currents. This led to the study of critical current measurement in a conduction-cooled environment. Meanwhile, some current transfer study was also being performed. Finally, I ended up scrutinising the dynamics of the quench origin and the effects of a measurement system on results.

At first, Aki and Risto advised me on my thesis. Though most of the ideas

were mine, the early papers would not have been generally comprehensible without their contribution. Jorma Lehtonen joined to the advisors in summer 2006, and thanks to his contribution, the thesis achieved its present scientific level. Though I was only starting all these studies, Jorma's e-mail help was indispensable with the detailed content of each publication.

This thesis is not a masterpiece, but it marks an intermediate stage in my life and research. I hope research of conduction-cooled measurement systems will continue and expand here at Electromagnetics, and I hope to participate in it at some level. At least, we have one very promising and eager candidate ready for a Ph.D.

* * *

I believe I have already named the people who contributed most to my Ph.D. studies, but I also wish to express my appreciation to many others, whose contribution I value. To end this preface, I wish to thank the following people and to apologise to those who, yet deserving thanks, have not been mentioned by name.

Aki Korpela, your ability to make a text more readable is beyond compare. Thanks for helping me efficiently to start Ph.D. thesis and for organising all the weekly football activities we had at IoE.
Family at Palokka, Joensuu, Oulu, sometimes Down Under, Mexico, wherever you are, having no problems at home helped me to concentrate on essentials in my life. The essentials changed many times over, but each time it was important to choose from what was there and not to choose too wrongly too often for a too long time, regardless of whether there was a wrong choice.
Friends from my Palokka time, mainly from PaRi, and also the ones who came to study in Tampere and friends from Soittorasia, we had good times off duty and hopefully also in future, though my family has certainly imposed me on new responsibilities, but I see also other growing families.
Giovanni Grasso, thanks for providing some material data and the MgB_2 conductors.
Iiro Hiltunen, thanks for invaluable help in the lab. We had nice time at conferences even though you were not a fan of Sly Fox. Still Risto liked Old Rasputin but both of us did not.
Jari Kangas, Pasi Raumonen and Saku Suuriniemi thanks for helping me to understand even a bit of computational electromagnetism and also coping with some practical computational issues.
Jonna Viljamaa, thanks for taking care of the coil manufacture.

Joonas Järvelä, thanks for making the MQE and v_{npz} measurements and helping with other tasks in the lab.
Jorma Lehtonen, without your contribution, this thesis would be of lower scientific value.
Joseph Horvat, thanks for carefully evaluating this thesis. I think your evaluation strengthened its argument.
Lasse Söderlund, when I had administrative problems... Well I had none. Wonder why? Thanks for that.
Lauri Kettunen, thanks for your support and leadership in several things. I am very grateful for having been accepted to the Graduate School of Applied Electromagnetism.
Lauri Rostila, Maria Ahoranta, Masi Koskinen Mika Masti, Teemu Hartikainen and others not mentioned here from IoE, TUT, in all Ph.D. and other work, it is important that one feels a part of a group of equals. Thanks for that. And special extra thanks to those who participated in our weekly football and futsal. I think that these happenings twice a week made this place the best working place in the whole universum, unless there is a place where these events are arranged three times a week, with the very same people.
Luca Bottura, I feel honoured to have an opponent from the very top of superconductor stability. Thanks.
Maija-Liisa Paasonen, like Lasse, you freed me to do my work.
Markus Rautanen, thanks for the multiplexer and your enjoyable company during your M.Sc. thesis work in Sc314.
Mervi, thanks and sorry. Without you, I would probably be also here, but my life would be wretched.
Nenna, your winning smile makes me rush home from work and refreshes me for another day at work.
Niilo, you are among the three most important persons in my life. Once when I came tired from work to pick you up from day-care, continued with you to the gym and then came home, you said with a happy sigh that finally you had time to play with daddy. It really breathed new life into me.
Osallistujat.com (Teamhappenings.com) helped greatly with many things and is likely to grow into a top web brand in Finland.
Pavol Kováč, you organised for me a two-week visit to Bratislava. I am also very pleased of our former and coming cooperation. I look forward to meeting you again at conferences or workshops.
Personnel from Protopaja are acknowledged for constructing parts for the measurement systems.
René Flükiger, I am pleased to have such a distinguished person as a pre-examiner and opponent. If you accept my thesis at the public defense and think I earned my Ph.D., I believe the work done was enough.

Risto Mikkonen, without you, I would never have made this Ph.D. When my son, Niilo, was born in July 2005, you reminded me that work was not the most important thing in the world. What kind of boss says that? The best.
Risto Ritala, thanks for giving me a chance to falimiarise myself with academic working environment. I really enjoyed summer 2003 under your guidance at the Institute of Measurement and Information Technology. When I came to IoE, I continued working the way I had learnt the year before and now all the way to this Ph.D.
Timo Lepistö, thanks for proof-reading the manuscript.
Timo Tarhasaari, thanks for helping me to become conscious, in my own level, about the difference between model and nature. Special thanks for your valuable comments while I was writing this thesis and rushing to ice-hockey games. Thanks to your help with the background, I can be satisfied with the thesis once it is off the press. If a year hence I am not, I have made progress.
Tomáš Holúbek thanks for showing me Bratislava and inspiring me to embark on my current trasfer studies.

This work was financially and materially supported by (in alphabetical order) Columbus Superconductors, Emil Aaltonen Foundation, the European Union (contract ALUHEAT-013683), Graduate School of Applied Electromagnetism (Ministry of Education), Magnet Technology Center (Prizztech), Slovak Academy of Sciences Institute of Electrical Engineering, Tampere University of Technology, Finnish Foundation for Technology Promotion and Ulla Tuominen Foundation.

In Tampere, 17 June, 2008

Antti

List of publications and author's contribution

Publication 1

Stenvall A, Korpela A, Mikkonen R and Kováč P 2006
Supercond. Sci. Technol. **19** 32
"Critical current of an MgB_2 coil with a ferromagnetic matrix"
doi:10.1088/0953-2048/19/1/006

Publication 2

Stenvall A, Korpela A, Mikkonen R and Grasso G 2006
Supercond. Sci. Technol. **19** 184
"Stability considerations of multifilamentary MgB_2 tape"
doi:10.1088/0953-2048/19/2/006

Publication 3

Stenvall A, Korpela A, Mikkonen R and Grasso G 2006
Supercond. Sci. Technol. **19** 581
"Quench analysis of MgB_2 coils with a ferromagnetic matrix"
doi:10.1088/0953-2048/19/6/028

Publication 4

Stenvall A, Hiltunen I, Korpela A, Lehtonen J, Mikkonen R, Viljamaa J and Grasso G 2007
Supercond. Sci. Technol. **20** 386
"A check-list for designers of cryogen-free MgB_2 coils"
doi:10.1088/0953-2048/20/4/014

Publication 5

Stenvall A, Korpela A, Lehtonen J and Mikkonen R 2007
Supercond. Sci. Technol. **20** 92
"Current transfer length revisited"

doi:10.1088/0953-2048/20/1/017

Corrigendum 2007
Supercond. Sci. Technol. **20** 1253
doi:10.1088/0953-2048/20/12/C01

Publication 6

Stenvall A, Korpela A, Lehtonen J and Mikkonen R 2007
Supercond. Sci. Technol. **20** 859
"Two ways to model voltage-current curves of adiabatic MgB_2 wires"
doi:10.1088/0953-2048/20/8/023

Publication 7

Stenvall A, Korpela A, Mikkonen R and Kováč P 2007
IEEE Trans. Appl. Supercond. **17** 2369
"Discrepancies in modelling magnets utilizing MgB_2 conductor with ferro- and non-magnetic matrix configurations"
doi:10.1109/TASC.2007.899269

Publication 8

Stenvall A, Korpela A, Lehtonen J and Mikkonen R 2008
Physica C **468** 968
"Formulation for solving 1D minimum propagation zones in superconductors"
doi:10.1016/j.physc.2008.04.011

Publication 9

Stenvall A and Mikkonen R 2008
Accepted for publication in a book "MgB_2 Superconductor Research", to be published by Nova Science Publishers
"Thermal transients in MgB_2 conductors"

Publication 10

Stenvall A, Hiltunen I, Järvelä J, Korpela A, Lehtonen J and Mikkonen R 2008
Supercond. Sci. Technol. **21** 065012
"The effect of sample holder and current ramp rate on a conduction-cooled $V - I$ measurement of MgB_2"
doi:10.1088/0953-2048/21/6/065012

Publication 11

Stenvall A, Magnusson N, Jelinek Z, Grasso G, Hiltunen I, Korpela A, Lehtonen J, Mikkonen R and Runde M 2008
Physica C **468** 487

"Electromagnetic viewpoints on a 200 kW MgB_2 induction heater"
doi:10.1016/j.physc.2008.02.001

Author's contribution

I (later the author) have written all the text in the publications, with following exceptions. G. Grasso provided section 2 for **Publication 3**, part of section 2 for **Publication 4** and section 2 for **Publication 11**. N. Magnusson provided section 3 for **Publication 11**. Z. Jelinek provided section 5 for **Publication 11**. The form of writing was unified by the author within these sections.

A. Korpela and R. Mikkonen helped with finalising the text of all the publications and with presenting the ideas in necessary form. J. Lehtonen provided similar help with **Publications 4-11** (except **Publication 7**) while discussing valuably about the contents. All the simulation work and design of computational models was done by the author.

For **Publication 1** and **Publication 7** P. Kováč provided the critical current characteristics and cross-section figures of the investigated conductors, whereas G. Grasso provided similar data for **Publication 2**, **Publication 3**, **Publication 4**, **Publication 10** and **Publication 11**. Conductor for **Publication 4**, **Publication 9** and **Publication 10** was provided by G. Grasso.

Coil design in **Publication 4** was performed by J. Viljamaa with the author. Measurements were performed by J. Viljamaa, I. Hiltunen and the author together. J. Järvela made the measurements for **Publication 9**, but the sample holder design was author's. J. Järvela and I. Hiltunen assisted the author with the measurement system for **Publication 10**, but the author performed all the measurements. TUT Protopaja made coil winding, sample holders and cryostat modifications when needed.

Contents

Abstract **i**

Preface **iii**

List of publications and author's contribution **ix**

Lists of symbols and abbreviations **xv**

1 Introduction **1**
1.1 Motivation 2
1.2 Structure of the thesis 3

2 Background **5**
2.1 Electromagnetic and thermal phenomena 6
2.1.1 Electric quantities 8
2.1.2 Magnetic quantities 11
2.1.3 Electromagnetic field 14
2.1.4 Temperature and heat transfer model 14
2.2 Superconductivity 17
2.2.1 Critical quantities 18
2.2.2 Classification of superconductors 22
2.2.3 Bean's critical state model 24
2.2.4 Stability aspects 25
2.2.5 Materials 30

3 Short sample characterisation **33**
3.1 Current transfer length 34

3.2 Spurious critical currents and n-values: a slab model 35
3.3 Spurious critical currents and n-values: measurements 36
3.4 Remarks 41

4 Ferromagnetic coils **43**
4.1 Critical current 44
4.2 Comparison of $I_{c,coil}$ computation models 47
4.3 SMES coil optimisation 49
4.4 Tests with a conduction-cooled solenoid 52
4.5 Remarks 54

5 Conductor stability analysis **55**
5.1 Formulation for minimum propagation zones 56
5.2 Comparison with analytical results 57
5.3 MQE and v_{nzp} measurements 59
5.3.1 Minimum quench energy 60
5.3.2 Normal zone propagation velocity 60
5.4 Remarks 62

6 Coil quench analysis **65**
6.1 Quench simulation algorithm 66
6.2 Implementing quench simulations 67
6.3 A 200 kW DC induction heater 70
6.4 Remarks 73

7 Conclusions **75**

Bibliography **79**

Lists of symbols and abbreviations

$\mathbf{A}$	Magnetic vector potential
A_{cond}	Area of conductor cross-section
A_{uc}	Area of unit cell
A_{z}	Magnetic vector potential z-component
a	Inner radius of solenoidal coil
$\mathbf{B}$	Magnetic flux density
B_0	Material parameter
B_{app}	Applied magnetic flux density
$B^{\mathrm{y}}_{\mathrm{app}}$	Applied magnetic flux density in y-direction
B_{ave}	Average magnetic flux density
$B^{\mathrm{y}}_{\mathrm{ave}}$	Average magnetic flux density in y-direction
B_{c}	Critical magnetic flux density
B_{c1}	Lower critical magnetic flux density
B_{c2}	Upper critical magnetic flux density
B_{irr}	Irreversible magnetic flux density
B_{p}	Magnetic flux density of full penetration
B_{y}	Magnetic flux density in y-direction
b	Outer radius of solenoidal coil
C_{p}	Volumetric specific heat
c_1	Constant
c_2	Constant
c_3	Constant
c_4	Constant
c_5	Constant
c_6	Constant
$\mathbf{D}$	Electric displacement
d	Distance between voltage taps
$\mathbf{E}$	Electric field
E_{ave}	Average electric field
E_{c}	Electric field criterion

E_{CTL}	Electric field criterion for current transfer length
E_{m}	Magnetic energy
e	Elementary charge
$\mathbf{F}_{\mathrm{q}}$	Force on mesoscopic particle with electric charge
G_{y}	Mapping from B^{y}_{ave} to B^{y}_{app}
G_{x}	Corresponding mapping than G_{y} but magnetic flux is x-directional
$\mathbf{H}$	Magnetic field intensity
H_{y}	Magnetic field intensity in y-direction
h	Height of solenoidal coil
I	Current
I_{c}	Critical current
$I_{\mathrm{c,coil}}$	Coil critical current
I_{CTL}	Current criterion for current transfer length
I_{op}	Operation current
I_{s}	Current produced by power supply
I_{sc}	Current in superconducting region
I_{tot}	Total current in conductor
I_{tr}	Thermal runaway current
$\mathbf{J}$	Current density
J_{ave}	Average current density
J_{c}	Critical current density
$J_{\mathrm{c}}^{\mathrm{eng}}$	Engineering critical current density
$\mathbf{K}$	Arbitrary vector field
L	Inductance
l	Length of superconductor
$l_{0\mathrm{S}}$	Length of minimum propagation zone according to proposed model
$l_{0\mathrm{W}}$	Length of Wilson's minimum propagation zone
l_{norm}	Length of normal zone
l_{wire}	Conductor length required for solenoidal coil
$\mathbf{n}$	Unit normal
n	Superconductor index number
P	Power
$\dot{\mathbf{Q}}$	Heat flux
Q	Heat generation
Q_1	Heat extracted from hot reservoir
Q_2	Heat delivered to coil reservoir
Q_{t}	Heat
q	Electric charge
R	Resistance

R_{norm}	Normal zone resistance
R_{s}	Resistance of dump resistor
$\mathbf{S}$	Arbitrary vector quantity
T	Temperature
T_1	Temperature of hot reservoir
T_2	Temperature of coil reservoir
T_{ave}	Average temperature in Wilson's minimum propagation zone
T_{c}	Critical temperature
T_{cs}	Current sharing temperature
T_{op}	Operation temperature
T^*	Temperature in disturbed region
t	Time
t_1	Time for V_{c} passing V_1
t_2	Time for V_{c} passing V_2
t^*	Constant
U	Internal energy
$\dot{U}$	Change of internal energy
U_α	Internal energy at thermodynamic state α
U_β	Internal energy at thermodynamic state β
V	Voltage
V_1	Voltage in normal zone propagation velocity measurement
V_2	Voltage in normal zone propagation velocity measurement
V_{c}	Voltage criterion
V_{s}	Voltage over power supply producing current I_{s}
$\hat{V}$	Volume of solenoidal coil
$\hat{V}_{\text{rel}}$	Relative volume of normal zone
$\mathbf{v}_{\text{q}}$	Velocity of mesoscopic particle
$\mathbf{v}_{\text{q},1}$	Velocity of mesoscopic particle
$\mathbf{v}_{\text{q},2}$	Velocity of mesoscopic particle
v_{nzp}	Normal zone propagation velocity
W	Work

$\mathcal{C}$	Line
$\mathcal{S}$	Surface
$\partial\mathcal{S}$	Boundary of surface
$\mathcal{V}$	Volume
$\partial\mathcal{V}$	Boundary of volume

α	Thermodynamic state
β	Thermodynamic state
γ	Temperature in Celsius
ΔT	Difference between temperature in disturbed area and operation temperature
Δt	Time step
Δx	Length of unit cell in x-direction
δ	Temperature in Kelvin
ϵ	Efficiency of heat engine
ϵ_{S}	Minimum quench energy computed for minimum propagation zone given by proposed model
ϵ_{W}	Minimum quench energy computed for Wilson's minimum propagation zone
λ	Thermal conductivity
μ	Permeability
μ_0	Vacuum permeability
μ_{eng}	Engineering permeability
$\mu_{\mathrm{eng}}^{\mathrm{y}}$	Engineering permeability in y-direction
ρ	Resistivity
ρ_{norm}	Superconductor's normal state resistivity
Φ	Magnetic flux
Φ_0	Magnetic flux quantum
φ	Electric potential
ψ	Arbitrary scalar field
Ω'	Whole space

AC	Alternating current
ALUHEAT	High efficiency aluminum billet induction heating, acronym for European project
Bi-2212	Bismuth based high temperature superconductor
Bi-2223	Bismuth based high temperature superconductor
BSCCO	Bismuth based high temperature superconductors
Conectus	Consortium of European companies determined to use superconductivity
CSM	Bean's critical state model
CTL	Current transfer length
$\mathrm{CTL_I}$	Current transfer length according to I-based criterion
$\mathrm{CTL_E}$	Current transfer length according to E-based criterion
D	Diode

DC	Constant current (direct current)
FEM	Finite element method
HTS	High temperature superconductor
LaBaCuO	Lanthanum based high temperature superconductor
LTS	Low temperature superconductor
MPZ	Minimum propagation zone
MQE	Minimum quench energy
MRI	Magnetic resonance imaging
NMR	Nuclear magnetic resonance
PDE	Partial differential equation
R	Rectangular initial guess for SMES optimisation
S	Switch
SI	International system of units
SMES	Superconducting magnetic energy storage
SQP	Sequential quadratic programming
SS	Stainless-steel
Tk	Thick initial guess for SMES optimisation
Tn	Thin initial guess for SMES optimisation
YBCO	Ytrium based high temperature superconductor

Chapter 1

Introduction

Magnesium diboride (MgB_2) has been available as a compound since 1953 [21], but it was found only in 2001 to superconduct [124]. However, because composite MgB_2 conductors are manufactured by using only low cost materials and familiar techniques commercial wires have been available for some years [23, 75].

The high critical temperature of MgB_2, 39 K, with its low cost and promising critical current density characteristics make it a tempting material for applications [81]. In January 2008, a three-year European project for developing MgB_2 into a technical superconductor was finished, resulting in advanced manufacturing processes of MgB_2 conductors [15, 32, 73, 99, 105, 141]. Intensive wire development has been underway also in, e.g., Australia, Japan and the United States [33, 34, 35, 93, 149, 150, 151, 154, 155]. In addition, the first serious applications have been demonstrated, including a magnetic resonance imaging (MRI) device [23, 121]. Within the MgB_2 community, it is generally estimated that some day conduction-cooled MgB_2 systems operating around 20 K can challenge the 50-year-old conventional superconductor NbTi, which is typically cooled by liquid helium at 4.2 K. NbTi is currently the most widely used superconducting material in large scale applications, and almost all superconducting MRI devices are made of it. To make commercial superconducting devices using MgB_2, its critical current characteristics must be improved and progress made in laboratories translated into commercial production. [81, 134, 162]

1.1 Motivation

According to Conectus[1], in 2007 the total superconducting markets were about € 4085 M. MRI devices constituted more than 80% of that figure, whereas the share of conventional low temperature superconducting materials was almost 99%. Currently, about 150 000 km of conductor is manufactured yearly from NbTi. The biggest MgB_2 conductor supplier, Columbus Superconductors, produced 100 km of MgB_2 wire in 2007. This is still a niche market, but, e.g, Columbus Superconductors aims to triple their production rate every year for the next four years. They also estimate that with production capacity reaching 10 000 km/year, the price becomes comparable to NbTi. [66]

Now when MgB_2 wire development has been commercialised on a small scale, and some applications have been demonstrated, a wide range of prototype devices using MgB_2 are required to highlight this fascinating material [32]. MRI devices operate at a low and intermediate field range, which is suitable for MgB_2. These devices can also be operated around 20 K with a conduction-cooled system, as demonstrated in [121]. Because of the large market share of MRI, it is a natural choice for the first demonstrations. However, also other, both conventional and new, applications seem to be promising, at least in a niche scale [160].

One good example is the induction heater. Conventional heaters apply water-cooled copper coils with the efficiency around 55-60%. With a superconducting one, the efficiency can rise to about 90% when the special characteristics related to superconductivity are fully exploited. Currently, the European project ALUHEAT is for demonstrating this application. [109] Other possible profitable applications are, e.g., fault current limiters, transformers, motors and generators. These days several projects are underway, e.g., in United States. [134, 160]

Several manufacturing and design techniques can be adopted for MgB_2 devices from other material systems, but not all. Because, most of the large scale superconducting applications consider coils, this thesis presents some special characteristics related to the design of MgB_2 coils operating at conduction-cooled systems. I consider here the performance modelling and stability analysis as well as basic characterisation.

[1] Conectus (for Consortium of European Companies Determined to Use Superconductivity) comprises of companies collaborating and having the shared vision that commercialisation of superconductivity will translate into significant benefits to Europe's economy and society [26].

1.2 Structure of the thesis

In the beginning, the background necessary for the thesis, including the attached publications, is reviewed. First the electromagnetic theory is briefly described. A very short note on observations of natural phenomena is given by way of an intuition for mathematical models. For more about the history of electromagnetism, readers are urged to browse parts of [18].

Thermodynamics play a crucial role in superconductors, because they operate at very low temperatures and very high current densities, which in fault situations can results in massive powers and fast temperature raise. Thus, I review briefly heat transfer in solids after the electromagnetic theory.

After the above, I familiarise the reader with superconductivity. Especial importance is paid on the stability issues, and thus, earlier research is introduced in a reasonable extent. Several references are given for the enthusiasts.

After the background, I will concentrate on the publications appended to this thesis. The headlines of the publications are presented in §3-§6. The main idea is to present specialities related to designing MgB_2 magnets. First, a magnet designer needs initial data for modelling. The most necessary piece of data is the conductor critical current characteristic. Specialities related to voltage-current characteristic measurement in conduction-cooled conditions are presented in §3. Chapters §3-§5 follow similar pattern, first theoretical considerations are presented and then measurements are scrutinised. Chapter §6 does not contain measurements. Each chapter ends with some remarks, summarising my contribution so far to this field and perhaps give ideas for future research too.

Based on §3, magnet design can be done in the sense of defining the coil critical current or the thermal runaway current. When the first MgB_2 conductors were produced, iron and nickel turned out to be very disposable matrix materials for manufacture, whereas, e.g., copper-clad conductors showed modest critical currents [58, 65, 83, 101, 141]. However, a copper matrix can be adopted with, e.g., a niobium diffusion barrier around the filaments [140, 159, 160]. Iron and nickel, though, unlike conventional matrices, magnetise. A computational model is proposed in §4 for including the non-linearity of matrix permeability in the computation of a coil's critical current. Then discrepancies between the proposed and the traditional model are discussed. Finally, this chapter ends with a discussion of measurements and practical problems faced in testing a conduction-cooled MgB_2 winding.

During magnet design, one must deal with stability issues too. In practice,

I suggest to study what kind of disturbances cause a thermal runaway in a magnet. Thus, a designer must be aware of typical disturbances and must know that the built magnet does not quench when these occur. To compare the disturbance tolerance of different conductors, minimum quench energies must be computed. To estimate how fast a thermal runaway can be detected the normal zone propagation velocities are considered. Chapter §5 discusses these issues.

Naturally, I study what happens if the minimum quench energy is exceeded. For that, a detailed quench analysis is performed in §6. A general algorithm for simulating quench is presented first. Then its implementation with a finite element method software is studied. Finally, the developed program is used to design a protection system for a 200 kW MgB_2 induction heater.

In practice, the stability issues and coil design are interconnected. In fact, the coil design and performance considerations can also be thought of as a stability issue. All in all, too high an operation current causes a fault in the operation of a superconducting device. The designer must thus be simultaneously aware of design targets and stability issues and perhaps form the optimisation problem by taking into account all these considerations. Consequently, these chapters provide a basic coil design algorithm including supplementary information about special characteristics related to MgB_2 coils and conductors.

As seen from the title, this thesis gives an electrical engineering point of view to the stability of MgB_2 superconductor; i.e., I seek to contribute to electromagnetic design and measurements from this particular angle. In superconducting magnets, thermal stresses and electromagnetic forces play a crucial role. However, I leave all this to the mechanical scientists. After all, such considerations are to some extent well established knowledge [175, p.41-67]. A more detailed study would require its own thesis [3]. In addition, the models presented in this thesis and specialities related to measurements can be considered disposable only for single strands and windings made of these strands, not for cables or windings made of cables. For example, see [14] for the review of stability in these cases.

Chapter 2

Background

Computational models are for predicting natural phenomena. Engineers exploit models to create apparatuses, whereas scientists try to sort out the mystery of the nature; however, the border between scientist and engineer is blurred. To understand and exploit a model, information about physics and possibly hidden preconditions is necessary. For me to understand a model means know-how about its structure and use environment, not understanding nature. However, the basis of any model reflects observations of natural phenomena on some level, though models are, of course, built on each other too. If a model predicts the natural behaviour, later observations either support to use the model in the future too or disqualify its validity. Models can also be corrected after new observations, and very often a correction means a limitation to the preconditions and, thereby, the models' use environment. Typically, the relevance of any model depends on time and space scales of an observer. The models do not explain nature nor control it, but approved models characterise nature.

In engineering science, models are very often formulated with second order partial differential equations (PDE). Several commercial programs have been developed to solve these equations. Many of them apply finite element method (FEM), which was also widely used in the computations of this thesis.

This chapter familiarises the reader with models needed in the research presented in the appended publications. Computational methods are not presented. An engineering approach was chosen here; i.e., I aimed to solve problems encountered by engineers dealing with superconductors. I do not look into the uniqueness and existence theorems for the solutions, but the methods are deemed valid if they seem to work in practise. In addition, even though superconductivity is a quantum phenomenon, the microscopic statistical per-

spective is ignored in this thesis; luckily, superconductivity can be observed in the macroscopic world!

First, electromagnetic models are presented to characterise nature where extreme changes do not occur. After this, temperature and heat transfer are briefly reviewed. Finally, from the broad field of superconductivity, I present how superconductors can be categorised and then introduce my conception of superconductor stability considerations. Finally, some general knowledge about superconducting materials is given for those not familiar with superconductivity.

2.1 Electromagnetic and thermal phenomena

This thesis deals with static, stationary, or low frequency phenomena. Here, low frequency means that changes are slow and dimensions short compared to propagation speeds; i.e. changes can be observed simultaneously everywhere with relevant accuracy. In other words, the electromagnetic wave phenomenon does not exist and charges do not pack.

I consider only mesoscopic or macroscopic models here. In [125], the mesoscopic model was defined for the needs of thermodynamics. However, my conception of the mesoscopic scale agrees best with the verbal, and probably informal, definition developed within the Wikipedia community. The mesoscopic scale refers to the length scale at which one can reasonably discuss material properties or physical phenomena without having to pay attention to individual atoms [173]. The macroscopic scale describes nature which can be observed with human senses. The following models are mesoscopic, even though they involve quantities related to points. Practically, on the mesoscopic scale, it becomes reasonable to talk about the average density, charge, or other characteristics of a material, and statistical properties, such as temperature, have a meaning. For many problems, such mesoscopic averaging yields very accurate predictions of macroscopic behaviour and properties.

This section presents mathematical models for electromagnetic and thermal phenomena and seeks to explain the intuition behind the models. However, intuition does not explain nature, even though mesoscopic intuition is often used in school books for this purpose. I use the presented field quantities as computational aid to characterise the observations of phenomena and do not commit to their real existence. For example [16, p.142-159] gives a fruitful discussion about the existence of magnetic vector potential and the famous Aharonov-Bohm effect [2]. Different approaches are available in [13, p.274-

275], [67, 161].

I begin with electric quantities and continue to magnetic ones. This leads to the interaction of electromagnetic field. Finally, I will briefly discuss a mathematical model of heat transfer in solids. I try to give first an observation of nature and then a mathematical formulation for a model of this phenomenon. Here, an explanation of an observation aims to support an intuition and does not necessary state what really happens. After all, for an engineer, a model is good if it can be profitably used in industry.

Here in the introduction of thermodynamics, and later when discussing about superconductivity, I provide several references in appropriate places, but not when I introduce electromagnetic models. For the reference of electromagnetic models, I suggest primarily the publication of Maxwell [119]. It is not that I, or many of my contemporaries, have first come upon these things while reading the publication of Maxwell's, but I think that it presents the basis of observable phenomena related to the electromagnetic theory in a very good spirit. In Maxwell's day, it was all about observations, which were displacements caused by forces. With care and criticism, I suggest [48] for a textbook. In Maxwell's time, vector algebra had not yet been developed. Heaviside formulated the Maxwell's equations into readable form in [71], though they still were not in the form used typically in today's vector algebra [133, p.389]. After all, while reading [119], it is useful to keep [169] handy.

The oncoming discussion is based on the electromagnetic force, called the Lorentz force, though it was introduced before the time of Lorentz. This force appeared first in [120] equation (77) and it is worded in [119] for equation (D). Lorentz introduced it in [106]. All this time, one has to keep in mind that in this thesis I consider the presented formulations of models as purely abstract mathematical constructs, which allow engineers, and scientists, to predict things we can actually perceive [132].

I present vector quantities as bold face letters, such as $\mathbf{S}$. When the direction and magnitude information packed in the vector quantities is not relevant, or when I mean only magnitude, I write S. In some cases when $\mathbf{S}$ in a fixed coordinate system has only one non-zero component, I refer to this with S. Then S can also be negative.

2.1.1 Electric quantities

As a starting point, I posit the existence of an electric charge q as a particle property. Here, particle is an instance of mesoscopic matter. The SI unit[1] of the electric charge is C. To derive most of the models, no units are needed. However, for example comparison of measurement results, these are irreplaceable. Thus, I want to present the SI units here. In the following only symbols of the units are introduced.

Electric field models forces on stagnant particles, i.e. on particles which do not move with respect to sources and observers, determined by only one property: the electric charge. I call these particles charges. The electric field is a pair {electric field intensity, electric displacement} i.e. $\{\mathbf{E}, \mathbf{D}\}$. $\mathbf{D}$ is only required if frequencies are high and thus electromagnetic wave phenomenon exists or if materials become electrically polarised, as happens with dielectrics. For example in capacitors polarisation plays important role. In this thesis, $\mathbf{D}$ is no longer mentioned and the electric field intensity is called the electric field or $\mathbf{E}$. The unit of $\mathbf{E}$ is V/m.

In electrostatics, $\mathbf{E}$ is defined as

$$\lim_{q \to 0} \frac{\mathbf{F}_\mathrm{q}(\mathbf{x})}{q} = \mathbf{E}(\mathbf{x}), \tag{2.1}$$

where $\mathbf{F}_\mathrm{q}$ is the force directed at a stagnant test charge. The unit of force is N. This model seems microscopic, but it is not. First, I'll go below the mesoscopic level. Although quasiparticles can have q equal to some fraction of the elementary charge e [24], it is generally believed that the charge can not go infinitely close to zero, as required by the limit operator. In fact, for this $\mathbf{E}$ one must measure forces with several charges of different magnitude on the mesoscopic scale and extrapolate $\mathbf{E}$. However, one is not allowed to go below the mesoscopic scale, because with, e.g., one electron or nucleon, it is not known what the primary particle is like. Does it have an internal charge distribution [78]? Where is it and where is it going [51]? Thereby, different measurements can result into different extrapolations of $\mathbf{E}$. On the other hand, these properties of microscopic matter inside a mesoscopic volume do not affect $\mathbf{E}$ in a measurable way. In addition, a test charge affects on the $\mathbf{E}$ distribution to be defined and may thus alter its source.

[1] To avoid any confusion, I present the units for all quantities under study, when I think a misunderstanding is possible. International System of Units (SI) includes 7 base units (meter, kilogram, second, ampere, kelvin, mole, candela) and several derived units. Twenty-two derived units have been given special names and symbols (e.g. hertz, joule, tesla). [126]

Equipotential surfaces exist in static and stationary current phenomena. A charge can be freely moved in the equipotential surface without doing any work or changing the system energy. Because $\mathbf{E}$ was derived from the force and is thus related to work, $\mathbf{E}$ must be an object with equipotential surfaces; i.e., it must be irrotational as

$$\nabla \times \mathbf{E} = \mathbf{0}. \tag{2.2}$$

This also means conservation of energy, which here states that if one moves a charge from one equipotential surface to another and returns, no energy is lost or gained.

Instead of a complicated $\mathbf{E}$, the voltage V is very often measured in electrotechnics. Voltage describes the work required to move the unit charge from one equipotential surface to another. However, measuring V means also most often measuring a force. For example, in many analog meters the displacement of a spring is monitored. Here, the original description of V may have been lost via Ohm's law (2.12) to a macroscopic body property. On the other hand, in an oscilloscope, charges are displaced between two equipotential surfaces to produce an image. Hence measurement of V is related to the model of the phenomenon, not to the measurement of the described work. In other words, voltages are not measured but something else which is then converted to a voltage. The unit of V is V.

The voltage is defined as the integral of the electric field along a line $\mathcal{C}$

$$V = \int_{\mathcal{C}} \mathbf{E} \cdot \mathrm{d}\mathbf{l}. \tag{2.3}$$

Thus object $\mathbf{E}$ is related to lines. In fact, V depends only on the boundary of the line, i.e., on the potentials of two equipotential surfaces. Therefore, V maps two points (or surfaces) to real numbers. In engineering superconductivity, the electric field is very often used almost synonymously with voltage. The average electric field E_{ave} on a line $\mathcal{C}$ is typically meant as

$$E_{\mathrm{ave}} = \frac{1}{\mathrm{d}(\mathcal{C})} \int_{\mathcal{C}} \mathbf{E} \cdot \mathrm{d}\mathbf{l}, \tag{2.4}$$

where $\mathrm{d}(\mathcal{C})$ gives the length of the line in the chosen metric. Typically with superconductors, voltage is measured between two points on the conductor, and the line is the shortest path between the measurement points; hence

$$E_{\mathrm{ave}} = \frac{V}{l}, \tag{2.5}$$

where l is the length of the described path.

Another very important quantity related to the superconductivity is the current density $\mathbf{J}$. Its unit is $\mathrm{A/m^2}$. The flux of $\mathbf{J}$ through the boundary of volume $\partial\mathcal{V}$ equals the change rate of the overall charge in a volume $\mathcal{V}$ as

$$\int_{\partial\mathcal{V}} \mathbf{J} \cdot \mathrm{d}\mathbf{a} = \frac{\mathrm{d}q(\mathcal{V})}{\mathrm{d}t}. \tag{2.6}$$

Very often in electrotechnics, the current I is discussed. It's unit is A, and it is related to $\mathbf{J}$ as

$$I = \int_{\mathcal{S}} \mathbf{J} \cdot \mathrm{d}\mathbf{a}, \tag{2.7}$$

where $\mathcal{S}$ is a surface. Thus, the current is moving charges. In this thesis, I assume for every volume that the same amount of charges enter and leave the volume simultaneously. In differential calculus, this can be expressed as a current continuity equation

$$\nabla \cdot \mathbf{J} = 0. \tag{2.8}$$

In addition, if I is constant, the flow of charges is said to be stationary. Figure 2.1 illustrates how $\mathrm{d}q/\mathrm{d}t$, I and $\mathbf{J}$ are related.

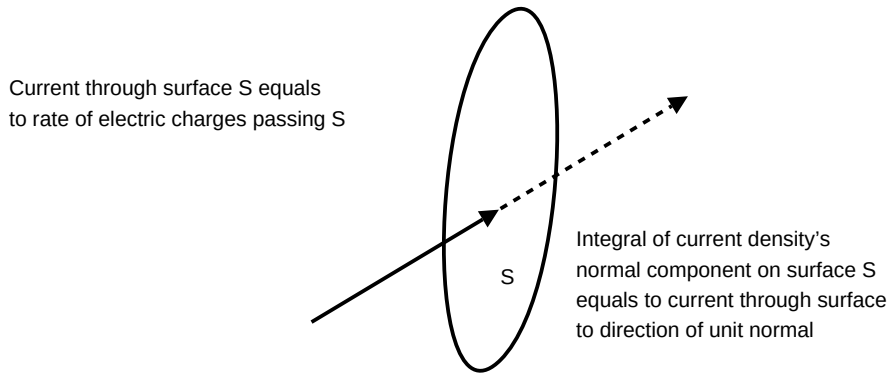

Figure 2.1: Schematic description between relations of charge rate, current and current density.

The constitution law between the current density and the electric field is of special interest within the field of superconductivity. Even though $\mathbf{E}$ and $\mathbf{J}$ are related to lines and surfaces, respectively, their relation is given as

$$\mathbf{E} = \rho\mathbf{J}, \tag{2.9}$$

where ρ [Ωm] is the resistivity. In some media, such as superconductors, ρ can also depend on $\mathbf{J}$. However, the mesoscopic nature of this model must be kept

in mind, i.e., ρ is a strictly statistic property, which can be defined only on the mesoscopic scale.

As I mentioned, it is convenient to derive models into second order PDEs for FEM programs. From vector algebra it is known that for all scalar fields ψ, it holds that $\nabla \times \nabla\psi = \mathbf{0}$. Thus, when (2.2) is expected, $\mathbf{E}$ has a scalar potential φ as

$$\mathbf{E} = -\nabla\varphi. \tag{2.10}$$

Then the second-order PDE for solving $\mathbf{E}$, and thereby the current density distribution, can be formed from (2.8) as the stationary current formulation

$$\nabla \cdot \frac{1}{\rho}\nabla\varphi = 0. \tag{2.11}$$

Typically measurements are done on a scale larger than what $\mathbf{J}$ and $\mathbf{E}$ represent. Like V, also I is typically considered. Then the macroscopic constitution law is known as Ohm's law, which states that

$$V = RI, \tag{2.12}$$

where R is the resistance with unit Ω. Resistance is related to a body and depends on the structure and constituents of the body as well as on the contacts between the electric circuit and the body, whereas resistivity is a material property. However, defining the resistivity requires also a body.

The power P [W] describes the conversion of energy or the rate of change of stored energy. Often, it reflects the electrical losses of the system, i.e., Ohmic heating

$$P = \mathbf{J} \cdot \mathbf{E}. \tag{2.13}$$

2.1.2 Magnetic quantities

It has been observed that a moving charge encounters a different force than a stagnant one. This force acting on a moving charge is called the electromagnetic force. In fact, the force introduced in (2.1) is also the electromagnetic force, but does not describe it fully. The magnetic field completes the mesoscopic model of forces acting on a moving charge. Like the electric field model, the magnetic field model is also composed of a pair {magnetic flux density, magnetic field intensity}, $\{\mathbf{B}, \mathbf{H}\}$. Now, the electromagnetic force acting on the particle is given as

$$\mathbf{F}_{\mathrm{q}}(\mathbf{x}) = q\mathbf{E}(\mathbf{x}) + q\mathbf{v}_{\mathrm{q}} \times \mathbf{B}(\mathbf{x}), \tag{2.14}$$

where $\mathbf{v}_\mathrm{q}$ is the velocity of the particle with charge q. In fact, one $\mathbf{v}_\mathrm{q}$ does not uniquely define $\mathbf{B}$, but two velocities with the condition $\mathbf{v}_{\mathrm{q},1} \times \mathbf{v}_{\mathrm{q},2} \neq \mathbf{0}$ do. The unit of $\mathbf{B}$ is T.

$\mathbf{E}$ and $\mathbf{B}$ are not completely independent. As known, the force on a charge cannot depend on an observer. I do not commit myself on the electromagnetic force when a particle is moving close to or at the speed of light. If the relative velocity of the charge and the observer is $\mathbf{0}$, all forces acting on the charge are packed in $\mathbf{E}$. That is, $\mathbf{B}$ can not be defined, or it is $\mathbf{0}$, according to (2.14). However, a stagnant observer may see $\mathbf{B} \neq \mathbf{0}$. This also emphasises why I use these mathematical formulae only as models. In fact $\mathbf{E}$ and $\mathbf{B}$ are interchangeable via Lorenz transformation in a coordinate transformation [48, ch.25-26]. These remarks do not belittle the importance of these models. On the contrary, electromagnetic models can be used with very high accuracy to predict natural phenomena and to design highly sophisticated apparatuses.

A Hall magnetometer (figure 2.2) can be used to give a value for magnetic flux density [70, 153]. Then, a constant current is applied to a sensor perpendicularly to the magnetic flux density to be determined. Because current consists of moving charges, they encounter a force in perpendicular to the current and the magnetic flux density, and thus a current in the direction of force is created. In principle at the centre of the sensor there is an excess of charge carriers in the one edge of the sensor while the other is neutral or has an excess of reversed charges. Then electric field can be determined and according to (2.3), voltage can be measured. In this measurement, the phenomenon model (2.14) is quite far off from the measured voltage, or its representative, but still the measurement is applicable.

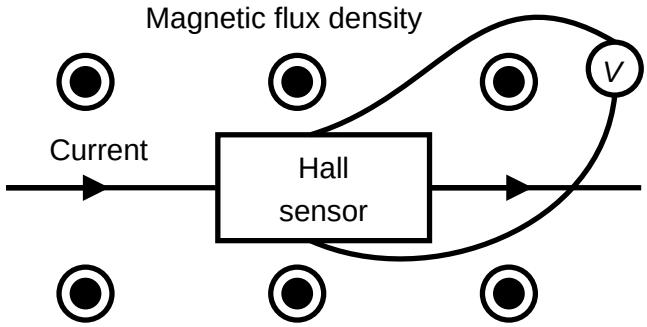

Figure 2.2: Schematic view of operational principle of Hall magnetometer.

Analogous to the current and current density is the pair of magnetic flux Φ and magnetic flux density. The unit of Φ is Wb. The magnetic flux density

is related to surfaces and is defined as

$$\Phi = \int_{\mathcal{S}} \mathbf{B} \cdot \mathrm{d}\mathbf{a}. \tag{2.15}$$

A magnetic flux line is a closed path, along which a charge can move without being exposed to a magnetic force. Thus, a charge can be moved along a flux line without doing or gaining work. Because the flux line is closed, magnetic flux density has to be sourceless, i.e,

$$\nabla \cdot \mathbf{B} = 0. \tag{2.16}$$

The pair of $\mathbf{B}$ and $\mathbf{H}$ [A/m] is coupled together with the magnetic constitution law as

$$\mathbf{B} = \mu \mathbf{H}, \tag{2.17}$$

where μ is a material property called the permeability. In some materials, μ is a non-linear function of $\mathbf{B}$, and such materials are said to magnetise. In ferromagnetic materials, magnetisation is especially strong. However, many materials do not magnetise, and their μ equals to the vacuum permeability μ_0 with adequate accuracy. Magnetisation is a model of material behaviour, in certain circumstances, and it can be used to predict how a body influences the surroundings.

Despite the fact that the existence of energy is a mystery to me, it can be characterised as an ability to work. In electrotechnics, people talk about electric, magnetic or electromagnetic energies, the distinction depends on an observer, which can be stored and then used when needed. In superconducting magnetic energy storage (SMES) systems, magnetic energy can be stored for a very long time and later almost fully exploited. In coils, energy is said to be stored in the magnetic field and called the magnetic energy E_m [J]. It is given in the whole space Ω' as

$$E_\mathrm{m} = \frac{1}{2} \int_{\Omega'} \mathbf{H} \cdot \mathbf{B} \mathrm{d}v. \tag{2.18}$$

Electromagnetic energy can not be divided into its partial constituents. That is, it is impossible to compute how much work is needed to get the energy into a proper subset of Ω' alone, but also the energy outside the subset is needed.

2.1.3 Electromagnetic field

As was already stated, $\mathbf{E}$ and $\mathbf{B}$ depend on each other. According to Faraday's law, for any surface $\mathcal{S}$ and to its boundary $\partial\mathcal{S}$

$$\int_{\partial\mathcal{S}} \mathbf{E} \cdot \mathrm{d}\mathbf{l} = -\frac{\partial}{\partial t} \int_{\mathcal{S}} \mathbf{B} \cdot \mathrm{d}\mathbf{a}. \tag{2.19}$$

Faraday's law is the first governing equation in the model of interaction between the electric and magnetic phenomena. It motivates that $\mathbf{E}$ and $\mathbf{B}$ are objects related to lines and to surfaces, respectively.

Furthermore, currents in conductors have been found to create an object similar to $\mathbf{B}$ in (2.14). In fact, the magnetic field intensity combines the current density with the magnetic field. The Ampère's law gives a second governing equation and represents the relation between $\mathbf{J}$ and $\mathbf{H}$

$$\nabla \times \mathbf{H} = \mathbf{J}. \tag{2.20}$$

To couple $\mathbf{J}$ and $\mathbf{B}$ into a second order PDE, magnetic vector potential $\mathbf{A}$ is introduced. From vector algebra, it is known that for all vector fields $\mathbf{K}$, $\nabla \cdot \nabla \times \mathbf{K} = 0$. Thus according to (2.16), $\mathbf{B}$ can be expressed as a curl of another vector field, here $\mathbf{A}$, and thus vector potential formulation for magnetostatics is obtained as

$$\nabla \times \frac{1}{\mu} \nabla \times \mathbf{A} = \mathbf{J}. \tag{2.21}$$

2.1.4 Temperature and heat transfer model

The concept of temperature T [K] is very different when compared to the field quantities in electromagnetic models. The temperature is a scalar quantity which takes the same value in two systems that are brought together and allowed to reach thermal equilibrium [131, p.3]. However, heat transfer models, which deal with, e.g., reaching the thermal equilibrium, resemble the electromagnetic models, at least in their mathematical representation.

To explain the concept of thermal equilibrium, I must now discuss system. A system is a macroscopic or at least mesoscopic entity in space and time. It is closed if it does not exchange material with its surroundings and isolated if it does not interact with its surroundings. An isolated system eventually reaches a state from which it does not subsequently depart. This state is called thermal equilibrium. Only a few parameters, including temperature, are required to describe the state of a system in thermal equilibrium. [131, p.4-6]

A law of thermodynamics is an axiom related to the concept of temperature. According to the zeroth law, temperature takes the same value in different systems which are individually in thermal equilibrium, and it remains when these two systems are brought into thermal contact [131, p.5]. To be able to assign numerical values to temperatures, the first and the second law of thermodynamics need to be introduced.

It is assumed that isolated systems have a quantity called internal energy U. If a system is in a thermodynamic state α, with an internal energy U_α, and is transferred to a thermodynamic state β with an internal energy U_β, the first law of thermodynamics gives the increase in the internal energy as

$$U_\beta - U_\alpha = W + Q_\mathrm{t}, \tag{2.22}$$

where W is the work done on the system and Q_t is the heat transferred to the system. [131, p.6-7] If $W = 0$, heat is the difference of internal energies between two states. The equivalence of heat and work was demonstrated by Joule in [85, 86].

Before defining the temperature, I present the second law of thermodynamics, even though the concept of temperature is needed there. Here temperature is related to feeling cold and warm, which I call unequal temperatures. The second law of thermodynamics states that it is impossible to devise an engine that works in a cycle and does nothing but transfers heat from a colder to a hotter body [131, p.7].

However, one can construct a heat engine that converts heat to work [146]. Carnot proposed that a simple heat engine is a machine between two thermal reservoirs, as schematically shown in figure 2.3. Here, Q_1 and Q_2 are the heat extracted from the hot and the heat delivered to the cold reservoirs, respectively. [43] According to the second law of thermodynamics, work is required in the grey area of figure 2.3 to transfer heat from the cold to the hot reservoir. Carnot believed in the caloric theory of heat; hence his postulates about the definition of temperature are not practical anymore. [146]

The efficiency of a heat engine ϵ is expressed as

$$\epsilon = \frac{W}{Q_1} = \frac{Q_1 - Q_2}{Q_1}. \tag{2.23}$$

The most precious of Carnot's inventions was that for an ideal Carnot cycle

$$\frac{Q_1}{Q_2} = \frac{T_1}{T_2}, \tag{2.24}$$

where T_1 and T_2 are the temperatures of the hot and cold reservoirs, respectively [43]. In 1848, Lord Kelvin realised that this relation can be used to

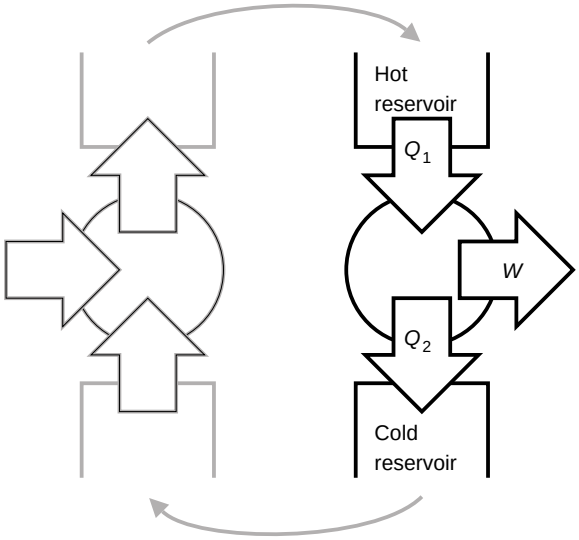

Figure 2.3: Schematic view of heat engine in black. Grey part completes cycle of heat engine. It is essential that input work on left is of different type than W on right. For example, input work can be used to heat fluid in cold reservoir, but output work has potential to do mechanical work.

define temperature when one temperature value is fixed [88], [131, p.8]. In Kelvin's honour, the absolute temperature scale has unit K.

Also, other temperature scales than the one postulated by Kelvin are in common use. In Europe, the Celsius scale of temperature is widely used. It does not belong to the SI units but it has an unit °C. I point this out because it is much better known than the Kelvin scale. The Celsius and Kelvin scales are related as

$$\gamma = 273.15 + \delta, \tag{2.25}$$

where γ and δ are the temperatures in °C and K [68, p.18].

Modelling of heat transfer in mesoscopic environment is based on formalising the first law of thermodynamics (2.22). In this thesis, I consider only heat transfer in solids. Fourier's law, is sort of a constitutive relation for thermodynamics, gives the heat flux $\dot{\mathbf{Q}}$ [W/m^2] as

$$\dot{\mathbf{Q}} = -\lambda \nabla T, \tag{2.26}$$

where λ [W/m^2/K] is the thermal conductivity [122, p.47]. The minus sign comes from the second law of thermodynamics. A change in the internal energy $\dot{U}$ [W/m^3] is expressed as

$$\dot{U} = C_\mathrm{p} \frac{\partial T}{\partial t} - Q, \tag{2.27}$$

where C_p [J/m^{3}K] is the volumetric specific heat and Q [W/m^3] is the heat generation. On the other hand, $\dot{U}$ corresponds to the point source of heat flux, i.e., its divergence, as positive $\nabla \cdot \dot{\mathbf{Q}}$ increases $\dot{U}$. Thus, finally, the formula for model of heat transfer states that [48, p.3-7]

$$\nabla \cdot \lambda \nabla T + Q = C_\mathrm{p} \frac{\partial T}{\partial t}. \tag{2.28}$$

This is already a second-order PDE, and FEM softwares can be used to solve it. Equation (2.28) has many names, e.g., heat balance equation or heat diffusion equation. In the steady state, it is also called the heat conduction equation. I use the term heat diffusion equation in this thesis.

In addition to (2.28), the boundary conditions of a heat transfer model are important. In principle, (2.28) models heat conduction and temperature changes in solid bodies, whereas boundary conditions describe heat transfer between solids and fluids, or radiation between solids. In addition, other boundary conditions may arise from the model symmetry or the known temperatures or heat fluxes.

2.2 Superconductivity

Two superconductivity specialists may have very little in common. In practice, everybody knows about critical quantities, but that is where it ends. One may specialise in manufacturing conductors, another in electronics and yet another in designing power engineering devices using superconductivity. My work focuses on designing power engineering devices and examining them in terms of MgB_2 perspective.

I begin with introduction of the critical quantities and go on an excursion to categorise superconductors, because the existence and nature of flux vortices have puzzled me. After this, I will change the tone and explain Bean's critical state model as a useful starting point for stability considerations on the qualitative level. Then I describe briefly the stability of superconductors from the viewpoint of magnet design. Finally, I give basic information about the most common superconducting materials, which is directed to readers specialised in some other field than superconductivity.

2.2.1 Critical quantities

Superconductivity is a quantum phenomenon which can be observed macroscopically. The microscopic model of superconductivity, the BCS theory, was published in 1957 by Bardeen, Cooper and Schrieffer [6]. The phenomenon of superconductivity had been found 50 year earlier. In 1911, Heike Kamerlingh Onnes observed that when the temperature of mercury was lowered somewhat below the boiling point of liquid helium at atmospheric pressure, 4.2 K, its electrical resistivity suddenly vanished [28]. This was the exact moment of discovery of superconductivity.

The vanishing resistivity is the easiest observable macroscopic manifestation of superconductivity. Typically, this is seen when the voltage remains zero in a voltage current measurement. In other words, no work is then needed to keep the current running. In fact, it is impossible to measure this, because a meter always takes energy out from the monitored system. In general, this is impossible to prove by experiments in general but can be illustrated verbally. Let us take a high quality persistent superconducting loop, in which the current is running and thus some energy is stored. When a meter, e.g., a Hall magnetometer [70] for measuring magnetic flux density decay in a system, is brought to the measurement area or taken away, the current in the superconducting loop may increase. However, the increase does not depend on the measurement duration. On the other hand, the voltage generated in the meter is related to the forces affecting the current, i.e., moving charges, and is thus doing work. This work reduces the energy stored in the superconducting loop. When the measurements are then continued, they cause decay in the measured magnetic flux density, because the stored magnetic energy is constantly being spent. Thus it is philosophically irrelevant whether the current decay in the persistent superconducting loop can be measured with a particular arrangement. A conventional thermometer gives another example. Without the meter, the temperature would not be the same.

Each superconducting material, pure or compound, has its critical temperature, T_c, below which the resistivity disappears. Therefore, superconducting devices can be designed in such a way that no work is needed at constant current operation. In addition to the temperature, the superconductive-normal transition defined here as the resistive transition, depends also on two other quantities: current density and magnetic flux density.

The direction of $\mathbf{B}$ can also have effect on the state of the superconductor. This is an instance of anisotropy. The effect depends on the material and the studied scale. For example, $Bi_2Sr_2Ca_2Cu_3O_{10}$ material can be used in a

textured thin film or in a flat tape, in which the anisotropy is easily seen, whereas rectangular $Bi_2Sr_2Ca_2Cu_3O_{10}$ conductors with no anisotropy can also be manufactured. However, anisotropy exists always on the crystal level, where texturing occurs. [163]

J, B and T form a critical surface below which the material is in the superconducting state and above in the normal state. Figure 2.4 presents critical surfaces of two commercial superconductors. As can be seen, operation is practically impossible at the critical temperature, because then neither J or B can be applied.

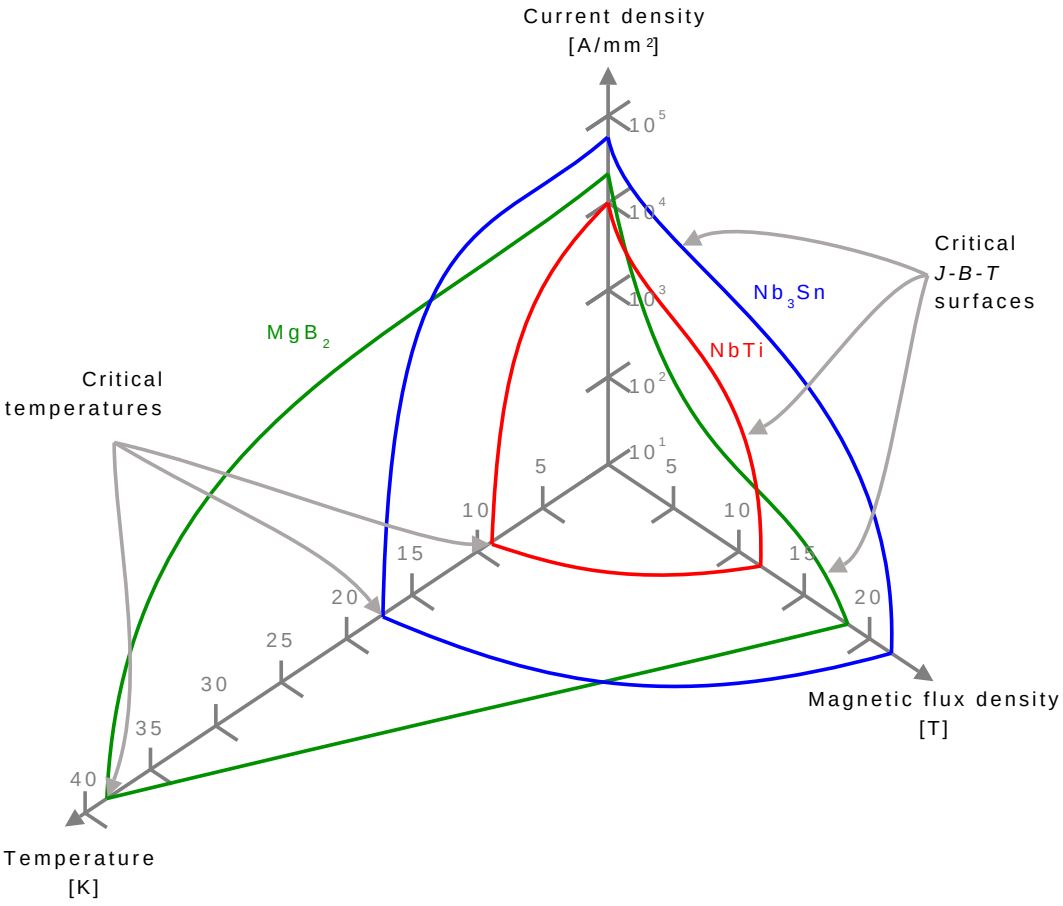

Figure 2.4: Critical surfaces of two commercial superconductors, NbTi and Nb_3Sn, and MgB_2 [41, 162].

The resistive transition is not as black and white as sketched above. The resistance of a wire rises monotonously as the current or the applied magnetic flux density is increased. Thus Voelker stated that a clear-cut critical current

cannot be defined from a measured voltage-current characteristic [166]. Many papers have claimed that increasing flux creep creates a flux flow resistance [4, 9, 90]. However, in practical superconductors, the flux flow resistance cannot adequately describe the voltage-current relationship whose non-linear part has been explained at least by the progressively increasing flux creep [5], the non-linear effect of Lorenz force [46] and local variations in the critical current [84].

According to Bruzzone [17], Walter has suggested in 1974 that the voltage-current relationship of a superconductor can be characterised with a power law. The suggestion was based only on observations, not on earlier phenomenon models like flux flow resistance. Thus the transition from the superconducting to the normal state in practical superconductors happens rapidly though not in a step. In fact, the critical current I_c of a superconductor is typically defined so that at the critical current a chosen electric field criterion E_c equals the average electric field in the measurement area. Typical E_c values are 0.1, 1 and 10 μV/cm. However, also other criteria exist for defining the critical current [17].

The superconductor index number n, also called exponent n or n-value, characterises the steepness of the superconductor resistivity growth between superconducting and normal states [175, p.236]. It is inversely related to the width of the transition, visible in the $V - I$ characteristic [57]. Normally, n-values are measured for composite conductors, in which case the electric field-current relation is assumed to be

$$E = E_\mathrm{c} \left(\frac{I}{I_\mathrm{c}} \right)^n . \tag{2.29}$$

It is then assumed that E does not vary in conductor cross-section. Equation (2.29) holds only near I_c at constant B and T. However, in this thesis, I have assumed it to be valid from zero current until the conductor's normal state resistivity, ρ_norm, is reached. Figure 2.5 shows a schematic view of the $E - I$ characteristic near the transition. According to (2.13), heat generation in low n-value conductors begins already at sub-critical currents and can thus limit the maximum continuous operation current of such devices.

Most practical superconductors are manufactured as multifilamentary wires, in which granular filaments are embedded in a normal conducting matrix. The local critical current density J_c varies in and between the grains, and sausaging can cause variation to the cross-sectional I_c [102, 168]. Here, I again speak about local in mesoscopic sense; otherwise, J_c has no meaning. When the n-value is measured as a global conductor quantity, given extrinsic reasons can have influence on it. Furthermore, it can also develop from intrinsic effects related, e.g., to a flux creep and thus also to flux pinning. I want to point out flux

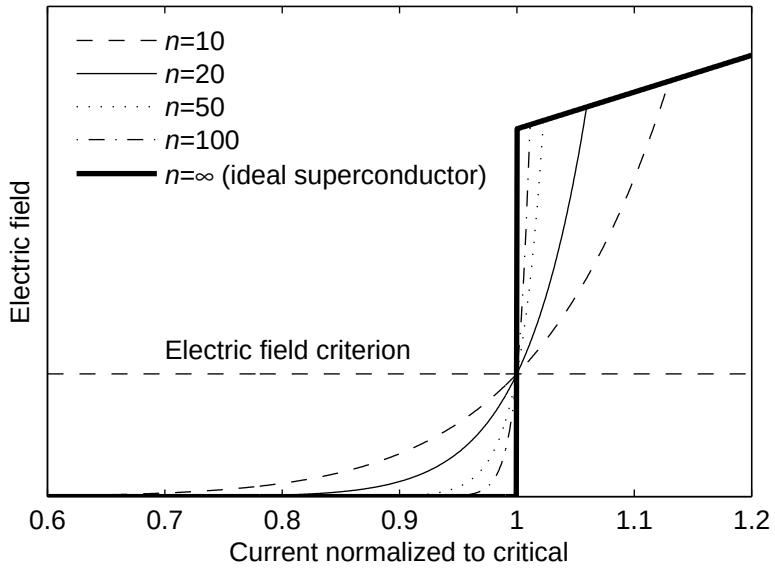

Figure 2.5: Schematic view of resistive transition.

pinning here because it, both intrinsic and extrinsic, has been studied widely for MgB_2, and because some breakthroughs have been achieved to increase the critical currents at high field regime [32, 145]. See discussion and reviews considering the n-value and the voltage-current characteristics from [17, 37, 57].

n-values are determined from the measured voltage-current characteristics. These measurements are sensitive to conductor temperature variations during the measurement. At conduction-cooled measurement stations, the cooling power is very limited when compared to liquid-cooled stations. During measurement, even low heat generation can then markedly raise the temperature. In a failed characterisation, temperature variations cause a sharp voltage-current characteristic, even though in isothermal operation conditions the transition is very gentle. **Publication 6** and **Publication 10** discuss pitfalls of I_c and n-value characterisation at conduction cooled measurement stations, focusing on heat generation. Methods for performing successful $V-I$ measurement in liquid helium are given in [64] and a detailed discussion on I_c measurement and data analysis in [39, p.351-490].

2.2.2 Classification of superconductors

Traditionally superconductors are categorised according to how **B** penetrates into them. Accordingly, the materials can be divided into type I and type II. In April 1986, the discovery of $La_{1-x}Ba_xCuO_3$ (LaBaCuO) revolutionised the field of superconductivity [10]. LaBaCuO was a ceramic compound, whereas all the earlier superconductors had been metallic, and its critical temperature was around 30 K, about 7 K higher than the highest T_c thus far [123]. After that, superconductors have been also categorised as low temperature superconductors (LTS) and high temperature superconductors (HTS). The two categorisations are not exclusive, but they are different.

Type I and type II superconductors

Superconductors can be divided into two groups according to a model which considers how they can tolerate applied magnetic fields. In type I superconductors, the external magnetic field generates surface currents which prevent the magnetic flux penetration deeper into the superconductor. This is the Meissner effect. After the applied magnetic flux density oversteps a critical value B_c, superconductivity vanishes. [27, p.28-30] The B_c values depend on the material and are typically of the order of 10 mT. Consequently, type I materials are totally unattractive even for moderate field applications. [135, p.46]

Type II superconductors have two critical magnetic flux densities: the lower B_{c1} and the upper B_{c2} [27, p.29-33]. Below B_{c1}, a type II superconductor behaves like a type I. After this, the magnetic flux can penetrate into the superconductor as magnetic vortices with a normal conducting core until at B_{c2} superconductivity vanishes. Each vortex carries one magnetic flux quantum $\Phi_0 = 2.07$ pWb [142, p.5], and B is directly linked to the number of vortices per m^2 [27, p.29]. Superconducting shielding currents surround the cores, which are usually pinned to anomalities, e.g., to impurities in the crystal structure. The quantised Φ is an exclusive property of superconductors. The flux vortex is a behavioural model of macroscopic observation via, e.g, magneto-optical imaging [12, 60]. Depending on the target, the flux vortex can be considered as a volume with a lowered probability for the existence of superconducting charge carriers, or as alternatively, it can be understood as a volume where the electromagnetic interaction occurs as predicted by (2.14).

All in all, the flux vortex is a microscopic object, and in fact, it should not be considered by the means of classical physics. However, the given intuition is

a mesoscopic description of the model for type II superconductivity and a more detailed approach is not in the scope of this thesis. For a deeper discussion about flux vortices see, e.g., [116] and for its background [142, p.17].

Anomalities act as pinning centres for the vortices. The basic mechanism of flux pinning is the difference in superconducting properties between the pinning centres and their surroundings [31]. When a vortex moves in the superconductor, some energy is released as heat. A vortex movement from a pinning centre to another is called flux creep [4]. When more and more vortices move, heat generation increases and the physicists speak about the flux flow resistance [90]. Thus it is advantageous to have strong pinning which tends to keep the vortices static. In some superconductors, the crystal structure of the compound creates significant intrinsic pinning centres in the material [36]. Whereas in some materials, artificial pinning centres by doping with non-superconducting nanoparticles, are needed to improve pinning [145, 167].

When the applied magnetic flux density increases, the critical current gradually decreases. When the irreversibility magnetic flux density B_{irr} is reached, the superconducting transport current drops practically to zero [117]. With the conventional superconducting materials, NbTi and Nb_3Sn, B_{irr} is very close to B_{c2}; in fact, the difference can not be always observed [181], but with MgB_2 they can differ several Teslas [52, 94, 102].

LTS and HTS materials

Superconducting materials are also typically divided into two groups. Low temperature superconductors (LTS) are metallic compounds and have $T_{\mathrm{c}} \leq 23.3$ K [123]. High temperature superconductors (HTS) are ceramic compounds and their T_{c} is roughly from 30 K upwards. So far the highest T_{c} has been claimed to be 185 K in $(SnPb_0.5In_0.5)Ba_4Tm_5Cu_7O_{20x}$ compound [152, 14 March 2008]. The superconducting material under consideration in this thesis, MgB_2, has T_{c} around 39 K, but it has not been strictly categorised as LTS or HTS. The BCS theory characterises well superconductivity in LTS materials and succesfully predicts some properties of MgB_2. However, according to BCS theory $T_{\mathrm{c}} \leq 30$ K. On the other hand, MgB_2 does not have copper oxide layers, which are characteristic of most HTS materials, and which cannot be described well by the BCS theory. [165]

To exploit their potential for large scale applications, superconductors must be manufactured as long conductors. If the superconducting state is lost, a massive heat generation occurs in a current carrying conductor. Therefore, conductors cannot be made only of bulk superconducting material but they

must include a stabilising material. The high thermal and electrical conductivities of the stabilising material can guarantee that the temperature does not rise dramatically during a fault. Therefore, copper is a good stabilising material, though it is not chemically compatible with all the superconductors [1, 101, 163]. Other matrix materials permit several different manufacturing routes [42, 49], and in some conductors, the matrix can consists of several materials. In addition to the stabilisation, the matrix also reinforces the conductor. [61, 92, 170]

Furthermore, no superconducting material suits the whole range of possible operation conditions and needs when also price is taken into account. Table 2.1 presents the most common superconducting materials. In practice B_{c2} and T_c are material properties on which conductor manufacturing cannot have much positive effect typically. Instead B_{irr} and I_c depend greatly on the manufacturing process. For example, heat treatment conditions, doping materials and purity of precursors play important roles [50, 104, 164, 167].

Table 2.1: Most common superconducting materials, their critical temperatures and upper critical magnetic flux densities at 4.2 K [11, 69, 164],[19, ch.B3.3.1,ch.B3.3.4]. Anisotropy means relative difference of J_c in textured crystal when orientation of applied **B** is varied.

Material	T_c [K]	Anisotropy	B_{c2}(4.2 K) [T]	B_{irr}(4.2 K) [T]	$\rho(T_c)$ [$\mu\Omega$cm]
NbTi	9	2-5	11-12	10-11	60
Nb_3Sn	18	Negligible	25-29	21-24	5
Nb_3Al	19	-	28-32	-	50
MgB_2	39	1.5-5	15-20	6-12	0.4
Bi-2223	110	50-200	>100	0.2 (77 K)	40-60
YBCO	92	5-7	>100	5-7 (77 K)	150-800

2.2.3 Bean's critical state model

One of the best-known models for current distribution in a superconductor is Bean's critical state model (CSM) [7]. Even when its assumptions are not strictly valid, it provides an useful tool for simple computations and illustrations in qualitative sense. In this work, the CSM has been applied in **Publication 6** when the dynamics of voltage-current measurement were discussed.

The CSM states that in an applied magnetic field, the shielding current penetrates into a superconductor from the edges. The magnitude of current density is J_c. After the shielding currents have decreased B to 0 in the superconductor, the current density equals to 0; for this CSM assumes that $\mu = \mu_0$

in (2.17) and (2.20). At the penetration field, B_p, the current flows everywhere in the superconductor. On the other hand, the transport current penetrates also on the edges of the superconductor. At the critical current, the current density equals J_c everywhere in the conductor. In the CSM, J_c does not depend on B. Figure 2.6 shows schematically J and B profiles in a slab carrying a transport current in the self-field according to CSM.

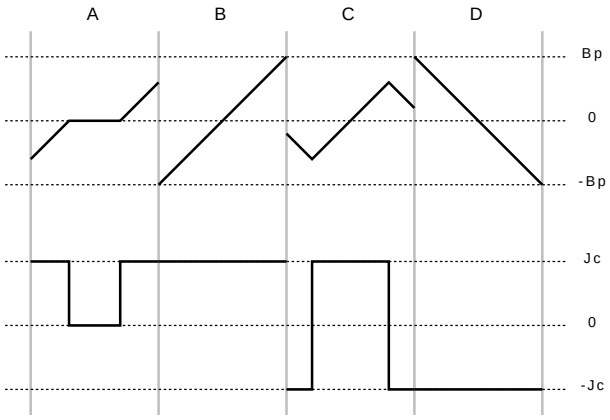

Figure 2.6: Transport current penetration and B profile according to CSM in slab. (A) Current has penetrated a little from initial state. (B) Current equals to critical current. (C) Net current is to same direction as in (A) and (B) but smaller than in (A). (D) Current equals to critical current but flows in opposite direction than in (B).

Models which are otherwise similar to CSM but B dependence of J_c is taken into account have also been presented. For example, according to the Kim's model

$$J_\mathrm{c}(B) = \frac{J_\mathrm{c}(0)}{1 + \frac{B}{B_0}}, \tag{2.30}$$

where B_0 is a material parameter [89]. The model can be further modified to include, e.g., the dependence of J_c on the direction of $\mathbf{B}$ [136, 179].

2.2.4 Stability aspects

Stability of superconductors means a lot in many levels. A conductor manufacturer has to make a conductor cabable of achieving its potential. There, the concepts of adiabatic and dynamic stability are important [175, p.133-135 and p.145-46], and they limit the size of a filament. Consequently, superconductors are often manufactured as multifilamentary wires. For simple suggestive computations of adiabatic and dynamic stability, the CSM can be used to study

the flux jump phenomenon, which was first qualitatively presented in [8] and quantitatively reviewed, e.g., in [175, p.130-134].

A conductor manufacturer also desires to make conductors which can tolerate disturbance energies well. Only then, the manufacturer can sell one's products. But these considerations give response to a magnet designer as well. Every magnet designer tries to design apparatuses that do not fail in typical disturbances, which depend on the conductor and the operation conditions. Sometimes the concept of cryogenic stabilisation and Stekly's criterion are used to design magnets which can in principle operate even though the whole superconductor is in the normal state [87, 147]. However, this leads to a low overall coil current density. Several coil stabilisation aspects are reviewed and discussed in [177], whereas conductor and cable stability is reviewed with especial emphasis on forced-flow cooling in [14].

In practice, a magnet designer must predict when the designed coil quenches and what happens during the quench. In the quench of a superconducting magnet, the disturbance initiates a propagating normal zone, which forces the magnet operator to discharge the stored energy. A part of it is always dissipated in the winding. In this thesis, it is relevant to present the concepts of minimum propagation zone, normal zone propagation velocity and quench. The first two are discussed on a conductor level, whereas quench is here related to magnets. To deal with quench, I must introduce the concepts of coil critical current and thermal runaway current. In this thesis, I concentrate only on conduction-cooled systems.

Normal zone evolution

In [176], Wilson and Iwasa presented the concept of minimum propagation zone (MPZ), based on studies in [111]. Wilson worded the definition of the MPZ by normal zone in a superconductor which is larger than the MPZ will grow and a smaller one collapses and full superconductivity will recover. [175, p.76] This concept is important because it allows to study the superconductor tolerance against disturbances in certain operation conditions. In fact, after having researched many stability aspects, Wilson pointed out that an essential design parameter is the size of the disturbance against which a coil is stabilised [177].

In [175, p.74-76], Wilson derived that in an adiabatic conductor the length of an MPZ, $l_{0\mathrm{W}}$, is obtained as

$$l_{0\mathrm{W}} = \sqrt{\frac{2\lambda(T_\mathrm{c} - T_\mathrm{op})}{J_\mathrm{c}\rho_\mathrm{norm}^2}}, \tag{2.31}$$

where T_{op} is the operation temperature. For (2.31) Wilson assumed, e.g., the steady-state of (2.28). The energy required to create this normal zone, the minimum quench energy (MQE), is computed from the required enthalpy increase of the conductor. When I use Wilson's model, I denote this MQE as ϵ_{W}.

In the approach of Ishibashi *et al* [79], (2.28) was solved in transient conditions to study whether a conductor quenches or not when an arbitrary heat pulse is applied. Recent measurements indicate that Wilson's, or other closed-form approaches [156], are not applicable to modelling the MQE of an MgB_2 conductor; instead (2.28) must be solved in transient conditions [112, 113, 162]. In **Publication 8** I formalised the model presented in [79] to compute minimum propagation zones. This model can be exploited also with conductors with a real n-value. **Publication 8** also includes a study of the effect of n-value on MQE. In **Publication 9** I compared the model with the measured results of a multifilamentary MgB_2 conductor.

The propagation of the initiated normal zone is of special interest. If the normal zone propagation velocity v_{nzp} is low, it can take a long time to detect a thermal runaway. By then the hot spot temperature can rise too high or electrical insulation may break. [20, 114],[175, p.200-208]

In [172], Whetstone and Roos presented an analytical formula for v_{nzp} and the analytical solutions of v_{nzp} were discussed in detail in [29]. In these the principles of CSM were used but Martínez *et al* considered also real n-values for MgB_2 conductors in [113]. However, the values of v_{nzp} cannot be directly used to estimate the hot spot temperature rise, because in actual coils, transverse heat conduction is also important and three dimensional normal zone propagation must be studied. On the other hand, v_{nzp} can be used to estimate if difficulties emerge in the quench detection based on one's earlier experimental knowledge. Based on the approach of Whetstone and Roos, v_{nzp} was compared between MgB_2 and other superconductors in **Publication 2**. In **Publication 9**, measured values of v_{nzp} were compared with the computed ones derived from the MPZ model.

Coil performance

Coil design always involves determining the maximum operation current. In constant current (DC) magnets, one of two well established criteria, either the coil critical current $I_{\mathrm{c,coil}}$ [82] or the thermal runaway current I_{tr} [80], determines the maximum operation current.

When a coil is operated at $I_{\mathrm{c,coil}}$, the maximum B in the coil volume equals

the applied B of the short sample measurement in which the critical current is $I_{\mathrm{c,coil}}$. Thus the lowest turn critical current defines $I_{\mathrm{c,coil}}$. The resistive transition is sharp in LTS materials, and thus $I_{\mathrm{c,coil}}$ can be used as a practical upper limit for the coil operation current. In practice, some margin is left for safety.

If no materials magnetise in the coil system, $I_{\mathrm{c,coil}}$ can be computed analytically, as presented by Wilson [175, p.20-22]. The computation is based on the Biot-Savart law, which is derived from the presented electromagnetic models to give $\mathbf{B}$ as a function of $\mathbf{J}$ [133, p.198]. Figure 2.7 presents schematically the determination of $I_{\mathrm{c,coil}}$. Here the load line represents a maximum value of B in the coil as a function of the operation current. However, in the vicinity of ferromagnetic materials, this approach is no more valid. In **Publication 1**, a model is proposed for the computation of I_{c} for coils that contain ferromagnetic constituents. In **Publication 9**, the proposed and linear models are compared, and in **Publication 7**, the proposed model is used to optimise a SMES coil. Based on [93], I expected high n-values for the MgB_2 conductors, but later in **Publication 10** and **Publication 4**, that hypothesis turned out invalid for the investigated conductor.

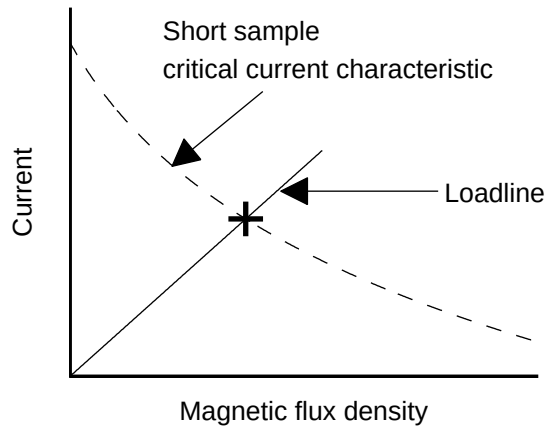

Figure 2.7: Schematic view of determining coil critical current, which is presented with +.

When conductor n-values are low, e.g., in $Bi_2Sr_2Ca_2Cu_3O_{10}$ and MgB_2, heat generation occurs also at subcritical currents. On the other hand, at slightly overcritical currents, heat generation is not as massive as with LTS materials. Thus overcritical operation can also be permitted for a short period, but some cooling is required at subcritical currents too. I_{tr} is the maximum operation current of a coil which can be continuously applied while the tem-

perature distribution in the coil remains constant. Even in the simplest coil geometry, the solenoid, solving I_{tr} requires a numerical approach. One descriptive example is given in [95]. There (2.28) was solved on the coil cross-section with a chosen operation current and specific boundary conditions, and it was studied if the temperature equilibrium can be attained. For computing heat generation, the turn critical currents and corresponding n-values at the operation current are needed. A thermal runaway occurs if the hot spot temperature increases, causing finally a quench.

Quench analysis

A superconducting wire can carry two orders of magnitude higher currents than a normal conducting wire of the same size without a blow out. Thus if a disturbance causes a propagating normal zone in a superconducting device, the device can suffer severe damage like insulation breakdown [53], melting [142, p.525-528] or mechanical strains [77]. The insulation on the conductor can be damaged if the voltage between adjacent turns rises too high. If the hot spot temperature rises too high, the coil may burn at the hot spot. If local temperatures rise rapidly, the thermal expansion of the hot spot can induce mechanical faults. In any of these cases, the expensive coil cannot be used any longer.

In a quench analysis, the magnet designer confirms that a coil can quench safely. The analysis includes quench simulations, design of protection system and possibly also considerations of quench detection. A numerical approach is always required for a detailed quench simulation. Accordingly, several programs have been introduced, including general and specialised for coils which require their own individual approaches [44, 45, 55, 56, 96, 127, 130, 158, 180]. One of the first such programs was Wilson's QUENCH [175, p.218].

Though quench simulation can be approached in various ways, all approaches couple the thermal problem and circuit theory problem to control the current decay. For example, actual coil domains have been discretised with a finite element [180] and finite difference [45] methods, whereas an analysis based on the propagation velocities was taken in [96]. In any case, hot spot temperature rise, coil intrinsic voltages or other quench characteristics are impossible to predict precisely. In addition, the functionality of quench simulation cannot even be tested accurately, because the hot spot temperature, typically, cannot be measured. Consequently, it is enough to have a quench simulation program that predicts with reasonable accuracy that a quench is safe with an appropriate safety margin. These depend on the designer's ambition, the time

available and also on the application. For example, one small research magnet in a series of prototypes can burn, whereas a destructive quench is not allowed, e.g., in an accelerator magnet or installed fusion magnet. In some commercial products, a quench must be quaranteed to be a very unlikely event. However, if it happens, no danger to bystanders is tolerated.

In **Publication 3**, I present my approach on quench simulation. This program was first developed for coils with a ferromagnetic matrix. Later in **Publication 9**, I studied how the philosophy of modelling a quench origin affects quench characteristics.

2.2.5 Materials

LTS materials have been widely industrialised, whereas HTS materials are at a turning point. Earlier bismuth based compounds have been intensively developed but now several companies have directed their HTS production research towards $(Y_{1-n}Ba_n)_2CuO_{4-x}$ based materials. MgB_2 is still a newcomer but already commercialised in a small scale. This subsection presents basic information concerning the most common materials and their applications. This is targeted to people not very familiar with superconducting materials. For further reading, I suggest [139] and references therein.

LTS and HTS

NbTi and Nb_3Sn are widely commercialised LTS materials with NbTi being the cheaper and easier to manufacture. In addition, coil winding from NbTi is easier than from fragile Nb_3Sn. Nb_3Sn was discovered in 1954 and NbTi in the early 1960s [62, 118]. NbTi is mainly used in low and medium-field applications in liquid helium. Its raw material and fabrication costs are the lowest among technical superconductors for magnetic flux densities in the 2-8 T range. It is a ductile alloy and very often manufactured in round wires. [19, ch.B3.3.2] Thus the anisotropy presented in table 2.1 does not play a role in technical superconductors. The main part of the commercial markets of superconducting devices are in magnetic resonance imaging (MRI) [107]. Commercial MRI devices operate today typically with 1.5-3 T field in the imaging area, which suits well for the relatively cheap NbTi. In high-field magnets, such as in nuclear magnetic resonance (NMR) spectrometer devices, Nb_3Sn must be applied. Copper is typically matrix material for NbTi. Because of the manufacturing requirements of Nb_3Sn, bronze is one matrix option for it [157].

Nb_3Al is an alternative of Nb_3Sn at high field large scale magnet appli-

cations such as nuclear fusion and high energy particle accelerators. It has high J_c at high B and excellent tolerance on mechanical strain. However, its manufacturing process is difficult when compared to Nb_3Sn. [19, ch. B3.3.4] With Ge additions B_{c2} can rise to around 40 T [76].

In February 1987, about a year after the discovery of the first HTS material, $(Y_{1-n}Ba_n)_2CuO_{4-x}$ (YBCO) was discovered to be superconductive [22, 178]. Long YBCO conductors can be manufactured only as thin films. The main application prospects for YBCO conductors are in AC power cables and in insert coils of high-field magnets. Because of the very thin layer of YBCO in a thin film, the losses due to time varying current, AC losses, of such cables can become very small and make them very competitive in high-power cables [137].

The best known superconducting bismuth-based compounds have an atomic structure of $Bi_2Sr_2Ca_nCu_{n+1}O_x$ (BSCCO), where n=0,1,2. Compounds with n=1 and n=2 are called as Bi-2212 and Bi-2223, respectively. These compounds were found superconducting in January 1988. The critical temperature of the compounds is for n=0 $\rightarrow T_c = 30$ K, n=1 $\rightarrow T_c = 85$ K and n=2 $\rightarrow T_c = 110$ K. It is difficult to manufacture BSCCO conductors, because the compounds form at high temperature (Bi-2223 around 830 °C) and within a very narrow temperature interval (only a few °C). Thus their production requires well controlled heat treatment to manufacture high-quality wires. In addition, only expensive silver or silver alloys can be used as a matrix to allow oxygen diffusion during heat treatment. For these reasons, the development of commercial HTS wires is now concentrated mostly on YBCO. BSCCO materials are currently developed only by Sumitomo Corporation in Japan. [62]

BSCCO conductors are applied mainly in superconducting current leads and specific coil applications, in which Bi-2212 covers the temperature range 4-25 K and Bi-2223 upward of that [62]. Because the B_{c2} of these HTS materials is superior to that of other common materials, they can be adopted in high field inserts [91, 171].

MgB_2

Though MgB_2 has been a widely known compound since 1950s, its superconductivity was discovered as late as in 2001 [21, 124]. MgB_2 conductors contain only relatively cheap and common materials. In addition, it is easy to manufacture, e.g., heat treatment temperature variation is not very crucial. These reasons make MgB_2 a very attractive compound. Currently, three companies, Columbus Superconductors in Italy, Hyper Tech Research in USA and Hitachi in Japan, are manufacturing MgB_2 conductors. [81]

According to some predictions, MgB_2 will replace NbTi in MRI magnets. But also opposite arguments have been made, and at least in 2006 MgB_2 had no advantages in terms of coil performance or cryogenics [128]. Thus more wire development and a successful shift from laboratory experiments to industrial production are required [32]. Yet already 5 years after the discovery of superconducting phase in MgB_2, a demonstration of an MgB_2 MRI was presented [121]. The device exploited the high critical temperature of MgB_2 and operated at 20 K. However, the current density was modest, and an iron yoke was applied to increase the field at the imaging volume. Currently, the most interesting application prospects of MgB_2 are those that require 0-3 T magnetic flux densities around 20 K. In addition to MRI, these applications include, e.g., fault current limiters, transformers and induction heating. In **Publication 11**, I present the quench analysis of an MgB_2-based DC induction heater.

Copper is an excellent matrix material for superconductors. However, it cannot be used in direct touch with MgB_2, because MgB_2 filaments would then get contaminated during heat treatment and degrade the critical current characteristics of the conductor [47, 58, 59, 129, 144, 149]. However, copper can be used at high formation temperatures if a barrier material is used between it and MgB_2 [151]. Already at an early stage of MgB_2 wire development, iron and nickel were found chemically good matrix materials [164]. However, compared to copper, their electrical resistivities are high and thermal conductivities low, which may pose challenges to stabilising high-current magnets. For a detailed survey of the properties and current status of MgB_2, I recommend [38, 162, 164, 165].

Chapter 3

Short sample characterisation

The design of superconducting applications is based on voltage-current characteristics measured on short samples in specific characterisation systems. In these systems, heat is generated in electrical contact resistances and a normal conducting sample holder. Even at sub-critical currents, losses arise also in a superconductor due to a finite n-value and changing self-field [80],[175, p.140-143].

In liquid- and gas-cooled systems, sample warming does not usually create problems, but in conduction-cooled systems, it can increase the n-values and decrease critical currents spuriously. For successful characterisation, the sample temperature must be constant enough during the measurement and the current sharing between the matrix and the superconductor is not allowed to change within the measurement accuracy in the measurement area. For the latter condition, the concept of current transfer length must be introduced.

In this chapter, the need for the current transfer length is first justified and the concept is then formally defined. Further information including numerical and analytical models for examining current transfer in a two-layer structure with a contact resistance between the layers can be found in **Publication 5**.

Next, simulation results illustrate how the critical current decreases and the n-value increases when a slab warms during a measurement. The results are based on **Publication 6**, which also includes numerical and analytical models for performing simulations in an adiabatic slab.

Finally, critical currents and n-values were measured in a conduction-cooled environment for a multifilamentary MgB_2 tape. In the measurement, the ramp rate was varied with two sample holders which had similar geometries and dimensions but were made of different materials. In addition, a

numerical model was built to study the effect of the sample holder material on heat generation and, thus, on sample warming. Experiment details and the computational model appear in **Publication 10**. Based on these results, future research is proposed on both thermal and electrical contact resistances in conduction-cooled measurement stations.

3.1 Current transfer length

Ekin suggested that a too short distance between the current contacts and the voltage taps can have an effect on a short sample test. Informally, he proposed that the current transfer length is the minimum distance from the current contact to a point where the voltage tap can be placed without the current transfer voltage interfering with measurements of the wire's intrinsic $V - I$ characteristics. [40]

I propose a formal definition for the current transfer length (CTL) and two different criteria to determine it.

Definition. The current transfer length is the distance from the beginning of the current contact to the point where a chosen criterion is satisfied. The criterion can be chosen from two alternatives:

1. The electric field on the surface of the matrix is E_{CTL}.

2. The dimensionless relative proportion of the current in the superconducting region $\frac{I_{\mathrm{sc}}}{I_{\mathrm{tot}}}$, where I_{sc} and I_{tot} are the current in the superconducting region and the conductor, respectively, is I_{CTL}.

Naturally, it is required that $I_{\mathrm{CTL}} \in [0, 1)$.

Depending on the criterion, the definition of the CTL is to be called either (i) the E-based definition or (ii) the I-based definition and denoted by $\mathrm{CTL_I}(I_{\mathrm{CTL}})$ [mm] or $\mathrm{CTL_E}(E_{\mathrm{CTL}})$ [mm].

Current transfer models can also be used to compute heat generation in current terminals and joints. Consequently, soldering lengths can be optimised.

3.2 Spurious critical currents and n-values: a slab model

To visualise the effect of sample warming on the critical current, I simulated $E - J_{\mathrm{ave}}$ curves with several ramp durations and determined the diminished J_{c} and the increase of n-values (figure 3.1). Here, J_{ave} is the average current density in the superconducting region. In this particular case, for a real n-value of 20, the J_{c} degraded 3%, 8% 16% and 24% from the initial temperature J_{c} when the ramp durations were 0.1 s, 1 s, 10 s and 100 s, respectively. Correspondingly, the n-values rose to 27, 70, 340 and 540.

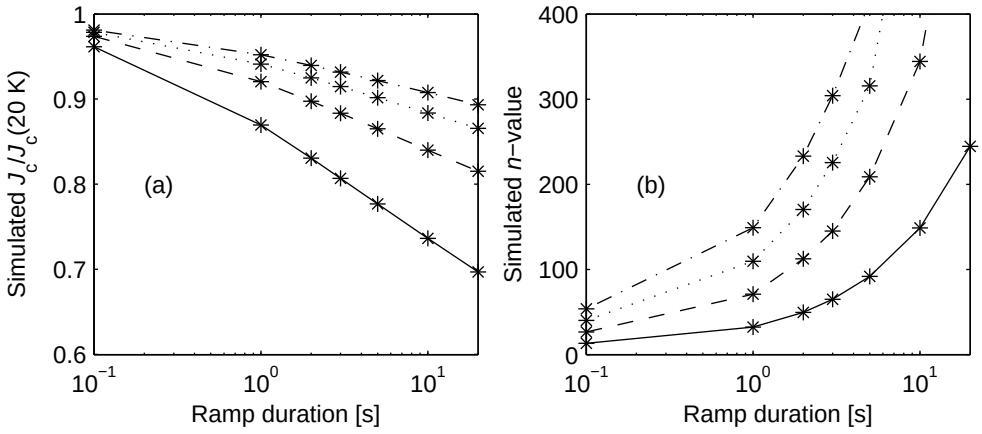

Figure 3.1: Simulated (a) J_{c} normalised to $J_{\mathrm{c}}(20\ \mathrm{K})$ and (b) n-value as a function of ramp duration. Solid lines (–) correspond to $n = 10$, dashed line (– –) to $n = 20$, dotted line ($\cdots$) to $n = 30$ and dash-dotted line ($- \cdot -$) to $n = 40$.

Though the simulations were run for an adiabatic bulk slab and though in practical superconductors a matrix stabilises a measurement, the above gave some practical hints. First, poor cooling easily leads to considerable errors in the critical currents in the high current density region, but fast ramps give the best results. At slow ramps, the losses due to finite n-value, the index losses [174], can ruin measurements. Thus I recommend that, if a conduction-cooled measurement station is used, the sample temperature is measured during the $V - I$ measurement and the temperature stability is reported with the other results. Furthermore, I suggest that the $V - I$ measurement is repeated at different ramp rates to check on any variation in critical currents and n-values. It is obvious that the temperature stability depends on the curvature

of $I_c(T)$. These guidelines apply to both coils and short samples.

3.3 Spurious critical currents and n-values: measurements

Critical currents and n-values at self-field were measured as a function of ramp rate for a Columbus Superconductors standard tape [23] (presented in figure 3.2), mounted on a copper or a stainless-steel (SS) sample holder (shown in figure 3.3). Figure 3.4 shows the results at 27.2 K. Even though this sample holder was against approved practice [39, p.297], it was designed to remove extrinsic stabilisation due to sample holder and to study intrinsic conductor properties. With a ramp rate of 1 A/s, the temperature rose considerably during the measurement and the critical currents degraded to 180 A and 83 A with Cu and SS sample holders, respectively. The temperature increased more with the SS sample holder at least because of a higher sample holder resistivity. Even though the soldering lengths of the conductor were equal (4.5 cm), the contact resistances between the sample holder and the conductor may be different, which can then be another reason for different heat generations. The corresponding n-values, 90 and 5440, were also unrealistically high. From these values, the critical current was smoothly increased until it saturated to about 245 A and 230 A at a ramp rate of 50 A/s for the Cu and SS sample holders. The n-value levelled at 15 and 13 after about 50 A/s and 15 A/s, respectively.

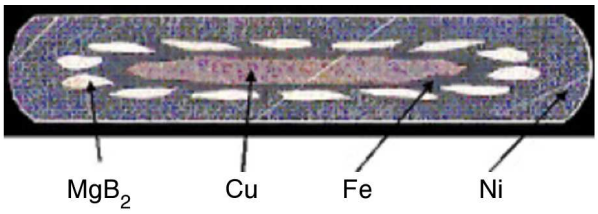

Figure 3.2: Columbus Superconductors standard tape including 14 MgB_2 filaments embedded in nickel matrix having copper stabiliser and iron diffusion barrier. Width of tape is 3.6 mm and height is 0.65 mm. Filling factor for MgB_2 is 9%.

Next, with the copper sample holder, the variation in the n-value and I_c was measured as a function of current ramp rate at different temperatures. As shown in figure 3.5, at 23 K I_c rose by 81% when the ramp rate was increased from 1 A/s to 150 A/s. Corresponding rises at the temperatures of 25 K, 27 K

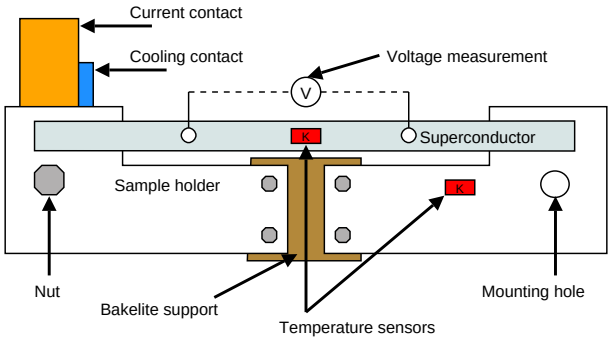

Figure 3.3: Sample holder design for $V - I$ curve measurement.

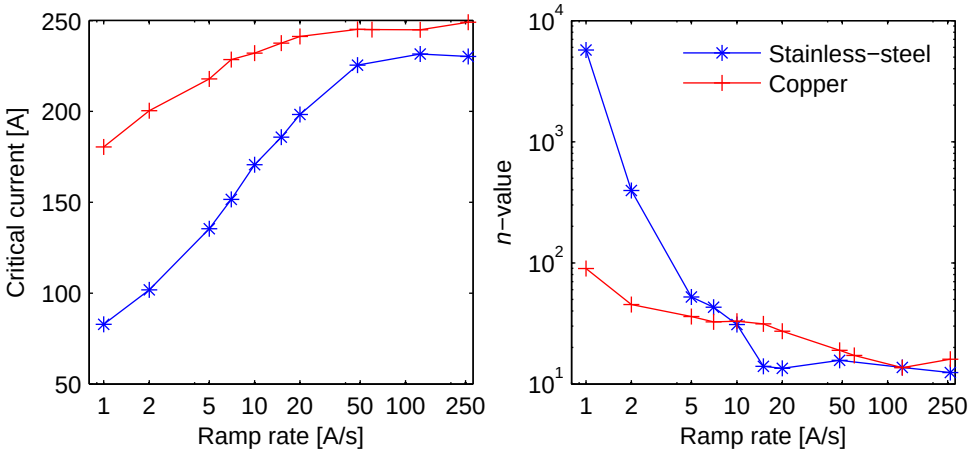

Figure 3.4: Effect of sample holder on critical current and n-value.

and 30 K were 60%, 41% and 20%. Thus the lower the temperature, the more prominent the change in I_c because I_c increased with decreasing temperature; hence heat generation surged during the measurement.

As a function of ramp rate, the critical current increased most visibly at low temperatures, i.e., with higher currents. Then sample holder warming and Ohmic losses in the material interfaces were higher. In addition, the specific heats of the constituents are monotonically increasing functions of temperature. At 35 K, heat conductivity and cooling fully compensated heat generation, enabling a $V - I$ measurement without an increase in temperature.

The n-value dropped dramatically as a function of ramp rate. Still, even the ramp rate of 10 A/s resulted in too high n-values, a situation creating a

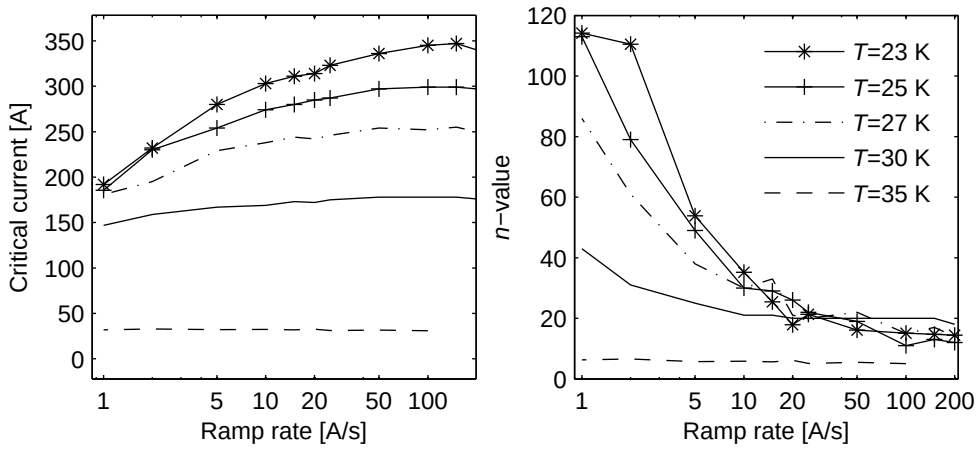

Figure 3.5: Effect of ramp rate on critical current and n-value at different temperatures.

dangerous pitfall for a magnet designer. For example, in a conductor with a critical current of 340 A and an n-value of 35 (10 A/s at 23 K), the index losses at 200 A equal the index losses in a conductor with the same critical current but with an n-value of 15 (100 A/s at 23 K) at 103 A. One can thus easily make too optimistic design decisions for magnet applications based on a short sample measurement when future I_c development is estimated and n-values are expected to remain. Also if n-values are high critical currents can be determined by using the magnetisation measurement, which also eliminates the losses in the contacts, sample holder and current leads. However, based on a recent experiment applying the standard voltage-current measurement is necessary to define the critical current of an MgB_2 conductor. [74]

Figure 3.6 shows critical currents as a function of temperature at a ramp rate of 100 A/s. At this ramp rate, all I_c values levelled out. In addition, a least squares fit is shown for the measured I_c. Thus the critical current can be expressed as a function of temperature as

$$I_c(T) = c_1 - c_2 T, \tag{3.1}$$

where $c_1 = 953.3$ A and $c_2 = 26.2$ A/K.

With a FEM model, the rise in the sample temperature was computed at the critical current with various ramp rates. The cryocooler's cooling power was measured and simulation results, computed with zero cooling and measured cooling, were compared with the measurements (figure 3.7). With a Cu sample holder, the temperature rise should be negligible also at the slowest

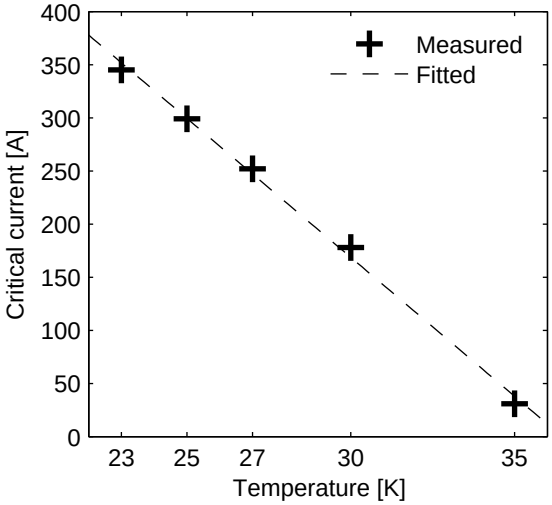

Figure 3.6: Measured critical currents as function of temperature; also shown is fitted critical current.

ramp rates according to the model, but in reality, then the apparent critical currents were considerable lower than at the high ramp rates. In simulation, due to small rises in temperature, cooling had almost no effect on the critical current. With cooling, only 10 mK temperature rises were observed with the slowest ramps. Without cooling, a ramp of 1 A/s caused the computed temperature rise of 0.1 K, whereas measurements showed a temperature rise of about 2.3 K.

With the SS sample holder, cooling had a significant effect. At a ramp of 1 A/s, the simulation of uncooled case showed a temperature rise of 1.8 K, which was 1.1 K higher than the cooled one. Yet the temperature calculated without cooling was 4.3 K lower than the one estimated from measured I_c data. When the ramp rate increased to 10 A/s, the sample temperature rose in the cooled case because the operation current increased and because the balance changed between heat generation and cooling; that is, a shorter ramp affords less time for both Ohmic loss generation and heat conduction. From 1 A/s to 10 A/s, the reduction in the energy removed by heat conduction contributed more to the sample temperature than reduction in Ohmic losses. However, after 10 A/s simulated temperatures decreased, even though the maximum current increased, because then decrease in Ohmic losses became dominant. This happened also when cooling was neglected.

When the ramp rate was increased, the simulated temperatures approached

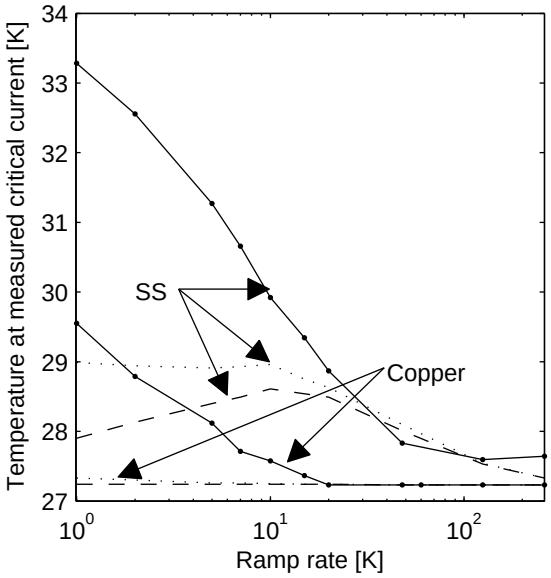

Figure 3.7: (lines with ·) Sample temperatures derived from measured critical currents according to (3.1) and computed at end of current ramp up to I_c in $(\cdots)$ uncooled and $(--)$ cooled simulations with Cu and SS sample holders.

those estimated from measurements. At ramp 48 A/s, the simulation gave 0.2 K higher temperature rise than the measurement. The non-isothermal temperature in the sample and sample holder can explain this small variation, but it does not explain the temperature differences at low ramps. Thus the electrical and thermal contact resistances must play a crucial role in the following three interfaces: between the current lead and the sample holder, between the sample holder and the MgB_2 tape, and between the matrix and the filaments. In addition, at least in some cases the tape is likely to have quenched at the contact between the tape and sample holder.

Simulated warming was negligible with the Cu sample holder in each case. However, at 1 A/s ramp rate 2.3 K sample warming was estimated from the measurements. Around ramp rate of 20 A/s the measured warming became also negligible. These also emphasise that the warming at contact resistances must play important role. Due to increasing AC losses as a function of ramp rate it is apparent that the critical current will start to decrease after some ramp rate value. However, in these measurements this did not play a role.

3.4 Remarks

In a short sample $V - I$ measurement, the current transfer length limits the possible voltage taps positions. According to measurable voltage levels, one can choose the correct alternative from the presented criteria and use one's current transfer model to determine voltage tap positions.

It is essentially important to monitor the sample temperature during the $V - I$ characterisation. Sample warming is a real problem with conduction-cooled measurement stations. If the temperature increases before the critical current is reached, too low critical currents and too high n-values can be derived from measured $V - I$ curves. Consequently, the too high n-values can create too optimistic expectations in the application designer, whereas the too low critical current can spell a pessimistic future for wire development.

In the future, the heat generation sources should be studied further. Based on the presented measurements and simulations, electrical and thermal contact resistances in the measurement station can significantly increase the sample temperature.

Chapter 4

Ferromagnetic coils

When the first MgB_2 conductors were made, nickel and iron were found to be chemically compatible materials with MgB_2, whereas copper contaminated the filaments during high temperature heat treatment [47, 58, 59, 129, 144, 149]. Earlier, nickel and iron had not been used as matrices of any other superconductor in a wide scale. Because the two are ferromagnetic materials, their magnetisation must be taken into account when coils including these are considered.

Chapter §3 discussed the short sample critical current and n-value characterisation. On that basis, the concepts of the coil critical and the thermal runaway currents have been well established, as presented in §2.2.4. If a coil includes a ferromagnetic constituent or if ferromagnetic bodies are placed near the coil, the linear methods for determining turn critical currents are not valid, even though the principles of $I_{\mathrm{c,coil}}$ and I_{tr} are feasible. This means that a numerical method must be used and one needs to take into account the effect of the ferromagnetic materials on the magnetic flux density distribution.

In this chapter, I first propose a model for computing the coil critical current of an MgB_2 coil, which consists of a conductor with a ferromagnetic matrix. The model was originally introduced in **Publication 1**. Then the linear and the proposed model are compared according to **Publication 9**. After this, the proposed model is used to optimise an SMES coil as presented in **Publication 7**. A linear MgB_2 SMES coil was optimised simultaneously and the results and required computational efforts are compared. Finally, I present the laboratory tests of a conduction-cooled MgB_2 coil with a ferromagnetic matrix. This discussion is based on **Publication 4**.

4.1 Critical current

A superconducting coil can consist of several thousands of turns. Each turn can include from tens to hundreds of filaments with electrical insulation and impregnation material between the turns. In other words, a coil cross-section can easily consist of several hundreds of thousands domains, each requiring at least a couple of elements in a two-dimensional finite element mesh. Thus with a finite element software in a personal computer, it is impossible to model the actual structure of the coil cross-section, much less the coil volume in three dimensions. Therefore, some kind of homogenisation is needed.

To solve the vector potential formulation for the magnetostatics (2.21) with a finite element software, an engineering permeability μ_{eng} is given to a homogeneous coil instead of describing each constituent separately. Depending on the conductor structure, homogenised coil material may be anisotropic.

To compute μ_{eng}, (2.21) is solved in a detailed conductor unit cell. The conductor unit cell includes the cross-sectional structure of the conductor and surrounding fill materials. The filling factor of the unit cell, i.e. the conductor area per total area, is the same as the coil's. Figure 4.1 shows schematically the model for solving the engineering permeability in y-direction. Here, I apply y-directional magnetic flux with a magnitude of $B_{\mathrm{app}}\Delta x$ from bottom to top. Then the engineering permeability is computed in the y-direction as

$$\mu^{\mathrm{y}}_{\mathrm{eng}}(B_{\mathrm{app}}) = \frac{\int |B_{\mathrm{y}}| \mathrm{d}a}{\int |H_{\mathrm{y}}| \mathrm{d}a}, \tag{4.1}$$

where the integrations are done over the unit cell cross-section. and B_{y} and H_{y} are the magnetic flux density and field intensity in y-direction, respectively. By repeating this with several values of B_{app} in the x- and y-directions, the engineering permeability is obtained as a function $\mathbf{B}$.

In a homogeneous coil, the computed $\mathbf{B}$ distribution cannot be used as such to give the turn critical currents from the short sample data. In this model, the whole coil cross-section magnetises because of μ_{eng}, but in practice this happens only in the ferromagnetic matrix. To overcome this problem, I formed a mapping between the computed $\mathbf{B}$ distribution on the homogeneous coil cross-section and the applied $\mathbf{B}$ in a short sample measurement. These kind of corrections are not totally new, but earlier self-field corrections have been made for cables with high self-fields at critical currents [142, p.340].

To compute the mapping, I placed the homogeneous unit cell with μ_{eng} in an external magnetic flux density with a constant magnitude of B_{app} to compute the average magnetic flux density B_{ave} in the unit cell, as schemati-

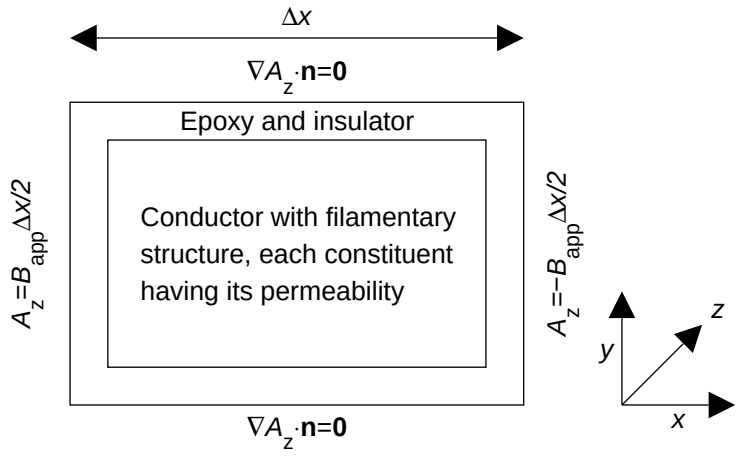

Figure 4.1: Schematic view of model for solving engineering permeability in y-direction.

cally shown in figure 4.2. Then (2.21) was solved in the virtual measurement situation and the average magnetic flux density in the y-direction $B^{\mathrm{y}}_{\mathrm{ave}}$ was calculated in the unit cell as

$$B^{\mathrm{y}}_{\mathrm{ave}} = \frac{1}{A_{\mathrm{uc}}} \int |B_{\mathrm{y}}| \mathrm{d}a, \tag{4.2}$$

where $A_{\mathrm{unit\,cell}}$ is the area of the unit cell and where the integration is performed in the unit cell cross-section. When this is repeated with several B_{app} values, first in y-direction $B^{\mathrm{y}}_{\mathrm{app}}$, the relation, or mapping,

$$G_{\mathrm{y}} : B^{\mathrm{y}}_{\mathrm{ave}} \rightarrow B^{\mathrm{y}}_{\mathrm{app}} \tag{4.3}$$

is obtained. Similarly G_{x} can be determined. Another option for computing the mappings G_{y} and G_{x} is to map maximum value of B to $B^{\mathrm{y}}_{\mathrm{app}}$. Experimental research is needed to compare and further develop these methods.

Finally, the computed $\mathbf{B}$ distribution in the coil cross-section is used, via the described mappings, to compute the turn critical currents. The coil critical current is found when the operation current equals the minimum of the turn critical currents. One must remember that because μ_{eng} depends on $\mathbf{B}$, the load line is not straight but it becomes a non-linear load curve.

Figure 4.3 presents the discrepancies in finding coil critical current according to the tradiational method illustrated in figure 2.7 and the proposed method.

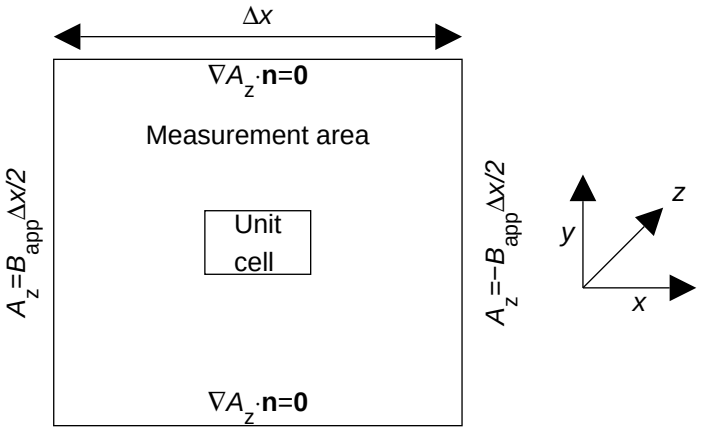

Figure 4.2: Schematic view of model with boundary conditions for computing relation between B^y_{ave} and B_{app} when B_{app} is y-directional. Here A_z is magnetic vector potential z-component and $\mathbf{n}$ unit normal.

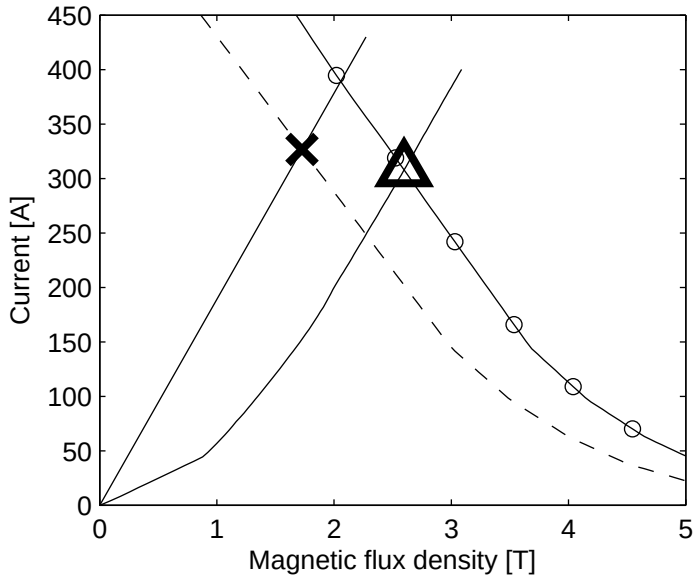

Figure 4.3: Discrepancies in solving $I_{\text{c,coil}}$. Conductor for this example case is presented in figure 4.6.a. Coil was solenoidal with height of 20 mm and thickness of 10 mm while filling factor for conductor was 65%. Dashed line and line with circles present measured and mappaed critical current characteristic, respectively. Cross and triangle present $I_{\text{c,coil}}$ for linear and non-linear cases at their load curves (solid lines), respectively.

4.2 Comparison of $I_{c,coil}$ computation models

I studied the $I_{c,coil}$ difference between the non-linear and linear models for five coil designs. Coil **1** had the dimensions of the Nb_3Sn SMES magnet built at the Tampere University of Technology, Institute of Electromagnetics [96]. The dimensions of coil **2** corresponded to the intermediate design dimensions for one of the two main coils designed for an MgB_2 DC induction heater in the ALUHEAT project [109]. Coils **1** and **2** represented a small and a large coil, respectively. Coils **3**, **4** and **5** had rectangular, thin and thick cross-sections, respectively. Coil **4** had a large bore, whereas coils **3** and **5** had smaller bores. The dimensions of the coils are presented in table 4.1. There, a, b and h are the inner and the outer radii and the height, respectively. The coils were assumed to be made of Columbus Superconductors 14-filament MgB_2/Ni/Fe/Cu standard tape [23]. Here I used the critical current characteristics presented in figure 4.4 with a 50% filling factor for each coil.

Table 4.1: Dimensions, critical currents and stored energies computed according to proposed and linear models. Both E_m values were computed with $I_{c,coil}$ given by proposed model.

Coil	a [mm]	b [mm]	h [mm]	$I_{c,coil}$ [A]		E_m [kJ]	
				Non-linear	Linear	Non-linear	Linear
1	200	243	90	158	189	5.3	5
2	450	550	200	99	120	124.1	118.6
3	100	200	100	118	125	8.9	8.1
4	200	250	200	136	156	19.1	18.3
5	100	300	50	130	134	14.7	13.8

In the linear method, the permeability was assumed to be μ_0 and the short sample critical current curves were used as such. To illustrate the effect of the matrix magnetisation on the stored energy, I computed E_m in both the modelling cases when the coils operated with $I_{c,coil}$ of the non-linear model. Table 4.1 presents the results of the analysis.

The difference between the $I_{c,coil}$ in the non-linear and linear models depended on the coil shape, but the linear model always gave higher $I_{c,coil}$. The biggest differences were noticed with coils **1** and **2**. Then, the linear model gave about 20% higher $I_{c,coil}$ than the non-linear model. In both cases, the weakest spot was located on the coil fringe because of anisotropic critical current characteristics. The third biggest difference, 15%, was observed in the thick coil **4**. Then the linear model gave $I_{c,coil}$ from the axial mid-point at the coil inner radius, whereas in the non-linear model $I_{c,coil}$ was found from the coil fringe.

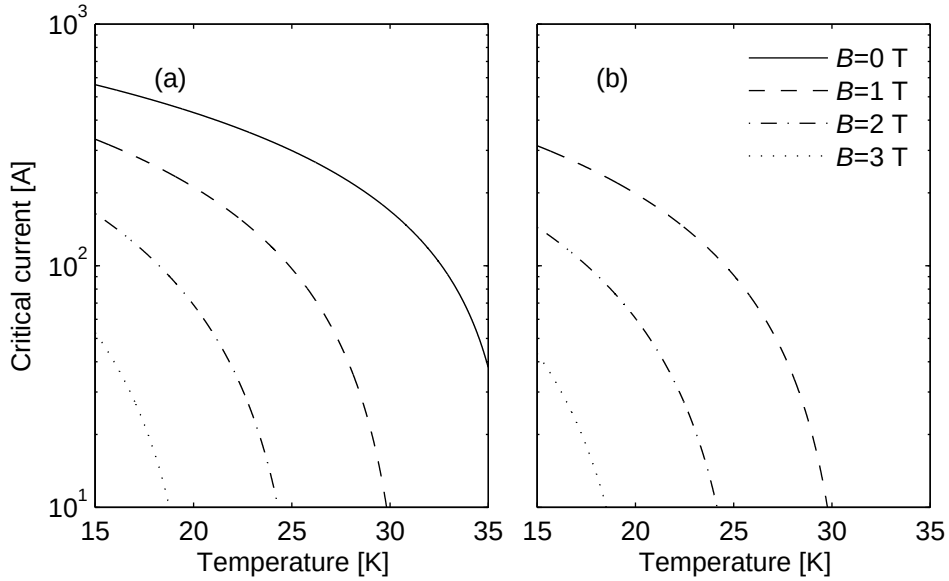

Figure 4.4: Critical currents in (a) parallel applied field and (b) perpendicular applied field.

Figure 4.5 presents the critical current contours of both models when coil **3** was operating at $I_{\mathrm{c,coil}}$. In fact, the critical current given by the linear model located at the coil inner radius and was lower than I_{c} at that location given by the non-linear model, but the fringe defined $I_{\mathrm{c,coil}}$ according to the non-linear model. Thus a ferromagnetic matrix can also be used to shield the filaments and to increase the operation current, but with this conductor configuration such behaviour was not observed in any of the coils. The shielding effects of the ferromagnetic matrix in MgB_2 conductors have been studied in [143].

When $I_{\mathrm{c,coil}}$ located in the coil inner radius, i.e. in coils **3** and **5**, the difference between the linear and non-linear models was only 6% and 3%, respectively. Thus, for this tape conductor, matrix magnetisation lowered the coil's maximum performance more when the critical current was defined in the coil fringe than in the coil inner radius. In other words, the perpendicular field was more damaging than the parallel field. Similar results have been obtained when shielding of saturated Bi-2223 tape with a partial nickel cover has been studied [63].

Due to the matrix magnetisation, the linear model naturally gave lower stored energies than the non-linear model at the same currents. The biggest difference occurred with coils **3** (9%) and **5** (6%), which had the shortest inner radii. The smallest differences (4%) were achieved with the ALUHEAT coil **2**

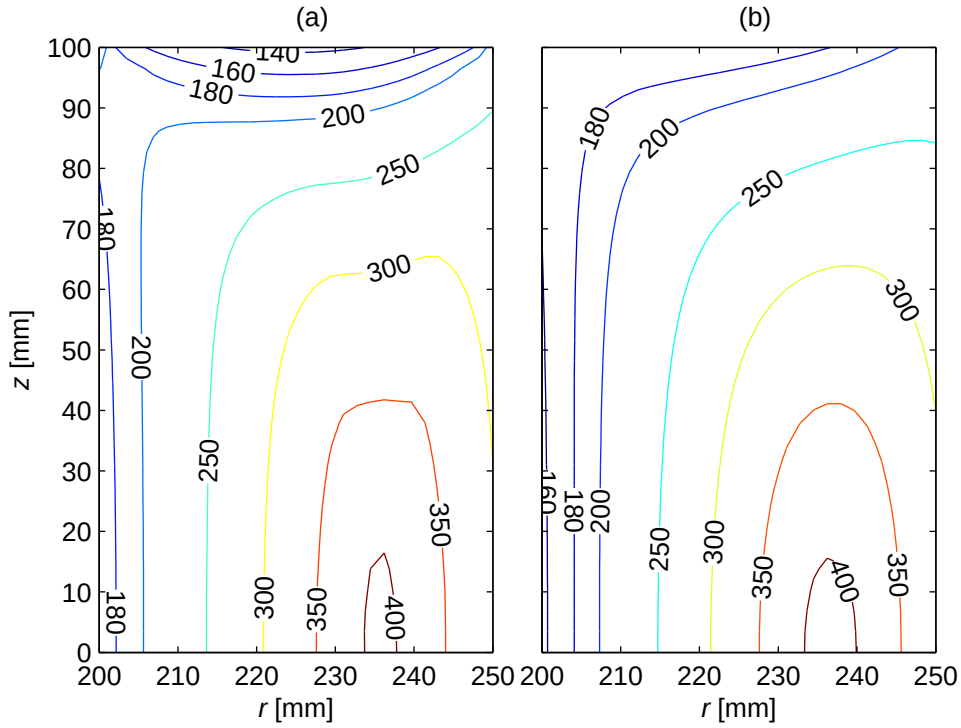

Figure 4.5: Critical current contours for half of coil **3** cross-section when operated at its critical current computed according to (a) non-linear model (136 A) and (b) linear model (156 A).

and the thin coil **4**. Although the linear model predicted energy with a few-percent accuracy, I recommend to scrutinise the effect of matrix magnetisation on the coil current carrying capability in the coil design phase. The traditional linear modelling tools can lead to an overly optimistic estimate of the coil critical current, if $I_{\mathrm{c,coil}}$ is found at the coil fringe and conductor critical current behaviour is anisotropic.

4.3 SMES coil optimisation

To compare the computational efforts required by the proposed model and the linear model, I optimised a, b and h to minimise the volume $\hat{V}$ of a solenoidal SMES coil

$$\hat{V} = \pi(b^2 - a^2)h, \tag{4.4}$$

with the following constraints:

1. Stored energy of the coil is at least 0.1 MJ when operating at 80% of its critical current.

2. The coil thickness $b - a$ and the height must be at least 10 mm.

3. The coil inner radius must be at least 50 mm.

Thirty-five percent of the coil cross-section was expected to consist of epoxy. Sequential Quadratic Programming (SQP), implemented in Matlab optimisation toolbox [115], was used in the optimisation. SQP is a method for finding a local minimum in a non-linearly constrained problem [97]. For a general discussion about the SMES magnet optimisation see [98].

In the optimisation, I studied two different MgB_2 conductors, one including ferromagnetic (Fe) and one non-magnetic matrix (Nb/AgMg). Their cross-sections are shown in figure 4.6 and their engineering critical current densities J_c^{eng} are presented in figure 4.7, which also includes the mapped data for the MgB_2-W/Fe conductor. Details of the MgB_2-W/Fe conductor are presented in [100] and MgB_2-Sic/Nb/AgMg is presented in [99].

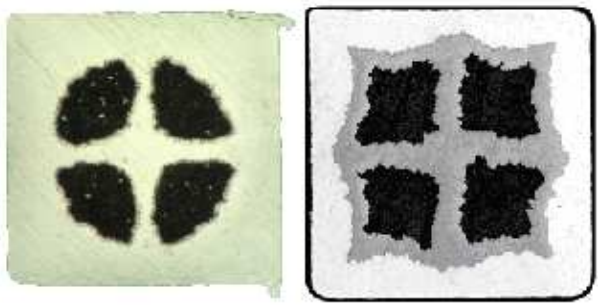

Figure 4.6: (a) MgB_2-W/Fe *ex situ* wire. Width and height of conductor are 1.0 mm. (b) MgB_2-SiC/Nb/AgMg *in situ* wire. Width and height of conductor are 1.2 mm.

Three different optimisations starting from different initial geometries were executed with both wires. The initial geometries Tn ($a = 0.2$ m, $b = 0.25$ m and $h = 0.4$ m), Tk ($a = 0.2$ m, $b = 0.6$ m and $h = 0.05$ m) and R ($a = 0.2$ m, $b = 0.4$ m and $h = 0.2$ m) represented a thin, thick and rectangular cross-section, respectively. Table 4.2 presents the optimisation results, where E_m was computed at the operation current of $0.8I_{c,coil}$ and l_{wire} is the required conductor length.

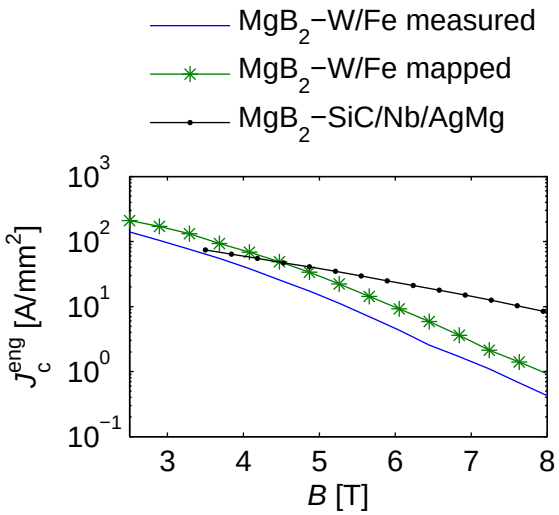

Figure 4.7: $J_{\mathrm{c}}^{\mathrm{eng}}(B)$ data for investigated conductors at 4.2 K when 35% epoxy addition to cross-section is taken into account.

Table 4.2: Results from SMES optimisation.

Init	(a, b, h) [mm]	$I_{\mathrm{c,coil}}$ [A]	E_{m} [kJ]	$\hat{V}$ [dm^3]	l_{wire} [km]
		MgB_2-SiC/Nb/AgMg			
R	(473, 496, 160)	262	100.0	11.6	5.2
Tn	(320, 339, 309)	267	100.0	11.6	5.2
Tk	(447, 474, 149)	255	100.0	11.6	5.2
		MgB_2-W/Fe			
R	(351, 558, 20)	213	100.0	11.9	7.7
Tn	(355, 365, 327)	296	100.0	7.4	4.8
Tk	(419, 589, 22)	211	100.0	11.8	7.6

With the MgB_2-SiC/Nb/AgMg wire, the optimisation algorithm found almost the same volumes in each case, but the dimensions differed notably between the different initial guesses. With the ferromagnetic MgB_2-W/Fe wire, the initial guess Tn led to a thin geometry, whereas R and Tk resulted in flat coils. These latter had almost identical volumes, which, however, were about 1.6 times larger than the one achieved with the initial guess Tn. In practice, thin and flat geometries are not very practical, which suggests that several initial guesses must be used in optimisation.

When FEM was applied, 10 minutes was a typical computation time for a linear optimisation. Non-linear optimisations took about 41 h, 25 h and 60 h for the initial guesses R, Tn and Tk, respectively. With both conductors, the minimum conductor consumption was almost the same. Thus, this analysis can

not be used to estimate if a ferromagnetic or a non-magnetic matrix results in a cheaper magnet manufacturing. More research is required for an optimal conductor manufacturing in long unit lengths. Also, different conductors can be specialised to certain operation conditions.

4.4 Tests with a conduction-cooled solenoid

I wanted to test the feasibility of the proposed model for estimating the current carrying capability of a ferromagnetic MgB_2 coil. Consequently, a coil was made of 46 m of the Columbus standard tape. The coil had the inner and outer radii of 40 mm and 60 mm, respectively and the height of 29 mm. The filling factor for the conductor was 58%. Based on the available information about the MgB_2 n-values [93], it was expected that the n-value of the conductor was relatively high. Hence, I applied directly the proposed $I_{c,coil}$ computational model. However, considerable heat generation was found at sub-critical currents, which led to premature quenches.

To verify the effect of coil warming on the coil n-value and critical current, $V-I$ curves were measured with different ramp rates. The temperature variation inside the winding was expected to be mainly due to the index losses. Thereby, it was low at fast ramps and the operation conditions tended towards isothermal. In each case, a current ramp was started when the coil temperature at the sensor locating in the coil inner radius, had cooled down to 16.9 K. Figure 4.8 presents the measured $V-I$ curves. The critical current increased and the $V-I$ curves became more gentle, i.e. the n-value decreased with increasing ramp rate. The n-values derived from the $V-I$ data are presented in figure 4.9 (a). At 0.1 A/s, the n-value was at its highest (6160) but plummeted to 40 at the ramp rate of 40 A/s.

Figure 4.9 (b) shows the critical currents normalised with the computed critical current, 189 A at 16.9 K. The normalised critical current increased from 61% to 76% when the ramp rate was increased from 0.1 A/s to 40 A/s. Yet degradation was noted at high ramps too, possibly stemming from intrinsic mechanical failures created during winding. In addition, the temperature distribution of a conduction-cooled coil is unlikely isothermal. That is, the isothermal conditions assumed in the computation are not valid in reality. Also, the proposed computational model may not after all adequately forecast the behaviour of a ferromagnetic coil. The measured $I_{c,coil}$ and n-values

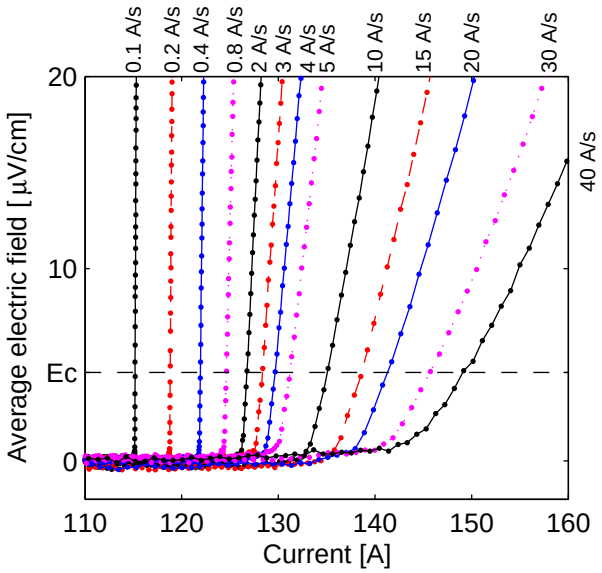

Figure 4.8: Measured $V - I$ curves at 16.9 K. Inductive voltage component was removed from curves.

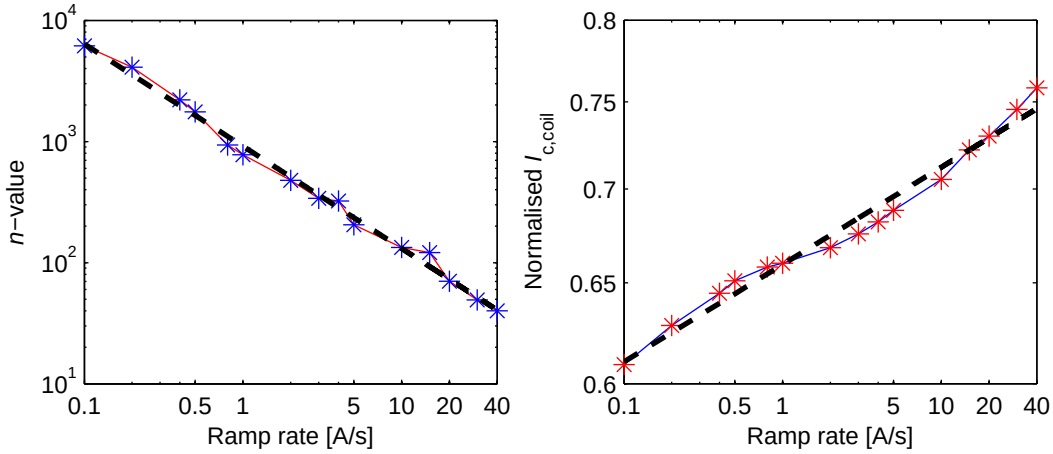

Figure 4.9: Lines with markers present n-value and normalised critical current as function of current ramp rate. Normalisation is done to computed critical current 189 A at 16.9 K. Dashed lines present fittings. Solid lines are only guides for eye.

followed with good accuracy the expressions

$$I_{\mathrm{c,coil}} = c_3 \left(\frac{\mathrm{d}I}{\mathrm{d}t} \right)^{c_4} \tag{4.5}$$

and

$$n = c_5 \left(\frac{\mathrm{d}I}{\mathrm{d}t} \right)^{c_6}, \tag{4.6}$$

where $c_3 = 125$, $c_4 = 0.033$, $c_5 = 915$ and $c_6 = -0.84$ are fitted constants.

Based on these results, it should be studied how close to the critical current the maximum attainable constant operation current can inch in MgB_2 coils. In fact, according to experiments by Takahashi *et al* [154], the maximum persistent current of a small MgB_2 coil was only 57% of the critical current. Thus a thermal runaway current can be a better indicator of the maximum operation current than $I_{c,coil}$. It is also worth studying in the future if the heat generation at the current terminals can limit the maximum operation current of a conduction-cooled coil. This may be a special problem when the resistivity of the matrix material is high when compared to high-purity copper.

4.5 Remarks

When designing a superconducting coil that includes conductor having a ferromagnetic matrix, the matrix magnetisation has to be taken into account in computation of the coil current carrying capability. Therefore, a model was proposed for estimating the critical current of ferromagnetic MgB_2 coils.

The proposed and linear $I_{c,coil}$ computation routines were compared and the difference in the resulting $I_{c,coil}$ reached up to 20%. After this, the model was used to optimise an SMES magnet. Optimisation took over 250 times longer with the non-linear model than with the linear model.

Finally, an MgB_2 coil was built, but unexpected problems emerged. At sub-critical currents, substantial heat generation was observed. Consequently, it was proposed that the thermal runaway current would better characterise the maximum performance of an MgB_2 coil than the coil critical current, at least in conduction-cooled environment.

Chapter 5

Conductor stability analysis

Until now, I have considered conductor characterisation and magnet design based on short-sample critical currents. From now on, I pay attention to stability issues and thus move on to next step in magnet designing. In this chapter, I use the concept of minimum quench energy to determine when magnet operation is stable. In the next chapter, I consider what happens when stability is lost.

To my best knowledge, there is no general definition for stability in superconducting magnets, but it can be derived from the earlier high-quality work bundled up largely in [30, 175]. In my opinion, magnet operation is stable when typical disturbances do not cause failures in normal operation; that is, the typical disturbances may generate local normal zones, but they contract and superconducting state recovers. The duration, intensity and distribution of the disturbances should be taken into account. However, the tolerance of different conductors to certain disturbances can be compared by computing the corresponding minimum quench energies. Then, one can begin from a disturbed initial temperature distribution or from a predetermined power pulse distribution and study if a conductor quenches or not. For example, the minimum length of a disturbed temperature profile leading to a quench determines the minimum propagation zone of the conductor for such a disturbance. From this the minimum quench energy can be computed.

According to recently measured minimum quench energies of MgB_2 conductors, the traditional closed-form formulae are not applicable [112, 113, 162]. Thus it is necessary to solve the heat diffusion equation in transient conditions (2.28). This was also done earlier for LTS conductors, in which the conductor n-value was not considered [79].

In this chapter, I first propose a formulation for determining minimum propagation zones in superconductors with finite n-values. The formulation was introduced in **Publication 8**, which also included the details of one possible implementation. This formulation is used to compute minimum quench energies with varying conductor n-values and the simulation results are compared with the Wilson's closed-form formula.

In addition to MQE, normal zone propagation velocities were also computed. Both of these were also measured and compared with the simulation results. In the simulations, the model based on the proposed MPZ formulation was used in such a way that the minimum quench energy was solved from power pulses applied to the conductor. Normal zone propagation velocities were then derived from the solutions according to **Publication 9**.

It is not always practical to measure material properties for the investigated conductors. Thus some formulae are given in **Publication 2** for computing the effective material properties based on literature data.

5.1 Formulation for minimum propagation zones

In my approach, I assume an isothermal conductor cross-section and, thus, take a one-dimensional approach. This approach is not applicable for cables where, e.g., gradual current diffusion from strand to strand or stabiliser at the quench frontier has to be taken into account [14, 56]. The approach is based on solving the heat diffusion equation (2.28) in a conductor to study whether a given initial temperature distribution leads to a thermal runaway or not. Any piecewise continuous temperature distribution can be used as the initial condition.

The heat generation is computed according to the power-law

$$Q(T) = \min\left\{\rho_{\mathrm{norm}}, \frac{E_{\mathrm{c}} A_{\mathrm{cond}}}{I_{\mathrm{c}}(T)} \left(\frac{I}{I_{\mathrm{c}}(T)}\right)^{n-1}\right\} \left(\frac{I}{A_{\mathrm{cond}}}\right)^2, \tag{5.1}$$

where A_{cond} is the area of the conductor cross-section. Because the n-value is in practice measured for composite conductors, not for pure superconductors, the power law takes into account the current sharing.

In this formulation, a piecewise constant temperature distribution is set as an initial temperature distribution. The temperature is set to T^* in the disturbed region, with length l, and to T_{op} elsewhere. Then formally, the length of the one-dimensional MPZ $l_{0\mathrm{S}}$ is solved as: Find such length of the

initial disturbance $l_{0\mathrm{S}}$ that

$$\begin{cases} \forall l < l_{0\mathrm{S}} \quad : \quad \left.\dfrac{\partial T(t)}{\partial t}\right|_{x=0} < 0 \\ \forall l \geq l_{0\mathrm{S}} \quad : \quad \left.\dfrac{\partial T(t)}{\partial t}\right|_{x=0} > 0 \end{cases} \quad \text{when} \quad t \geq t^*. \tag{5.2}$$

Here, $x = 0$ refers to the middle point of the disturbance and t^* is a constant. The same problem can also be formulated as a minimisation problem:

$$\min_{l_{0\mathrm{S}}} \quad : \quad \forall l \geq l_{0\mathrm{S}} \quad : \quad \left.\frac{\partial T(t)}{\partial t}\right|_{x=0} > 0 \quad \text{when} \quad t \geq t^*. \tag{5.3}$$

Finally, after $l_{0\mathrm{S}}$ and, thereby, the volume of MPZ are determined, MQE ϵ_{S} is computed as

$$\epsilon_{\mathrm{S}} = l_{0\mathrm{S}} A_{\mathrm{cond}} \int_{T_{\mathrm{op}}}^{T^*} C_{\mathrm{p}}(T) \mathrm{d}T. \tag{5.4}$$

In my approach, I utilised COMSOL Multiphysics [25] to solve minimum propagation zone problem.

5.2 Comparison with analytical results

It is well known that HTS magnets, which have low n-values, allow a short-term overcurrent operation without a thermal runaway. In LTS windings immersed in liquid helium, this is possible only for cryostable magnets [87, 147] and coils which satisfy the equal-area condition [108]. Therefore, it was expected that the results will differ considerably when the n-value was decreased from infinity to a realistic value.

I considered here disturbances at 20 K and 1 T parallel field. I studied the Columbus Superconductors standard tape [23] and varied its n-value. Figure 5.1 presents the $l_{0\mathrm{S}}$ and ϵ_{S} as a function of $\Delta T = T^* - T_{\mathrm{op}}$ for the n-values of 20, 50, 100 and ∞ when the normalised operation current was 0.5, 0.7 or 0.9. For comparison, $l_{0\mathrm{W}}$ and ϵ_{W} are also presented. Here T_{cs} is the current sharing temperature and it is obtained as an inverse function of $I_{\mathrm{c}}(T)$. The illustrated temperature in the Wilson's model was chosen to be the average temperature within the disturbance T_{ave}, and it was computed as

$$T_{\mathrm{ave}} = \frac{2}{l_{0\mathrm{W}}} \int_0^{l_{0\mathrm{W}}/2} T(x) \mathrm{d}x. \tag{5.5}$$

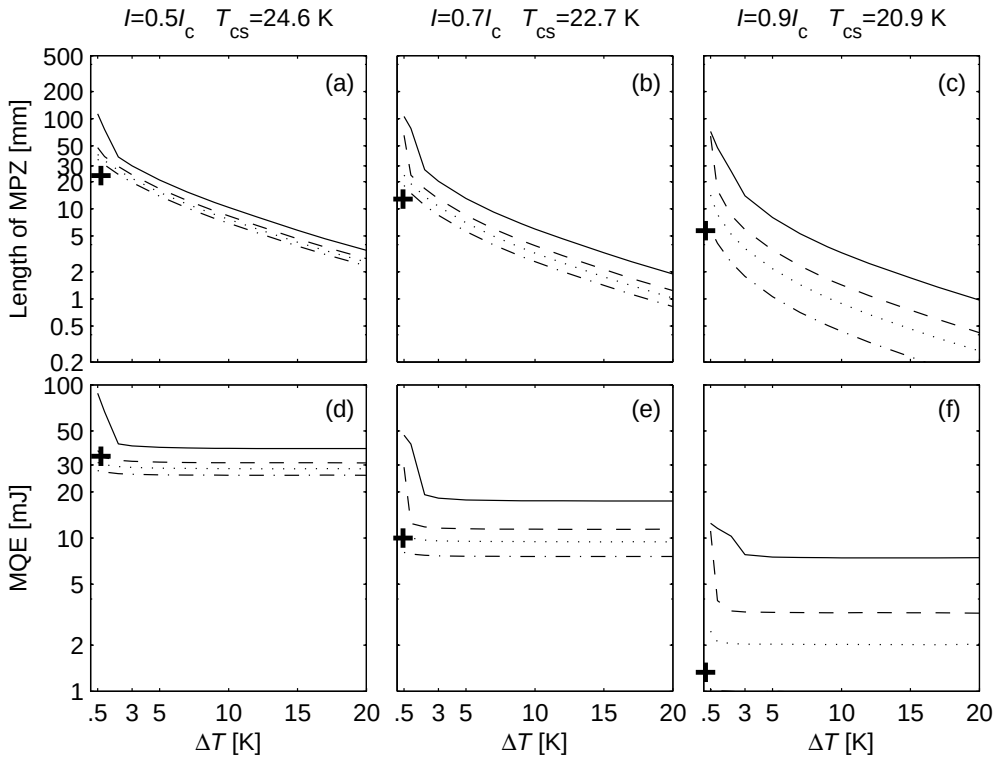

Figure 5.1: Values of $l_{0\mathrm{S}}$ and MQE for n-values of (—) 20, (– –) 50, ($\cdots$) 100 and (– · –) ∞. + presents $l_{0\mathrm{W}}$ and MQE at T_{ave}. Operation current is in (a) and (d) $0.5I_{\mathrm{c}}$, (b) and (e) $0.7I_{\mathrm{c}}$ and (c) and (f) $0.9I_{\mathrm{c}}$.

When ΔT was above a current dependent limit, ϵ_{S} did not change much but $l_{0\mathrm{S}}$ varied. At $n = 20$, the limit was 2, 2 and 3 K corresponding to $0.5I_{\mathrm{c}}$, $0.7I_{\mathrm{c}}$ and $0.9I_{\mathrm{c}}$. Below the limit, the tolerated disturbances were considerably high. This means that very high disturbance energies can be tolerated by low n-value conductors if they are distributed in a long conductor length.

At $0.5I_{\mathrm{c}}$, $0.7I_{\mathrm{c}}$ and $0.9I_{\mathrm{c}}$, ϵ_{W} agreed best with ϵ_{S} at $n = 50$, $n = 100$ and $100 < n < \infty$, respectively. That is, even though Wilson did not consider in his formulation current sharing, it gives reasonable estimates for MQE of practical LTS conductors. However, for a detailed analysis, it is necessary to take into account the conductor n-value.

5.3 MQE and v_{nzp} measurements

The MQE and normal zone propagation measurements were carried out with an early-stage development version of the Columbus Superconductors standard tape. Based on §3.3, at self-field the conductor n-value was about 15 and critical current was given by (3.1).

Figure 5.2 shows a schematic view of the setup for measuring MQE and the normal zone propagation velocity v_{nzp}. To measure real one-dimensional propagation, the sample was not in contact with the sample holder in the measurement area. Then heat was exchanged only by conduction along the sample and by radiation. Yet it was discovered that the cold mass of the sample holder affected the results at low currents. The ends of the sample holder were electrically separated with a bakelite plate to make sure that no current was shared between the sample holder and conductor in the measurement area. With this setup, one must be very careful in order not to burn the conductor when a quench occurs. However, with an automated sample current control this was not a problem.

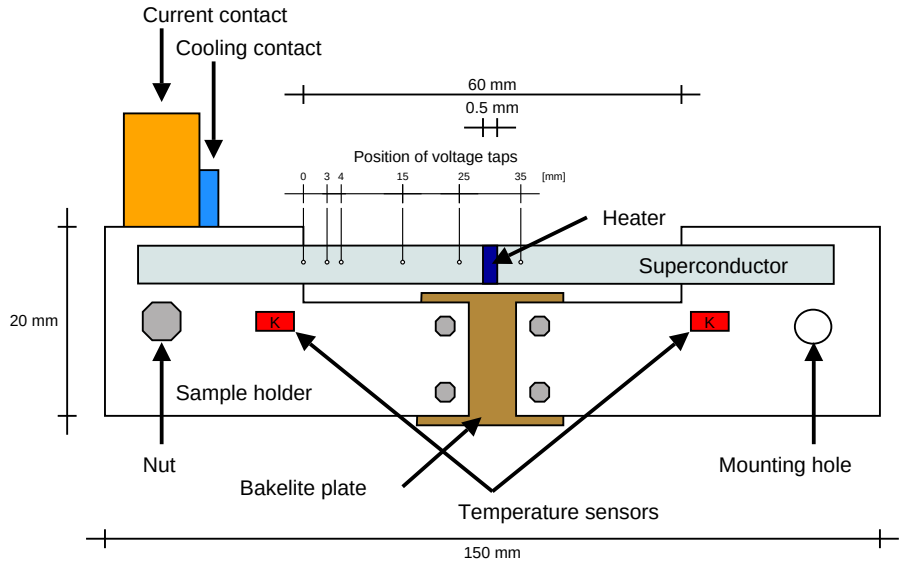

Figure 5.2: Schematic view of MQE and v_{nzp} measurement system.

5.3.1 Minimum quench energy

In the MQE measurement, a constant power (about 1 W) was applied to the heater for a specific time, and the minimum time causing a quench determined MQE. Now in the simulation, the initial temperature distribution was constant, but I applied the heater power to the 1 mm distance corresponding to the heater length and used (5.2) with obvious modifications. The typical heater operation time was in the range of 10-200 ms. In the computations, I used the resolution of 0.1 ms.

Figure 5.3 presents the measured and modelled minimum quench energies at 25.5 K and 28.0 K. At low currents, computed values of MQE were lower than the measured. At 100 A and 25.5 K, measured MQE was 188 mJ, while the computed value was 139 mJ, i.e. 27% smaller. The corresponding values at 28 K were 136 mJ and 119 mJ. Then the computed one was a little less than 13% smaller. The difference arised most likely due to the cold mass of the sample holder, which received some of the energy from the heater. In the simulations at 25.5 K and 100 A, I discovered that the temperature had already risen to 29.7 K at the sample holder edge when the superconductor below the heater reached its $T_{\mathrm{cs}} = 32$ K 19 ms after the heater start-up. Thus, the sample holder naturally affected the measurements when the temperature margin was several degrees.

The relative and absolute difference between the measured and computed MQE decreased when the operation current was increased and, thereby, the temperature margin lowered. For example, at 150 A, the computed MQEs were about 10% lower than the measured ones at both the investigated temperatures. Surprisingly, at 200 A and 28 K, the measured MQE exceeded the computed one. With the operation current of 250 A, the measurements could be done only at 25.5 K because at 28 K the conductor critical current was only 221 A. Also then, the computed value was 4% (3 mJ) higher than the measured one. Presumably, the current generated heat at joints which also raised the tape temperature and, thus, decreased the temperature margin. Thus, the same conclusion like in §3.4 could be drawn; in conduction-cooled measurement systems, the effect of various contact resistances on MQE measurement must be studied.

5.3.2 Normal zone propagation velocity

v_{nzp} was determined by using a voltage criterion, $V_{\mathrm{c}} = 2$ mV, and by measuring voltages V_1 between voltage taps at 4 mm (tap A) and 25 mm (tap C) and V_2

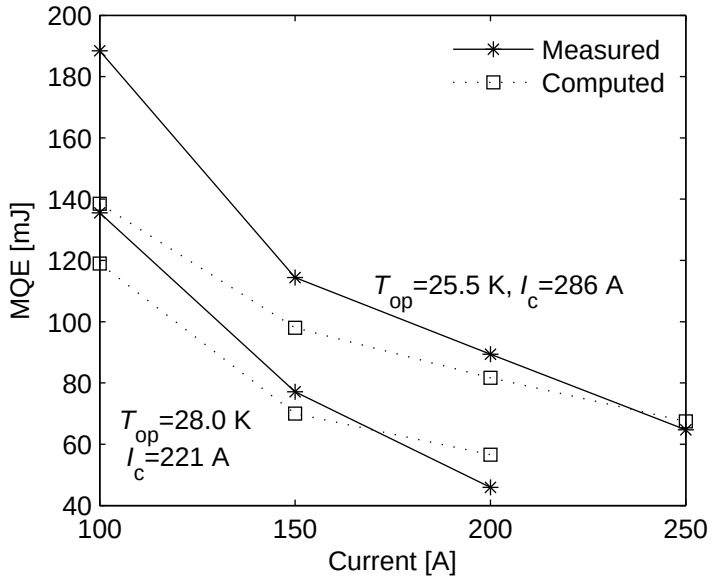

Figure 5.3: Computed and measured MQE as a function of operation current at temperatures 25.5 K and 28.0 K.

between tap A and tap B at 15 mm as a function of time. Thus the quench propagated from tap C towards B and finally passed A. v_{nzp} was then obtained from the measurement data as

$$v_{\mathrm{nzp}} = \frac{t_2 - t_1}{d}, \tag{5.6}$$

where $V_2(t_2) = V_{\mathrm{c}}$, $V_1(t_1) = V_{\mathrm{c}}$ and d is the distance between the voltage taps B and C.

In the simulation, the quench was ignited with MQE, and the corresponding voltage curves were then computed. V_1 was computed as

$$V_1(t) = \int_{\mathrm{tap\,C}}^{\mathrm{tap\,A}} \min \left\{ \frac{I}{A_{\mathrm{cond}}} \rho_{\mathrm{norm}}(T(x,t)), E_{\mathrm{c}} \left(\frac{I}{I_{\mathrm{c}}(T(x,t))} \right)^n \right\} \mathrm{d}x. \tag{5.7}$$

V_2 was correspondingly integrated between taps B and A.

Figure 5.4 presents the measured and simulated voltages V_1 and V_2 at 200 A and 28 K. The times of voltage V_1 passing V_{c} in the measurements and simulations were matched. Above 150 A, the simulated voltages fit well to the measurement data until the normal zone reached voltage tap A and the increase in the voltage slowed down. Then, the computed voltage rose more rapidly than the measured one. Most likely, the cold sample holder prevented the rapid

temperature rise in the sample during the experiment, but in simulations the sample was adiabatic allowing a faster temperature rise.

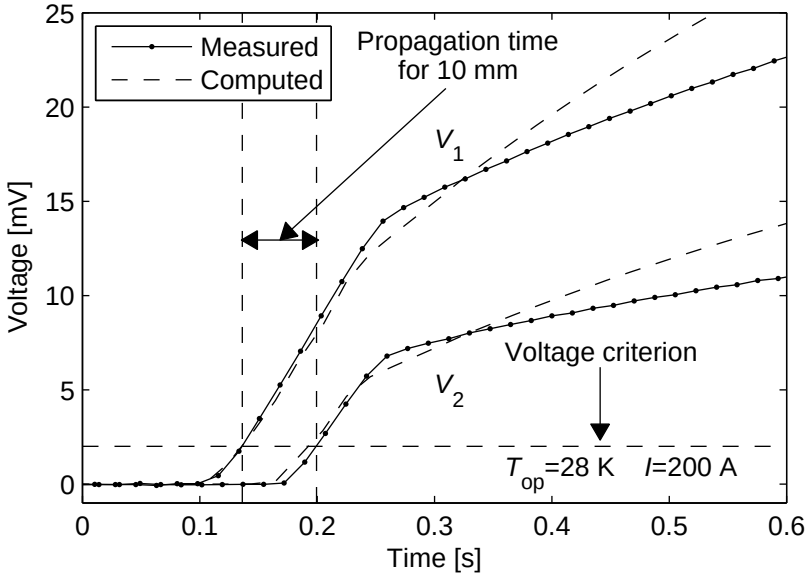

Figure 5.4: Measured and computed voltages V_1 and V_2 at 28 K and 200 A.

However, at 100 A the correspondence was poor. Both the measured voltages V_1 and V_2 rose more gently than the simulated ones. The computations gave a three times higher v_{nzp} than the measurements at 100 A and 25.5 K. The cooling effect of the sample holder's cold mass affected the measurement results at low current as also in the corresponding MQE measurements. However, inside an insulated coil cooling is negligible; thus simulated results can be more accurate than short sample measurements. Finally, figure 5.5 shows the measured and computed values of v_{nzp} at 25.5 K and 28.0 K. The best correspondence was achieved at 25.5 K and 250 A. Then the computations resulted only 12% higher value than the measurements.

5.4 Remarks

A formulation for solving minimum propagation zones for superconductors was introduced. When I used the formulation for computing MQEs, I found that the n-value has significant influence on MQE. Thus, the traditional closed-form solutions for MQE do not serve for detailed stability analysis.

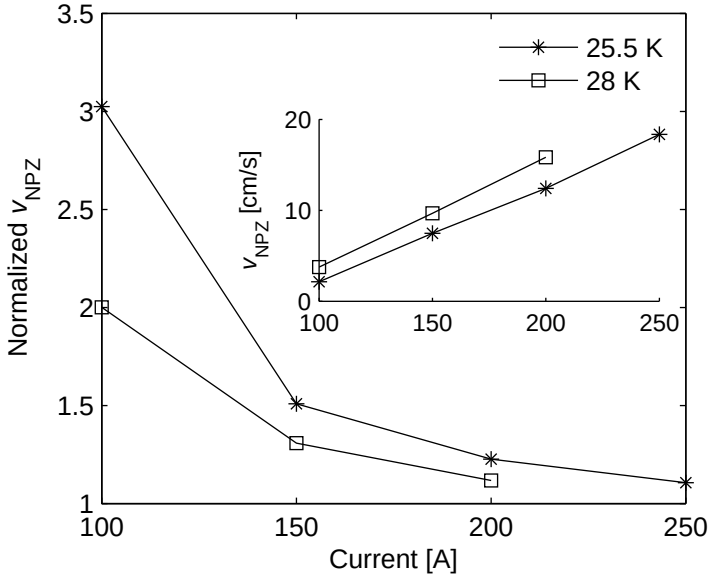

Figure 5.5: Computed values of normal zone propagation values normalised to corresponding measured values at operation temperatures of 25.5 K and 28.0 K. Inset presents measured v_{nzp} values.

The proposed model for solving MPZ was also successfully coupled with a measurement of quench onset. This included MQE and normal zone propagation velocity measurements. However, it turned out that when the stability margin is high (few degrees) the sample holder's cold mass can cause the measured MQE values to be too high and v_{nzp} too low. Hence simulation can reflect the conditions of an insulated magnet better than the short sample measurement.

Chapter 6

Coil quench analysis

When an unexpected, serious disturbance occurs, a coil quenches. In practice, coils quench, especially in research use where the magnets are run to the limits. Thus, a magnet designer must ensure that when a quench happens, a coil and accessories are not damaged. Therefore, the coil design must include a quench analysis which comprise quench simulations, design of a protection system and possibly quench detection considerations. Here, I concentrate on quench simulations. Quench protection and detection are discussed, e.g., in [142, p.542-554].

Several computer programs have been developed to simulate quench [44, 45, 55, 56, 96, 127, 130, 158, 175, 180]. In my finite element method based approach, matrix magnetisation was incorporated into the computation of local critical currents to make the program applicable to ferromagnetic MgB_2 coils. However, this program can be used also with linear coils.

This chapter introduces first the easy-to-implement quench algorithm presented in **Publication 3** and, then, presents some views on the quench origin models according to **Publication 9**. The developed program has been exploited in the European Project ALUHEAT, which aims to design, construct and test of a 200 kW DC MgB_2 induction heater [109]. The quench analysis is briefly reviewed at the end of this chapter according to **Publication 11**. My contribution to the project, quench analysis and considerations about the attractive forces between magnets were also published in [138]. In addition to the ALUHEAT project, the quench simulation program was also used to study the effect of the quench origin location on quench characteristics [148].

6.1 Quench simulation algorithm

A detailed quench simulation can be divided into three parts: preparation, primary analysis and post-processing. Preparation contains tasks that do not depend on the thermal behaviour. In a non-linear MgB_2 coil, it consists of computing the engineering permeability, mapping the measured short sample critical current surface to correspond to the homogenised unit cell used in analysis, computing the current dependent magnetic flux density distribution in the coil volume and computing the coil critical current.

Primary analysis means computing the quench characteristics, which consist current decay, hot spot temperature rise, power dissipation, normal zone resistance and voltages in the coil. The electromagnetic circuit analysis has to be coupled with the thermal analysis; hence a numerical approach is needed for detailed simulation. The thermal analysis is based on the heat diffusion equation (2.28), in which the effective material properties can be used.

Crucial parameters in the quench analysis are the maximum voltage over the normal zone and the hot spot temperature rise. The former is limited by the electrical insulation of the conductor, and the latter must be limited in order not to burn the coil. If a quench simulation indicates a danger of coil damage, a protection system must be designed. Naturally, the protection system design involves new quench simulations. Even though the simulation of an unprotected coil suggests a safe quench, some protection scheme is typically applied to guarantee safety and to reduce heat dissipation in the cryogenic environment. If the stored energy can be directed outside the coil, e.g., dissipated in a dump resistor or a secondary circuit, or fed back to grid, the coil re-cooling time and the energy required for cooling are cut down and quench costs accordingly reduced.

In post-processing, computed results are illustrated via graphs, key figures and animations of the temperature rise in the coil volume. In addition, the coil design can receive feedback, such as suggestions to choose another protection scheme or to lower the operation current.

A simplified electric circuit of a DC superconducting magnet is presented in figure 6.1. In normal operation, switch S is closed and the normal state resistance $R_{\mathrm{norm}} = 0\ \Omega$. When a quench occurs, the normal zone starts to propagate and R_{norm} increases. A quench can be detected by measuring the terminal voltage or picking up acoustic emissions [54]. When the quench is detected, S is opened. Then, diode D and the dump resistor with the resistance R_{s} are connected in series with the magnet. The current decay is determined by the coil inductance L, R_{norm} and R_{s}. Here, the ideal behaviour of the diode

is expected.

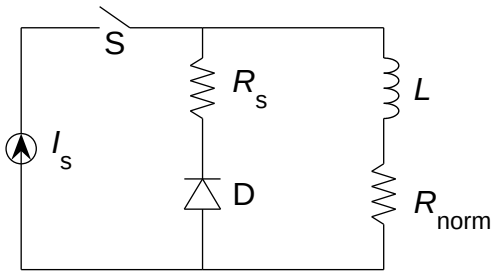

Figure 6.1: Basic electric circuit of DC superconducting magnet.

According to Kirchhoff's voltage law

$$L\frac{\mathrm{d}I}{\mathrm{d}t} + IR_{\mathrm{norm}}(t) = V_{\mathrm{s}} \qquad \text{if S is closed} \tag{6.1}$$

$$L\frac{\mathrm{d}I}{\mathrm{d}t} + I\left(R_{\mathrm{norm}}(t) + R_{\mathrm{s}}\right) = 0 \qquad \text{if S is open} \tag{6.2}$$

where V_{s} is the voltage of the power supply producing current I_{s}.

In (6.1) and (6.2), R_{norm} depends on time, on operation conditions before the quench and on the material properties. With ideal current source and closed S, $\mathrm{d}I/\mathrm{d}t = 0$ and with forward Euler type discretisation of (6.1) and (6.2), the current update is computed as

$$I^{k+1} = I^k \qquad \text{if S is closed} \tag{6.3}$$

$$I^{k+1} = I^k - I^k\left(R^k_{\mathrm{norm}} + R_{\mathrm{s}}\right)\frac{\Delta t}{L} \qquad \text{if S is open} \tag{6.4}$$

where k refers to the time step and Δt is the length of the time step. An algorithm for the numerical simulation of a quench is presented in algorithm 1. Here I_{op} is the initial operation current. In addition to the presented algorithm, a quench ignition is required. It can be implemented, e.g., by adding an artificial heater to a desired location in the model.

6.2 Implementing quench simulations

In quench simulations, the transverse heat conduction of the winding, the modelling of quench origin and the propagating normal zone front pose especial

Algorithm 1 Instructions for performing quench simulation.

1: $T(\Omega) \leftarrow T_{\mathrm{op}}$ {everywhere}
2: $I^0 \leftarrow I_{\mathrm{op}}$
3: $t^0 \leftarrow 0$
4: set Δt
5: set k=0
6: **while** "End condition" **do**
7: solve heat diffusion equation in coil volume using existing T distribution from t^k to $t^{k+1} = t^k + \Delta t$
8: save new T distribution
9: compute R^k_{norm}
10: compute I^{k+1}
11: $k = k + 1$
12: **end while**

problems. Here I study how the modelling of the quench origin affects simulation results in a finite element method software. In coils wound of cables, the current re-distribution at the normal zone front needs to be considered with care, because it can result to very severe heat generation [14, 56]. In my approach, I used a detailed mesh in the subdomains of the model, where I expected the most severe normal zone propagation. The transverse heat conduction was computed according to a model presented in [103].

The investigated coil had the same dimensions and properties as the SMES coil **1** in §4.2 in table 4.1, but improved critical current characteristics. The operation current I was 200 A at 20 K while $I_{\mathrm{c,coil}}$ was 300 A in the coil fringe, and the critical current at the coil inner radius was 317 A. Here matrix magnetisation was neglected to shorten the simulation time. The coil was assumed to be equipped with a protection system, in which the current source was switched off and the coil short-circuited when the voltage over normal zone exceeded 2 V.

I had three approaches to modelling the coil near the quench origin volume, which was a 2 cm long piece of conductor at the coil inner radius where the magnetic flux density reached its maximum. In cases **I** and **II** the whole winding was homogenised and a bulk heat conductivity tensor was given for it. In **I**, heat generation in the quench origin was evenly distributed over the coil unit cell, whereas in **II** it was evenly distributed over the conductor cross-section. In case **III**, I also modelled the actual coil structure near the quench origin. In addition to the conductor where the quench was ignited, one adjacent turn and epoxy layers between were modelled along 10 cm length.

Elsewhere, homogenised properties were assumed. In all cases, a heater was used to trigger a quench by adding a power of 5 W to the quench origin for a specific time.

Figure 6.2 presents results of the three quench analyses. The coil initial temperature was homogeneous 20 K. If the heater operated for 100 ms, the quench did not start in simulations **I** and **II**. When the 5 W heater was on for 200 ms, a quench started in each case. Thus 200 ms was chosen as the heater operation time. After the heater was turned off, the temperature decreased to 35 K, 39 K and 54 K in cases **I**, **II** and **III**, respectively, because heat was conducted away after a sudden decrease in local heat generation. After that, the hot spot temperature began rising again.

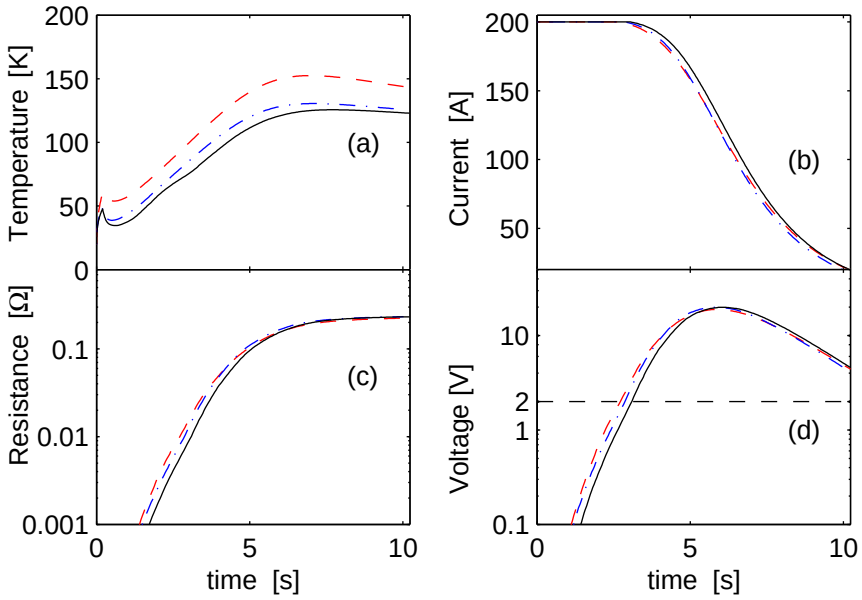

Figure 6.2: Results from quench analysis of (—) case **I**, (– · –) case **II** and (– –) case **III**.

Because of the considerably large temperature margin, it took about 3 s to detect the quench. Meanwhile, the hot spot temperature had risen to 77 K, 83 K and 93 K in cases **I**, **II** and **II**, respectively. Then, the current started to decay. For example, in case **III**, the hot spot temperature reached its maximum value 152 K at 7.0 s, while the current was 83 A. Simulation was continued until 1% remained of the total coil energy (9.6 kJ), i.e., at $I = 20$ A. In cases **I** and **II** the maximum hot spot temperatures were 126 K and 131 K, respectively.

According to the results, the thermally insulating epoxy around the tape

had considerable effect on the quench origin temperature; therefore, the actual coil structure needs to be modelled near the quench origin. This applies also if minimum quench energies in windings are computed for various disturbances.

With regard to the low stored energy, the hot spot temperature rise was quite high. However, from the practical point of view, the biggest concern was the temperature rise before the quench detection. In YBCO coils operating around 20 K, slow quench propagation has posed real problems in detecting the quench before a coil is damaged [114]. In the investigated coil, the hot spot temperature at the quench origin was 93 K in the detailed model at the time of detection. Typically tolerable maximum temperature during a quench is at most 300 K.

6.3 A 200 kW DC induction heater

The ALUHEAT project aims to demonstrate a new concept for induction heaters. Conventional induction heaters apply copper AC coils, and their efficiency is typically 55-60%. In the new concept, a billet to be heated is rotated in a DC magnetic field generated by MgB_2 coils. Rotation induces eddy currents which create the desired temperature distribution in the billet. The efficiency of the heater is primarily determined by the motor efficiency and coil cooling. In this project, the coils are cooled by cryocoolers, and the efficiency can reach 90%. Detailed description of the project is presented in [109].

The coil design is restricted by the dimensions of the billets, design of the mechanical system, the required field distribution and the conductor properties. The coil system outlined here was designed for billets with the diameter of 215 mm and with lengths up to 700 mm. The design principles of the coils were presented in [109, 110] and the mechanical system was outlined in [72].

The system consists of two identical solenoids located 800 mm apart, and the billet is placed between the coils. Thus, the magnetic field is oriented in perpendicular with the billet axis. The coils have an inner diameter of 450 mm, an outer diameter of 500 mm and an height of 180 mm as shown in figure 6.3.[1]

The current in the coils and, hence, the magnetic field, depend somewhat on the particular billet to be heated. When the billet is at rest, a typical value of the magnetic flux density is about 0.5 T in the centre of the billet, and the coils are exposed to the maximum magnetic flux densities of about 1.6 T at

[1]These dimensions differ from the values given in §4.2 because these studies were done at different phases while the final coil dimensions were not yet established. See future conferences for the dimensions of the manufactured coil.

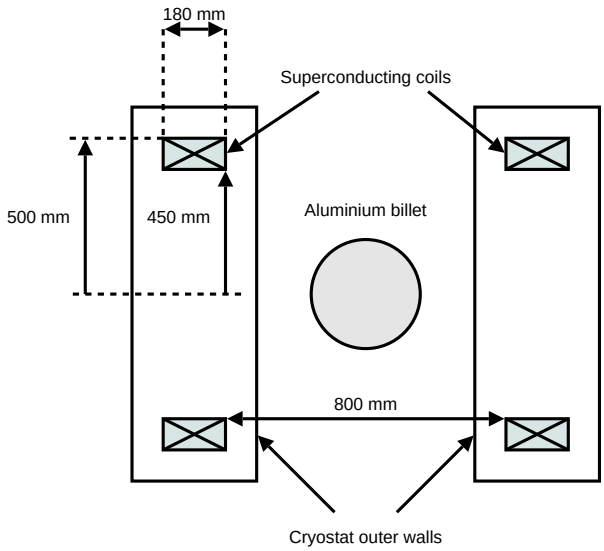

Figure 6.3: Schematic view of heater and coil dimensions.

the corners closest to the billet. These values are achieved with an operation current of 200 A. The total inductance of the coils connected in series is about 11 H.

Two types of quench analyses were performed. In the standard analysis, homogeneous degradation of the measured short-sample critical current characteristic in the coil was assumed. Then, the coil critical current was assumed to be degraded to 200 A in the fringe (figure 6.4). In the disturbance analysis, the coil critical current was assumed to be 300 A, but a local disturbance or a conductor weak spot quenched the coil at 200 A in the fringe, which determined the coil critical current (figure 6.5). Simulations were carried out with 2 Ω and 4 Ω dump resistors and also without any protection scheme. In all the cases, a quench was detected when the normal zone voltage exceeded 2 V. In the worst-case scenario, only one coil of the pair connected in series quenches. Then, the total stored energy, 220 kJ at 200 A, is dissipated in one coil and in a possible dump resistor.

The simulations were terminated when the current had decayed to 20 A because then the hot spot had started to cool down and only 1% remained of the total magnet energy. According to the standard analysis, the quench was detected 0.33 s after its onset. The maximum hot spot temperature was 84 K without a dump resistor. The current decay time from the quench current to 20 A was 14.0 s. The relatively long decay time was due to a slow normal zone propagation, which led to a sluggish rise in the normal zone resistance.

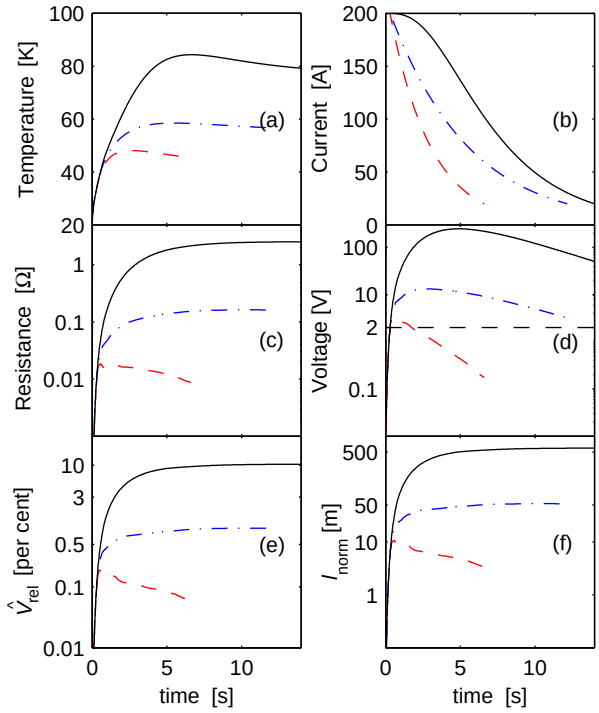

Figure 6.4: Quench simulation results of standard analysis (– –) without dump resistor, with (– · –) 2 Ω dump, and (—) 4 Ω dump resistor. Subplots present (a) hot spot temperature rise, (b) current decay, (c) normal zone resistance, (d) normal zone voltage, (e) relative volume of normal zone $\hat{V}_{\mathrm{rel}}$, and (f) length of normal zone l_{norm}. In (d) horizontal dashed line (– –) presents the quench detection voltage.

However, because of the modest average current density (42 A/mm^2), the hot spot temperature remained tolerable. A dump resistor could lower the maximum hot spot temperature to 58 K (2 Ω) or to 48 K (4 Ω).

The effectiveness of a dump resistor can be described explicitly by comparing the energy dissipations inside the winding. Without a dump resistor, 10% of the coil volume became resistive during a quench. All the stored energy was dissipated inside the cryostat and, has to be removed by a cryocooler. With the 2 Ω dump resistor, the volume was decreased to 0.9%, and only 9 kJ were dissipated in the coil. With the 4 Ω dump resistor, the volume decreased as low as 0.2% and dissipation diminished to 0.9 kJ.

In the disturbance analysis, the quench was detected about 7 s after the onset. Due to the slow normal zone growth, the temperature at the hot spot

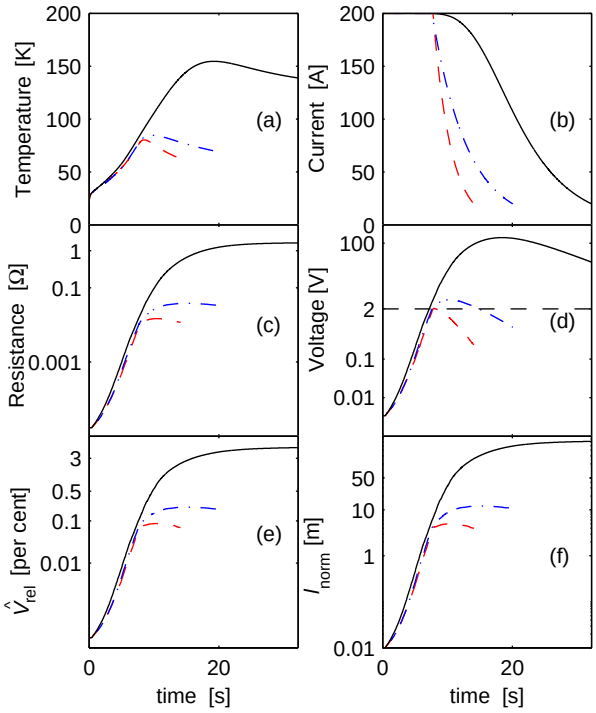

Figure 6.5: Results from analysis of disturbance originated quench. Curves and subplots correspond to those in figure. 6.4

reached 78 K before the quench was detected. With a dump resistor, the temperature started to decrease immediately after the detection due to a fast current decay. Without a dump resistor, the maximum hot spot temperature remained at an acceptable 155 K. The energy dissipation inside the coil was 2.9 kJ and 1.1 kJ when 2 Ω and 4 Ω dump resistors were used, respectively.

Finally, it was concluded that simple insulation is enough for 400 V terminal voltage, and thus it was decided to use a 2 Ω dump resistor in the coil protection system.

6.4 Remarks

Quench analysis is a very important phase of magnet design, because it aims to guarantee that an expensive coil is not damaged during fault conditions. An easy-to-implement algorithm was presented here for simulating quench.

Different ways of modelling the quench origin were studied. When detailed

coil structure near the quench origin was modelled, the hot spot temperature rose considerably higher than when only effective material properties were used. Also, in the latter case, more energy was required for quench ignition. Consequently, in quench simulation, modelling decisions must be made carefully. A special characteristic of a quench in an MgB_2 coil is slow normal zone propagation velocity, and thus a relatively long time to quench detection.

Finally, the developed program was used in the quench analysis of an MgB_2 DC induction heater coil. Based on the results, it was decided to use a 2 Ω dump resistor for protection.

Chapter 7

Conclusions

This thesis aims to help engineers to design MgB_2 coils. I began by discussing how to get initial data from short-sample measurements to model a coil. I concentrated on conduction-cooled systems and pointed that a characterisation can easily backfire due to sample warming. Then I scrutinised the sizing of the coil operation current and proposed a model to include the magnetisation of a ferromagnetic matrix in the computation of the coil critical current. However, laboratory tests of a small MgB_2 coil suggested that it is also necessary to consider the thermal runaway current. After these, I moved to stability considerations. First, I studied the conditions in which stability is lost by adopting the concept of minimum quench energy for conductors with a finite n-value. Finally, I considered the simulation of coil quench and adopted the presented information in a scientific industrial-scale project to size protection for a 200 kW MgB_2 induction heater.

Even though I presented in this thesis a compendium of specialities related to designing MgB_2 coils, each publication has a point which I want to emphasise:

Publication 1 and **Publication 7**: Consider matrix magnetisation when modelling coil performance.

Publication 2: This paper briefly reviews computation of basic stability parameters, minimum quench energy and normal zone propagation velocities, and presents computations for an MgB_2 tape. In addition, it gives formulae for determining effective material properties.

Publication 3: You can use this algorithm as a starting point, in various ways, when you program a new and more sophisticated quench simulation program to satisfy your needs.

Publication 4: Be aware of the conductor and coil n-values, because the cooling power of a conduction-cooled system is very low.

Publication 5: Define well any concept you use. Here, I define the current transfer length.

Publication 6 and **Publication 10**: When you measure $V - I$ curves in a conduction-cooled environment, repeat the measurements with various ramp rates. Check the results if I_c and n-values vary.

Publication 8: Use this tool to compute minimum quench energies for you conductors. Do not apply this to cables as such.

Publication 9: This publication gathers together things that a coil designer has to take into account from electromagnetic perspective. Still, do not forget analysis of mechanical stresses or forces!

Publication 11: A credible application is required to get funds for research. In my opinion, induction heating seems a promising, but a challenging, one.

The structure of this thesis stems from linking together all the above points. When designing a superconducting magnet, one needs initial data from short-sample measurements. This includes deriving critical current and n-value characteristics from measured $V - I$ curves. In conduction-cooled environment, sample warming can be devastating which leads to false characterisation. This can also arise from a bad sample holder.

DC magnet design often starts from a need to store certain energy or to produce certain magnetic field distribution to the working volume. The financier is typically interested mainly in achieving this target cost-effectively. To achieve the minimum cost of a superconducting magnet, it is outstandingly important to be able to exploit the full current carrying capacity of conductors. Therefore, I proposed a model for computing the critical current of an MgB_2 coil with a ferromagnetic matrix.

The financier is also definitely interested in system reliability. Thus by selecting a reliable conductor, a magnet designer can ensure future financing. Furthermore, by comparing conductor minimum quench energies, the endurance of different conductors on local disturbances can be studied.

In spite of the chosen conductor, a superconducting magnet may sometimes lose its stability. The worst-case scenario is quench. Detailed quench analysis is required to design the coil protection system and it also assures that the coil is not damaged during a quench.

The above issues have been discussed in detail for more than 20 years, and

also conduction-cooled coils have been used for more than 10 years. This thesis focuses on special characteristics related to conduction-cooled coils applied to systems using MgB_2 superconductor.

I provide in this thesis supplementary information to engineers who have already been designing conduction-cooled systems made of other materials, and also introduce the basics of some important concepts needed for designing of superconducting magnets. Therefore, newcomers can use this also as a source book for starting to familiarise themselves with superconducting magnet design. For complementary information useful references are given in many locations. However, for designing a specific application, I suggest to search also for more comprehensive references. This thesis awakes questions for future research too. I emphasise that especially the dynamics of a conduction-cooled short-sample characterisation needs more research. The effects of thermal and electrical contact resistances on the temperature variation during the measurement needs especially more study. And, finally, it would be interesting to study how matrix material of a superconductor effects the heat generation in the coil current terminations.

Bibliography

[1] Abhilash Kumar R G, Vinod K, Varghese N and Syamaprasad U 2007 *Supercond. Sci. Technol.* **20** 222 "Reactivity of sheath materials with Mg/B in MgB_2 conductor fabrication" doi:10.1088/0953-2048/20/3/018

[2] Aharonov Y and Bohm D 1959 *Phys. Rev.* **115** 485 "Significance of electromagnetic potentials in quantum theory" doi:10.1103/PhysRev.115.485

[3] Ahoranta M to appear 2008 *Modelling Mechanical Stress and Strain in Filamentary Superconductors with Finite Element Method* (PhD Thesis, Tampere University of Technology, Finland)

[4] Anderson P W 1962 *Phys. Rev. Lett.* **9** 309 "Theory of flux creep in hard superconductors" doi:10.1103/PhysRevLett.9.309

[5] Anderson P W and Kim Y B 1964 *Rev. Mod. Phys.* **36** 39 "Hard superconductivity: theory of the motion of Abrikosov flux lines" doi:10.1103/RevModPhys.36.39

[6] Bardeen J, Cooper L N and Schrieffer J R 1957 *Phys. Rev.* **108** 1175 "Theory on superconductivity" doi:10.1103/PhysRev.108.1175

[7] Bean C P 1962 *Phys. Rev. Lett.* **8** 250 "Magnetization of hard superconductors" doi:10.1103/PhysRevLett.8.250

[8] Bean C P and Doule M V 1962 *J. Appl. Phys.* **33** 3334 "Superconductors as permanent magnets" doi:10.1063/1.1931166

[9] Beasley M R, Labusch R and Webb W W 1969 *Phys. Rev.* **181** 682 "Flux creep in type-II superconductors" doi:10.1103/PhysRev.181.682

[10] Bednorz J G and Müller K A 1986 *Z. Phys. B* **64** 189 "Possible high T_c superconductivity in the Ba-La-Cu-O system" doi:10.1007/BF01303701

[11] Best K, Genevey D, Hillmann H, Krempasky L, Polak M and Turck B 1979 *IEEE Trans. Magn.* **15** 395 "Anisotropy of the critical current in solid solution superconductor NbTi"

[12] Bonevich J E, Harada K, Matsuda T, Kasai H, Yoshida T, Pozzi G and Tonomura A 1993 *Phys. Rev. Lett.* **70** 2952 "Electron holography observation of vortex lattices in a superconductor" doi:10.1103/PhysRevLett.70.2952

[13] Bossavit A 1998 *Computational Electromagnetis* (Boston: Academic Press), available online at `http://natrium.em.tut.fi/~bossavit/`

[14] Bottura L 1998 *Physica C* **310** 316 "Modelling stability in superconducting cables" doi:10.1016/S0921-4534(98)00482-1

[15] Braccini B, Nardelli D, Penco R and Grasso G 2007 *Physica C* **456** 209 "Development of *ex situ* processed MgB_2 wires and their applications to magnets" doi:10.1016/j.physc.2007.01.030

[16] Brown J R 2002 *Smoke and Mirrors How science reflects reality* (Taylor & Francis e-Library)

[17] Bruzzone P 2004 *Physica C* **401** 7 "The index n of the voltage-current curve, in characterization and specification of technical superconductors" doi:10.1016/j.physc.2003.09.005

[18] Calle C I 2001 *Superstrings and Other Things: A Guide to Physics* (Bristol and Philadelphia: Institute of Physics Publishing/CRC Press)

[19] Cardwell D A and Ginley D S Editors 2003 *Handbook of Superconducting Materials* (Bristol: Institute of Physics Publishing)

[20] Caspi S, Chiesa L, Ferracin P, Gourlay S A, Hafalia R, Hinkins R, Lietzke A F and Prestemon S *IEEE Trans. Appl. Supercond.* **13** 1714 "Calculating quench propagation with ANSYS" doi:10.1109/TASC.2003.812867

[21] Cava R J 2001 *Nature* **410** 23-24 "Genie in a bottle" doi:10.1038/35065177

[22] Chu C W 1987 *Proc. Natl. Acad. Sci.* **84** 4681 "Superconductivity above 90 K"

[23] Columbus Superconductors srl `http://www.columbussuperconductors.com/`

[24] Comforti E, Chung Y C, Heiblum M, Umansky V and Mahalu D 2002 *Nature* **416** 515 "Bunching of fractionally charged quasiparticles tunnelling through high-potential barriers" doi:10.1038/416515a

[25] COMSOL Multiphysics is a product of COMSOL AB, `http://www.comsol.com/`

[26] Conectus, Consortium of European Companies Determined to Use Superconductivity `http://www.conectus.org/`

[27] Cyrot M and Pavuna D 1992 *Introduction to Superconductivity and High-T_c Materials* (Singapore: World Scientific)

[28] de Bruyn Ouboter R 1997 *Scientific American* **Mar** 98 "Heike Kamerlingh Onnes's discovery of superconductivity"

[29] Devred A 1989 *IEEE Trans. Magn.* **25** 1698 "General formulas for the adiabatic propagation velocity of the normal zone" doi:10.1109/20.92628

[30] Devred A 1992 *AIP Conf. Proc.* **249** 1262 "Quench origins" doi:10.1063/1.41993

[31] Dew-Hughes D 1974 *Philos. Mag.* **30** 293 "Flux pinning mechanisms in type II superconductors" doi:10.1080/14786439808206556

[32] Dhallé M "Highlights of the FP6 'HIPERMAG' project" *Presented at European Workshop on MgB_2-based Conductors State-of-the-art and Applications, 25 January, 2008, University of Twente, The Netherlands*

[33] Dou S X, Soltanian S, Yeoh W K and Zhang Y 2005 *IEEE Trans. Appl. Supercond.* **15** 3219 "Effect of nano-particle doping on the upper critical field and flux pinning in MgB_2"
doi:10.1109/TASC.2005.848799

[34] Dou S X, Collings E W, Shcherbakova O and Shcherbakov A 2006 *Supercond. Sci. Technol.* **19** 333 "Aluminium-stabilized magnesium diboride - a new light-weight superconductor"
doi:10.1088/0953-2048/19/4/015

[35] Dou S X, Shcherbakova O, Yeoh W K, Kim J H, Soltanian S, Wang X L, Senatore C, Flükiger R, Dhallé M, Husnjak O and Babic E 2007 *Phys. Rev. Lett.* **98** 097002 "Mechanism of enhancement in electromagnetic properties of MgB_2 by nano SiC doping"
doi:10.1103/PhysRevLett.98.097002

[36] Doule R A, Campbell A M and Somekh R E 1993 *Phys. Rev. Lett.* **71** 4241 "Direct observation of intrinsic pinning in YBCO thin films"
doi:10.1103/PhysRevLett.71.4241

[37] Edelman H S and Larbalestier D C 1993 *J. Appl. Phys.* **74** 3312 "Resistive transitions and the origin of the n value in superconductors with a Gaussian critical-current distribution"
doi:10.1063/1.354554

[38] Eisterer M 2007 *Supercond. Sci. Technol.* **20** R47 "Magnetic properties and critical currents of MgB_2"
doi:10.1088/0953-2048/20/12/R01

[39] Ekin J W 2006 *Experimental Techniques for Low-Temperature Measurements* (New York: Oxford University Press)

[40] Ekin J W 1978 *J. Appl. Phys.* **49** 3406 "Current transfer in multifilamentary superconductors. I. Theory"
doi:10.1063/1.325245

[41] Ekin J W 2004 in *Gaseous Dielectrics X* (edited by Christophorou L C, Olthoff J K and Vassiliou P, Springer) "Superconductors: An emerging power technology"

[42] Embury D J and Han K 1998 *Curr. Opin. Solid State Mater. Sci.* **3** 304 "Conductor materials for high field magnets"
doi:10.1016/S1359-0286(98)80106-X

[43] Erlicson H 1999 *Eur. J. Phys.* **20** 183 "Sadi Carnot, 'Founder of the second law of thermodynamics'"
doi:10.1088/0143-0807/20/3/308

[44] Eyssa Y M and Markiewicz W D 1995 *IEEE Trans. Appl. Supercond.* **5** 487 "Quench simulation and thermal diffusion in epoxy-impregnated magnet system"
doi:10.1109/77.614453

[45] Eyssa Y M, Markiewicz W D and Miller J 1997 *IEEE Trans. Appl. Supercond.* **7** 159 "Quench, thermal, and magnetic analysis computer code for superconducting solenoids"
doi:10.1109/77.402572

[46] Farrell D E, Dinewitz I and Chandrasekhar B S 1966 *Phys. Rev. Lett.* **16** 91 "Nonlinear flux flow in type-II superconductors"
doi:10.1103/PhysRevLett.16.91

[47] Feng Y, Yan G, Zhao Y, Liu C F, Liu X H, Zhang P X, Zhou L, Sulpice A, Mossang E and Hebral B 2004 *J. Phys. Condens. Matter* **16** 1803 "Preparation and enhancement of critical current density in MgB_2 wires and tapes"
doi:10.1088/0953-8984/16/10/012

[48] Feynman R, Leighton R B and Sands M 1964 *The Feynman Lectures on Physics II Mainly Electromagnetism and Matter* (Reading: Addison-Wesley)

[49] Field M, Hentqes R, Parrel J, Zhang Y and Hong S 2001 *IEEE Trans. Appl. Supercond.* **11** 3692 "Progress with Nb_3Sn conductors at Oxford Instruments, superconducting technology"
doi:10.1109/77.919866

[50] Flükiger R, Suo H L, Musolino N, Beneduce C, Toulemonde P and Lezza P 2003 *Physica C* **385** 286 "Superconducting properties of MgB_2 tapes and wires"
doi:10.1016/S0921-4534(02)02307-9

[51] Folland G and Sitaram A 1997 *J. Four. Anal. Appl.* **3** 207 "The uncertainty principle: A mathematical survey"
doi:10.1007/BF02649110

[52] Fuchs G, Müller K-H, Handstein A, Nenkov K, Narozhnyi V N, Eckert D, Wolf M and Schultz L 2001 *Solid State Commun.* **118** 497 "Upper

critical field and irreversibility line in superconducting MgB_2"
doi:10.1016/S0038-1098(01)00157-0

[53] Fujino H 1990 *IEEE Elec. Ins. Mag.* **6** 7 "Electrical insulation technology for superconducting devices in Japan"
doi:10.1109/57.50800

[54] Fujita H, Takaghi T, Bobrov E S, Tsukamoto O and Iwasa Y 1985 *IEEE Trans. Magn.* **21** 380 "The training in epoxy-impregnated superconducting coils"

[55] Gavrilin A V 1993 *IEEE Trans. Appl. Supercond.* **3** 293 "Computed simulation of thermal process during quench in superconducting winding solenoid"
doi:10.1109/77.233484

[56] Gavrilin A V, Dudarev A V and ten Kate H H J 2001 *IEEE Trans. Appl. Supercond.* **11** 1693 "Quench modeling of the ATLAS superconducting toroids"
doi:10.1109/77.920108

[57] Ghosh A K 2004 *Physica C* **401** 15 "$V - I$ transition and n-value of multifilamentery LTS and HTS wires and cables"
doi:10.1016/j.physc.2003.09.006

[58] Glowacki B A, Majoros M, Vickers M, Evetts J E, Shi Y and McDougall I 2001 *Supercond. Sci. Technol.* **14** 193 "Superconductivity of powder-in-tube MgB_2 wires"
doi:10.1088/0953-2048/14/4/304

[59] Glowacki B A, Majoros M, Vickers M, Eisterer M, Toenies S, Weber H W, Fukutomi M, Komori K and Togano K 2003 *Supercond. Sci. Technol.* **16** 297 "Composite Cu/Fe/MgB_2 superconducting wires and MgB_2/YSZ/Hastelloy coated conductors for ac and dc applications"
doi:10.1088/0953-2048/16/2/330

[60] Goa P E, Hauglin H, Baziljevich M, Il'yashenko E, Gammel P L and Johansen T H 2001 *Supercond. Sci. Technol.* **14** 729 "Real-time magneto-optical imaging of vortices in superconducting $NbSe_2$"
doi:10.1088/0953-2048/14/9/320

[61] Goldacker W, Schlachter S I, Obst B, Liu B, Reiner J and Zimmer S 2004 *Supercond. Sci. Technol.* **17** S363 "Development and performance of thin steel reinforced MgB_2 wires and low-temperature *in situ* processing for

further improvements"
doi:10.1088/0953-2048/17/5/055

[62] Goldacker W "BSCCO materials" *Presented at Summer School on Materials and Applications of Superconductivity, 23-27 July, 2007, Forschungszentrum Karlsruhe, Germany*

[63] Gömöry F, Šouc J, Seiler E, Klinčok B, Vojenčiak M, Alamgir A K M, Han Z and Gu C 2007 *IEEE Trans. Appl. Supercond.* **17** 3083 "Performance improvement of superconducting tapes due to ferromagnetic cover on edges"
doi:10.1109/TASC.2007.900886

[64] Goodrich L F and Ficket F R 1982 *Cryogenics* **22** 225 "Critical current measurements: a compendium of experimental results"
doi:10.1016/0011-2275(82)90120-5

[65] Grasso G, Malagoli A, Ferdeghini C, Roncallo S, Braccini V and Siri A S 2001 *Appl. Phys. Lett.* **79** 230 "Large transport critical currents in unsintered MgB_2 superconducting tapes"
doi:10.1063/1.1384905

[66] Grasso G "MgB_2 conductors: technical and economical issues and perspectives (1)" *Presented at European Workshop on MgB_2-based Conductors State-of-the-art and Applications, 25 January, 2008, University of Twente, The Netherlands*

[67] Gronwald F and Nitsch J 2001 *IEEE Antennas Propagat. Mag.* **Aug** 64 "The structure of the electromagnetic field as derived from first principles"
doi:10.1109/MAP.2001.951560

[68] Guggenheim E A 1967 *Thermodynamics* (Amsterdam: North Holland)

[69] Gurvitch M, Ghosh A K, Lutz H and Strongin M 1980 *Phys. Rev. B* **22** 128 "Low-temperature resistivity of ordered and disordered A15 compounds"
doi:10.1103/PhysRevB.22.128

[70] Hall E H 1879 *Am. J. Math.* **2** 287 "On a new action of the magnet on electric currents"

[71] Heaviside O 1892 *Philos. Trans. R. Soc. London, Ser. A* **183** 423 "On the forces, stresses and fluxes of energy in the electromagnetic field"

[72] Hiltunen I, Stenvall A, Korpela A, Lehtonen J, Mikkonen R, Runde M, Magnusson N and Kalkowski G *AIP Conf. Proc.* **985** 1015 "Cryogenic design of the ALUHEAT project"
doi:10.1063/1.2908448

[73] HIPERMAG homepage, FP6 EU project, `http://lt.tnw.utwente.nl/research/HCS/Projects/HIPERMAG/`

[74] Horvat J, Yeoh W K, Kim J H and Dou S X 2008 *Supercond. Sci. Technol.* **21** 065003 "Transport and magnetic critical current in superconducting MgB_2 wires"
doi:10.1088/0953-2048/21/6/065003

[75] Hyper Tech Research Inc. `http://hypertechresearch.com/`

[76] Iijima Y, Kikuchi A and Inoue K 2000 *Cryogenics* **40** 345 "New Nb_3Al-based A15 multifilamentary wires with high J_c in high fields"
doi:10.1016/S0011-2275(00)00038-2

[77] Imbasciati L, Bauer P, Ambrosio G, Lamm M J, Miller J R, Miller G E, Zlobin A V 2003 *IEEE Trans. Appl. Supercond.* **13** 1718 "Effect of thermo-mechanical stress during quench on Nb_3Sn cable performance"
doi:10.1109/TASC.2003.812871

[78] Ioffe A, Vrana M, Arif M and Jacobson D 2000 *Physica B* **276-278** 968 "The study of the electrical charge distribution inside the neutron by neutron scattering methods"
doi:10.1016/S0921-4526(99)01687-7

[79] Ishibashi K, Wake M, Kobayashi M and Katase A 1979 *Cryogenics* **19** 633 "Thermal stability of high current density magnets"
doi:10.1016/0011-2275(79)90064-X

[80] Ishiyama A and Asai H 2001 *IEEE Trans. Appl. Supercond.* **11** 1832 "A stability criterion for cryocooler-cooled HTS coils"
doi:10.1109/77.920204

[81] Iwasa Y, Larbalestier D C, Okada M, Penco R, Sumption M D and Xi X 2006 *IEEE Trans. Appl. Supercond.* **16** 1457 "A round table discussion on MgB_2 toward a wide market or a niche production? - a summary"
doi:10.1109/TASC.2006.873235

[82] Iwasa Y 1979 *Cryogenics* **18** 705 "A critical current-margin design criterion for high performance magnet stability"
doi:10.1016/0011-2275(79)90188-7

[83] Jin S, Mavoori H, Bower C and van Dover R B 2001 *Nature* **411** 563 "High critical currents in iron-clad superconducting MgB_2 wires" doi:10.1038/35079030

[84] Jones R G, Rhoderic E H and Rose-Innes A C 1967 *Phys. Lett.* **24A** 318 "Non-linearity in the voltage-current characteristic of a type-2 superconductor"

[85] Joule J P 1850 *Philos. Trans. R. Soc. London* **140** 61 "On the mechanical equivalent of heat"

[86] Joule J P 1845 *Philos. Mag.* **27** 205 "On the existence of an equivalent relation between heat and the ordinary forms of mechanical power"

[87] Kantrowitz A R and Stekly Z J J 1965 *Appl. Phys. Lett.* **6** 56 "A new principle for the construction of stabilized superconducting coils" doi:10.1063/1.1754162

[88] Lord Kelvin (William Thomson) 1848 *Phil. Mag.* Also on *Math. Phys. Pap.* **1** (Cambridge University Press 1882) 100 "On an absolute thermometric scale founded on Carnot's theory of the motive power of heat, and calculated from Regnault's observations"

[89] Kim Y B, Hempstead C F and Strnad A R 1964 *Rev. Mod. Phys.* **36** 43 "Resistive states of hard superconductors" doi:10.1103/RevModPhys.36.43

[90] Kim Y B, Hempstead C F and Strnad A R 1965 *Phys. Rev.* **139** A1163 "Flux-flow resistance in type-II superconductors" doi:10.1103/PhysRev.139.A1163

[91] Kim J H, Joo J, Choi S, Nah W, Ha D-W, Ha H-S, Matsumoto A, Kumakura H, Koizumi T, Sugano M and Kiyoshi T 2005 *IEEE Trans. Appl. Supercond.* **15** 2470 "Characteristics of critical current and index n of Bi-2223/Ag tape up to 30 T at 4.2 K" doi:10.1109/TASC.2005.847482

[92] King C G, Grey D A, Mantone A, Herd K G and Laskaris E T *IEEE Trans. Appl. Supercond.* **7** 2046 "Mechanical stabilization of BSCCO-2223 superconducting tapes" doi:10.1109/77.620993

[93] Kitaguchi H, Matsumoto A, Hatakeyama H and Kumakura H 2004 *Physica C* **401** 246 "V - I characteristics of MgB_2 PIT composite tapes: n-values under strain, in high fields, or at high temperatures" doi:10.1016/j.physc.2003.09.047

[94] Kobayashi Y, Kitaguchi H, Doi T, Kumakura H, Hakuraku Y, Sosiati H, Yoshidome T, Hata S and Kuwano N 2006 *Teion Kogaku (Journal of Cryogenic Society of Japan)* **41** 481 In Japanese, but see figures. "J_c anisotropy and the columnar-grain texture in MgB_2 thin films" doi:10.2221/jcsj.41.481

[95] Korpela A, Lehtonen J and Mikkonen R 2003 *Supercond. Sci. Technol.* **16** 355 "Quench current in conduction-cooled HTS magnets" doi:10.1088/0953-2048/16/3/306

[96] Korpela A, Lehtonen J, Mikkonen R and Perälä R 2003 *Supercond. Sci. Technol.* **16** 1262 "Quench in a conduction-cooled Nb_3Sn SMES magnet" doi:10.1088/0953-2048/16/11/002

[97] Korpela A, Lehtonen J and Mikkonen R 2003 *Supercond. Sci. Tehcnol.* **16** 833 "Optimization of HTS superconducting magnetic energy storage magnet volume" doi:10.1088/0953-2048/16/8/301

[98] Korpela A, Lehtonen J, Mikkonen R and Paasi J 2000 *IEEE Trans. Appl. Supercond.* **10** 780 "Optimization of SMES magnet volume with electromagnetic and mechanical constraints" doi:10.1109/77.828347

[99] Kováč P, Birajdar B, Hušek I, Holúbek T and Eibl O 2008 *Supercond. Sci. Technol.* **21** 045011 "Stabilized *in situ* rectangular MgB_2 wires: the effect of B purity and sheath materials" doi:10.1088/0953-2048/21/4/045011

[100] Kováč P, Hušek I, Melišek T, Dhallé M, Müller M and Den Ouden A 2005 *Supercond. Sci. Technol.* **18** 615 "The effect of shape and deformation in *ex situ* MgB_2-W/Fe composite wires" doi:10.1088/0953-2048/18/5/007

[101] Kumakura H, Matsumoto A, Fujii H and Togano K 2001 *Appl. Phys. Lett.* **79** 2435 "High transport critical current density obtained for powder-in-tube-processed MgB_2 tapes and wires using stainless steel and Cu-Ni tubes" doi:10.1063/1.1407856

[102] Larbalestier D, Gurevich A, Feldmann M D and Polyanskii A 2001 *Nature* **414** 368 "High-T_c superconducting materials for electric power applications"
doi:10.1038/35104654

[103] Lehtonen J, Mikkonen R and Paasi J 2000 *Cryogenics* **40** 245 "Effective thermal conductivity in HTS coils"
doi:10.1016/S0011-2275(00)00030-8

[104] Lezza P, Abächerli V, Clayton N, Senatore C, Uglietti D, Suo H L, Flükiger R 2004 *Physica C* **401** 305 "Transport properties and exponential n-values of Fe/MgB_2 tapes with various MgB_2 particle sizes"
doi:10.1016/j.physc.2003.09.060

[105] Lezza P, Senatore C and Flükiger R 2006 *Supercond. Sci. Technol.* **19** 1030 "Improved critical current densities in B_4C doped MgB_2 based wires"
doi:10.1088/0953-2048/19/10/007

[106] Lorentz H A 1904 *KNAW Proc.* **6** 809 "Electromagnetic phenomena in a system moving with any velocity smaller than that of light"

[107] Lvovsky Y and Jarvis P 2005 *IEEE Trans. Appl. Supercond.* **15** 1317 "Superconducting systems for MRI-present solutions and new trends"
doi:10.1109/TASC.2005.849580

[108] Maddock B J, James G B and Norris W T 1969 *Cryogenics* **9** 261 "Superconductive composites: heat transfer and steady state stabilization"
doi:10.1016/0011-2275(69)90232-X

[109] Magnusson N and Runde M 2006 *J. Phys. Conf. Ser.* **43** 1019 "A 200 kW MgB_2 induction heater project"
doi:10.1088/1742-6596/43/1/249

[110] Magnusson N, Bersås R, and Runde M 2004 *Inst. Phys. Conf. Ser.* **181**, 1104 "Induction heating of aluminum billets using HTS DC coils"

[111] Martinelli A P and Wipf S L 1972 *Proc. 5th Appl. Supercond. Conf., IEEE* 331 "Investigation of cryogenic stability and reliability of operation of Nb_3Sn coils in helium gas environment"

[112] Martínez E, Lera F, Martínez-López M, Yang Y, Schlachter S I, Lezza P and Kováč P 2006 *Supercond. Sci. Technol.* **19** 143 "Quench development and propagation in metal/MgB_2 conductors"
doi:10.1088/0953-2048/19/1/024

[113] Martínez E, Young E A, Bianchetti M, Munoz O, Schlachter S I and Yang Y 2008 *Supercond. Sci. Technol.* **21** 025009 "Quench onset and propagation in Cu-stabilized multifilament MgB_2 conductors" doi:10.1088/0953-2048/21/02/025009

[114] Masson P J, Rouault V R, Hoffmann G and Luongo C A 2008 *IEEE Trans. Appl. Supercond.* **18** 1321 "Development of quench propagation models for coated conductors" doi:10.1109/TASC.2008.921260

[115] MATLAB is a product of The MathWorks, Inc., `http://www.mathworks.com/`

[116] Matsushita T 2000 *Supercond. Sci. Technol.* **13** 730 "Flux pinning in superconducting 123 materials" doi:10.1088/0953-2048/13/6/320

[117] Matsushita T, Fujiyoshi T, Toko K and Yamafuji K 1990 *Appl. Phys. Lett.* **56** 2039 "Flux creep and irreversibility line in high-temperature oxide superconductors" doi:10.1063/1.103011

[118] Matthias B T, Geballe T H, Geller S and Corenzwit E 1954 *Phys. Rev.* **95** 1435 "Superconductivity of Nb_3Sn" doi:10.1103/PhysRev.95.1435

[119] Maxwell J C 1865 *Philos. Trans. R. Soc. London* **155** 459 "A dynamical theory of the electromagnetic field"

[120] Maxwell J C 1861-62 *Phil. Mag.* **21** "On a physical lines of force"

[121] Modica M, Angius S, Bertora L, Damiani D, Marabotto M, Nardelli D, Perrella M, Razeti M and Tassito M 2007 *IEEE Trans. Appl. Supercond.* **17** 2196 "Design, construction and tests of MgB_2 coils for the development of a cryogen free magnet" doi:10.1109/TASC.2007.898107

[122] Moran M J and Shapiro H N 1988 *Fundamentals of Engineering Thermodynamics* (New York among others: John Wiley & Sons, Inc.)

[123] Müller K A and Bednorz J G 1987 *Proc. Natl. Acad. Sci.* **84** 4678 "High-temperature superconductivity"

[124] Nagamatsu J, Nakagawa N, Muranaka T, Zenita Y and Akimitsu J 2001 *Nature* **410** 63 "Superconductivity at 39 K in magnesium diboride" doi:10.1038/35065039

[125] Nagakomi T 1981 *J. Stat. Phys.* **26** 567 "Mesoscopic thermodynamics of nonequilibrium open systems. I. Negentropy consumption and residual entropy" doi:10.1007/BF01011436

[126] National Institute of Standards and Technology, International System of Units (SI), `http://physics.nist.gov/cuu/Units/introduction.html`

[127] Oshima M, Thome R J, Mann W R and Pillsbury R D 1991 *IEEE Trans. Magn.* **27** 2096 "PQUENCH - a 3-D quench propagation code using a logical coordinate system" doi:10.1109/20.133624

[128] Overweg J "MRI magnets" *Presented at 2nd Nordic Seminar on Superconductors and their Industrial Applications, 15-16 November, 2006, Pori, Finland*

[129] Pachla W, Presz A, Kováč P, Hušek I and Doduszko R 2004 *Supercond. Sci. Technol.* **17** 1289 "Structural characterization of multifilament heat treated *ex situ* MgB_2 superconducting wires with Cu and Fe sheaths" doi:10.1088/0953-2048/17/11/009

[130] Picaud V, Hiebel P and Kauffmann J-M 2002 *IEEE Trans. Magn.* **38** 1253 "Superconducting coils quench simulation, the Wilson's method revisited" doi:10.1109/20.996320

[131] Quinn T J 1983 *Temperature* (London: Academic Press)

[132] Rautio J C 2005 *IEEE Microwave Mag.* **Jun** 46 "Maxwell's legacy"

[133] Reitz J R, Milford F J and Christy R W 1993 *Foundations of Electromagnetic Theory* (Addison Wesley)

[134] Rindfleisch M "MgB_2 conductors: technical and economical issues and perspectives (2)" *Presented at European Workshop on MgB_2-based Conductors State-of-the-art and Applications, 25 January, 2008, University of Twente, The Netherlands*

[135] Rose-Innes A C and Rhoderick E H 1969 *Introduction to Superconductivity* (Glasgow: Pergamon Press)

[136] Rostila L, Lehtonen J, Mikkonen R, Šouc J, Seiler E, Melišek T and Vojenčiak M 2007 *Supercond. Sci. Technol.* **20** 1097 "How to determine critical current density in YBCO tapes from voltage-current measurements at low magnetic fields"
doi:10.1088/0953-2048/20/12/002

[137] Rostila L 2008 *Electromagnetic Design of Superconducting Coated Conductor Power Cables* (PhD Thesis, Tampere University of Technology, Finland)

[138] Runde M, Stenvall A, Magnusson N, Grasso G and Mikkonen R 2008 *J. Phys.: Conf. Ser.* **97** 012159 "MgB_2 coils for a DC superconducting induction heater"
doi:10.1088/1742-6596/97/1/012159

[139] Scanlan R M, Malozemoff A P and Larbalestier D C 2004 *IEEE Proc.* **92** 1639 "Superconducting materials for large scale applications"
doi:10.1109/JPROC.2004.833673

[140] Schlachter S I, Goldacker W, Frank A, Ringsdorf B and Orschulko H 2006 *Cryogenics* **46** 201 "Properties of MgB_2 superconductors with regard to space applications"
doi:10.1016/j.cryogenics.2005.11.003

[141] Schlachter S I, Frank A, Ringsdorf B, Orschulko H, Obst B, Liu B and Goldacker W 2006 *Physica C* **445-448** 777 "Suitability of sheath materials for MgB_2 powder-in-tube superconductors"
doi:10.1016/j.physc.2006.05.021

[142] Seeber B Editor 1998 *Handbook of Applied Superconductivity* (Bristol: Institute of Physics Publishing)

[143] Sivasubramaniam K, Laskaris E T and Ryan D 2003 *IEEE Trans. Appl. Supercond.* **13** 3277 "Suitability of MgB_2 tapes with iron sheaths for multiturn superconducting coils"
doi:10.1109/TASC.2003.812224

[144] Soltanian S, Horvat J, Wang X L, Tomsic M and Dou S X 2003 *Supercond. Sci. Technol.* **16** L4 "Transport critical current of solenoidal MgB_2/Cu coils fabricated using a wind-reaction in situ technique"
doi:10.1088/0953-2048/16/1/102

[145] Soltanian S, Horvat J, Wang X L, Munroe P and Dou S X 2003 *Physica C* **390** 185 "Effect of nano-carbon particle doping on the flux pinning properties of MgB_2 superconductor"
doi:10.1016/S0921-4534(03)00960-2

[146] Srinivasan J 2001 *Resonance* **Nov** 42 "Sadi Carnot and the second law of thermodynamics"

[147] Stekly Z J J and Zar J L 1965 *IEEE Trans. Nucl. Sci.* **12** 367 "Stable superconducting coils"
doi:10.1109/TNS.1965.4323653

[148] Stenvall A, Korpela A, Lehtonen J and Mikkonen R 2008 *IEEE Trans. Appl. Supercond.* **18** 1271 "The effect of local damage inside a winding on quench behavior in an Nb_3Sn magnet"
doi:10.1109/TASC.2008.920616

[149] Sumption M D, Bhatia M, Wu X, Rindfleisch M, Tomsic M and Collings E W 2005 *Supercond. Sci. Technol.* **18** 730 "Multifilamentary, *in situ* route, Cu-stabilized MgB_2 strands"
doi:10.1088/0953-2048/18/5/026

[150] Sumption M D, Bhatia M, Dou S X, Rindfliesch M, Tomsic M, Arda L, Ozdemir M, Hascicek Y and Collings E W 2004 *Supercond. Sci. Technol.* **17** 1180 "Irreversibility field and flux pinning in MgB_2 with and withoud SiC additions"
doi:10.1088/0953-2048/17/10/017

[151] Sumption M, Bhatia M, Rindfleisch M, Tomsic M and Collings E W 2006 *Supercond. Sci. Technol.* **19** 155 "Transport properties of multifilamentary, *in situ* route, Cu-stabilized MgB_2 strands: one metre segments and the $J_c(B,T)$ dependence of short samples"
doi:10.1088/0953-2048/19/2/001

[152] Superconductors.org, `http://www.superconductors.org`

[153] Tahar M 1999 *Scientific American* **Mar** 15 "How do Hall effect transducers work?"

[154] Takahashi M, Tanaka K, Okada M, Kitaguchi H and Kumakura H 2005 *Supercond. Sci. Technol.* **18** S373 "Relaxation of trapped magnetic field in a 100 m long class MgB_2 solenoid coil in persistent current mode operation"
doi:10.1088/0953-2048/18/12/025

[155] Tanaka K, Kitaguchi H, Kumakura H, Hirakawa M, Yamada H and Okada M 2005 *IEEE Trans. Appl. Supercond.* **15** 3180 "Fabrication and trasport properties of MgB_2 mono-core wire and solenoidal coil" doi:10.1109/TASC.2005.848778

[156] ten Kate H H J, Boschman H and van de Klundert L J M 1987 *IEEE Trans. Magn.* **23** 1557 "Longitudinal propagation velocity of the normal zone in superconducting wires"

[157] Thoner M, Krauth H, Szulczyk A, Heine K and Kemper M 1991 *IEEE Trans. Appl. Supercond.* **27** 2027 "Nb_3Sn multifilamentary superconductors: an updated comparison of different manufacturing routes" doi:10.1109/20.133987

[158] Tominaka T, Mori K and Maki N 1992 *IEEE Trans. Magn.* **28** 727 "Quench analysis of superconducting magnet systems" doi:10.1109/20.119982

[159] Tomsic M, Rindfleisch M, Yue J, McFadden K, Doll D, Phillips J, Sumption M D, Bhatia M, Bohnenstiehl S and Collings E W 2007 *Physica C* **456** 203 "Development of magnesium diboride (MgB_2) wires and magnets using *in-situ* strand fabrication method" doi:10.1016/j.physc.2007.01.009

[160] Tomsic M, Rindfleisch M, Yue J, McFadden K, Phillips J, Sumption M D, Bhatia M, Bohnenstiehl S and Collings E W 2007 *Int. J. Appl. Ceram. Technol.* **3** 250 "Overview of MgB_2 superconductor applications" doi:10.1111/j.1744-7402.2007.02138.x

[161] Tonomura A and Nori F 2008 *Nature* **452** 298 "Disturbance without the force" doi:10.1038/452298a

[162] van Weeren H 2007 *Magnesium Diboride Superconductors for Magnet Applications* (PhD Thesis, University of Twente, The Netherlands)

[163] Vase P, Flükiger R, Leghissa M and Glowacki B 2000 *Supercond. Sci. Technol* **13** R71 "Current status of high-T_c wire" doi:10.1088/0953-2048/13/7/201

[164] Vinod K, Abhilash Kumar R G and Syamaprasad U 2007 *Supercond. Sci. Technol.* **20** R1 "Prospects for MgB_2 superconductors for magnet application" doi:10.1088/0953-2048/20/1/R01

[165] Vinod K, Varghese N and Syamaprasad U 2007 *Supercond. Sci. Technol.* **20** R31 "Superconductivityof MgB_2 in the BCS framework with emphasison extrinsic effects on critical temperature" doi:10.1088/0953-2048/20/10/R01

[166] Voelker F 1970 *Particle Accel.* **1** 205 "Resistance in small, twisted, multicore superconducting wires"

[167] Wang X L, Soltanian S, James M, Qin M J, Horvat J, Yao Q W, Liu H K and Dou S C 2004 *Physica C* **480-410** 63 "Significant enhancement of critical current density and flux pinning in MgB_2 with nano-SiC, Si, and C doping" doi:10.1016/j.physc.2004.02.030

[168] Warnes W H and Larbalestier D C 1987 *IEEE Trans. Magn.* **23** 1183 "Determination of the average critical current from measurements of the extended resistive transition"

[169] Waser A 2000 *AW-Verlag* "On the notation of Maxwell's field equations"

[170] Watanabe K, Hoshi A, Awaji S, Katagiri K, Noto K, Goto K, Sugimoto M, Saito T and Kohno O 1993 *IEEE Trans. Appl. Supercond.* **3** 1006 "Nb_3Sn multifilamentary wires with CuNb reinforcing stabilizer" doi:10.1109/77.233868

[171] Weijers H W, Trociewitz U P, Marken K, Meinesz M, Miao H and Schwarz J 2004 *Supercond. Sci. Technol.* **17** 636 "The generation of 25.05 T using a 5.11 T $Bi_2Sr_2CaCu_2O_x$ superconducting insert magnet" doi:10.1088/0953-2048/17/4/012

[172] Whetstone C N and Roos C E 1965 *J. Appl. Phys.* **36** 783 "Thermal phase transitions in superconducting Nb-Zr alloys" doi:10.1063/1.1714218

[173] Wikipedia Contributors, Mesoscopic scale, *Wikipedia, The Free Encyclopedia* Revised 16 December 2007 19:26 UTC, `http://en.wikipedia.org/w/index.php?title=Mesoscopic_scale&oldid=178344513`

[174] Williams J E C, Baker M, Bobrov E S, Iwasa Y, Leupold M J, Stejskal V J, Weggel R J, Zhukovsky A, Gung J, Miller J Painter T and van Sciver S 1994 *IEEE Trans. Magn.* **30** 1633 "The development of a niobium-titanium cable-in-conduit coil for a 45 T hybrid magnet" doi:10.1109/20.305572

[175] Wilson M N 1983 *Superconducting Magnets* (Oxford: Oxford University Press)

[176] Wilson M N and Iwasa Y 1978 *Cryogenics* **18** 17 "Stability of superconductors against localized disturbances of limited magnitude" doi:10.1016/0011-2275(78)90132-7

[177] Wilson M N 1977 *IEEE Trans. Magn.* **13** 440 "Stabilization of superconductors for use in magnets"

[178] Wu M K, Ashburn J R, Torng C J, Hor P H, Meng R L, Gao L, Huang Z J, Wang Y Q and Chu C W 1987 *Phys. Rev. Lett.* **58** 908 "Superconductivity at 93 K in a new mixed-phase Yb-Ba-Cu-O compound system at ambient pressure" doi:10.1103/PhysRevLett.58.908

[179] Xu M, Shi D and Fox R 1990 *Phys. Rev. B* **42** 10773 "Generalized critical-state model for hard superconductors" doi:10.1103/PhysRevB.42.10773

[180] Yamada R, Marscin E, Lee A, Wake M and Rey J-M 2003 *IEEE Trans. Appl. Supercond.* **13** 1696 "3-D/2-D quench simulation using ANSYS for epoxy impregnated Nb_3Sn high magnetic field magnets" doi:10.1109/TASC.2003.812870

[181] Zheng D N, Ingle N J C and Cambpell A M 2000 *Phys. Rev. B* **61** 15429 "Irreversibility fields of superconducting niobium alloys" doi:10.1103/PhysRevB.61.15429